EXPLORING THE ROLE OF HYDROLOGIC RESIDENCE TIME AND CHEMISTRY IN THE PROCESSING OF NITRATE AT THE SEDIMENT-WATER INTERFACE

By

Tyler Barbee Hampton

A THESIS

Submitted to
Michigan State University
in partial fulfillment of the requirements
for the degree of

Geological Sciences - Master of Science

ABSTRACT

EXPLORING THE ROLE OF HYDROLOGIC RESIDENCE TIME AND CHEMISTRY IN THE PROCESSING OF NITRATE AT THE SEDIMENT-WATER INTERFACE

By

Tyler Barbee Hampton

The concentrations of inorganic nitrogen, including nitrate (NO₃-), are fundamental controls on the trophic state of aquatic ecosystems. Excess NO₃ degrades drinking water quality, and therefore there is a need to understand processes that remove inorganic nitrogen. Controls on NO₃ removal at the sediment-water interface (SWI) of aquatic ecosystems include both biogeochemical and hydrologic conditions, however the relative importance and interactions of these controls are poorly understood. This thesis explores these controls on NO₃ removal using a series of in-situ experiments involving both biogeochemical and hydrologic manipulations of the SWI in both lake and stream settings. Specifically, manipulative experiments altered dissolved organic carbon (DOC) and NO₃⁻ concentrations, as well as physical hydrologic residence times. The fate of NO₃⁻ in these manipulation experiments was traced by pairing isotopically labeled ¹⁵N-NO₃ tracer experiments with controlled variable-head infiltrometer rings to isolate the sediment-water system and control the hydrology of the SWI. With these experiments, I was able to isolate biogeochemical versus hydrologic controls on rates of NO₃⁻ removal and denitrification rates. I found that increasing NO₃⁻ and DOC concentrations increased NO₃⁻ removal and denitrification rates in the SWI, but that increases in physical residence time had a stronger effect on increasing NO₃⁻ removal and denitrification rates, especially under conditions where DOC and NO₃ availability were not limiting.

ACKNOWLEDGEMENTS

The completion of this master's thesis would not have been possible without the support from my mentors, peers, friends, and family. First and foremost, I want to thank my advisor, Jay Zarnetske, for his guidance throughout this project. I also want to thank my committee members Stephen Hamilton and Nathaniel Ostrom for their feedback on the direction of this research and on this thesis. Many thanks also to coauthors on this work, including Martin Briggs and Kamini Singha, whose support I have appreciated throughout my graduate school career. I am very grateful for the help of Farzaneh MahmoodPoor Dehkordy and Courtney Scruggs who implemented the design of these studies and without whom this work would not have been possible. I owe many thanks to my labmates, including Joseph Lee-Cullin, Sydney Ruhala, Stephen Plont, and Sinchan Roy Chowdhury; who all offered a combination of expertise, institutional knowledge, feedback, field assistance, and emotional support. Furthermore, I would like to offer my appreciation to all my peers in the Department of Earth and Environmental Sciences and across Michigan State University for their support throughout my degree and in my growth as a person during this time. In particular, I am grateful to the fostering of an environment that has destigmatized mental health issues and encouraged me to seek help for issues that affect approximately half of graduate students. Thanks also to my foster dogs, who gave so much love: Noodle, Indigo, Leia, Jack, Fiona. This research and derived presentations were funded or supported by the National Science Foundation, the Kellogg Biological Station, the Geological Society of America, the Society for Freshwater Science; and the Graduate School, the Council of Graduate Students, and the Department of Earth and Environmental Sciences at Michigan State University. Finally, to my family and friends, who have shown so much love and support, and encouraged me to pursue my path at every step: thank you.

TABLE OF CONTENTS

LIST OF TABLES	S	vi
LIST OF FIGURE	S	vii
KEY TO ABBRE	VIATIONS	xi
CHAPTER 1: INT	RODUCTION	1
CHAPTER 2: EX	PERIMENTAL MODIFICATIONS OF REACTANT AND HYDROLOGI	C
CONTROLS ON I	NITROGEN PROCESSING: RESULTS FROM FLOW-THROUGH	
LAKEBED SWI S	EDIMENTS	6
2.1. Introd	luction	6
2.2. Mater	rials and Methods	10
2.2.1.	Site Description	10
2.2.2.	Experimental Setup	12
2.2.3.	N, C, and Residence Time Manipulations	15
2.2.4.	Porewater Sampling and Laboratory Methods	17
2.2.5.	Calculations	19
2.2.6.	Sediment Characterization	22
2.3. Result	ts and Discussion	23
2.3.1.	Sediment Characterization	23
2.3.2.	Hydrologic and Chemical Setting	25
	Experimental Outcomes	27
	Residence Time Controls N Cycling	35
2.4. Concl	• •	38
CHAPTER 3: EX	PERIMENTAL MODIFICATIONS OF HYDROLOGIC FLUX AND	
RESIDENCE TIM	E REVEAL CONTROLS ON NITROGEN PROCESSING IN THE	
SEDIMENT-WAT	TER INTERFACE OF A HEADWATER STREAM	39
3.1. Introd	luction	39
3.2. Mater	ials and Methods	44
3.2.1.	Site Description	44
3.2.2.	Experimental Setup	46
3.2.3.	Porewater Sampling Methods	49
3.2.4.	Laboratory Analyses	51
3.2.5.	Calculations of Residence Time and Reaction Rates	51
3.3. Result	· · · · · · · · · · · · · · · · · · ·	52
3.3.1.	Hydrologic and Chemical Setting	52
3.3.2.	Solute Removal with Depth	55
3.3.3.	Scaling by Residence Time	61
3.4. Discus	· .	65
3.4.1.	Biogeochemical Reaction Rates in the SWI Controlled by Residence Time	65
3.4.2.	Role of Anoxic Microzones and POC	67
3.4.3.	Implications of Dynamic Stream Hydrology for N export	69

3.5. Conclusions	72
CHAPTER 4: SYNTHESIS & IMPLICATIONS	74
APPENDICES APPENDIX A: 2016 Snake Pond Sampling Data APPENDIX B: 2017 Sawmill Brook Experimental Data	78 79 83
REFERENCES	9(

LIST OF TABLES

- **Table 1: Details of the Snake Pond experiments.** Details are provided on the addition of reactants and changing flux rates. Concentrations of the reactant tanks are reported, as well as the measured pump rate from the tank into the surface water of the injection ring. The addition rate is the concentration in the addition tank multiplied by the pump rate. The hydraulic flux through the ring is also reported for each experiment, either directly measured or interpolated.
- Table 2: Parameter values for calculation of Bunsen solubility coefficients for N₂ and N₂O gasses in water. Values from Weiss (1970) and Weiss and Price (1980).
- **Table 3: Details of the Sawmill Brook Experiments.** The measured hydraulic flux through the ring is reported for each experiment.
- **Table 4: Tabulated data from Figure 12.** Concentrations are as either μmol/L or nmol/L. Experiment is listed, with A for Ambient or the experiment number. Type is the mean with standard deviation of points in parentheses, when more than one measurement was available. 80
- **Table 5: Tabulated data from Figure 13, as well as data for SO**₄²- **and NO**₂⁻. Rates are calculated as in Section 2.2.5. For the ambient profile, rates are calculated between 0 and 18 cm depth. For gases (O₂, N₂, and N₂O), rates are between 9.5 and 19.5 cm depths. For NO₃⁻ and DOC, rates are calculated between 9.5 and 19.5 cm for Experiments 1-2, and between 0 and 19.5 cm for Experiments 3-5.
- **Table 6: Sediment core data from Snake Pond.** Also including Loss on Ignition results from Figure 11.
- **Table 7: Tabulated data from Figure 20 and Figure 22.** Concentrations are as either μmol/L or nmol/L. Experiment is listed, with the flux rate and ring (US or DS). Type is the mean with standard deviation of points in parentheses, when more than one measurement was available. 84
- **Table 8: Tabulated data from Figure 21 and Figure 23.** Rates are calculated as in Section 2.2.5, as μ mol/L/h or nmol/L/h, with mean \pm standard deviation, when multiple points were available for the calculation.
- **Table 9: Injection and Flush porewater velocities from the Sawmill Brook Experiments.** Velocities were determined by the depth (10 or 20 cm) divided by the median arrival time of the conductivity plume at that depth, as shown in Figure 27.

LIST OF FIGURES

- **Figure 1: Diagram of the sediment-water interface (SWI).** In streams and lakes, groundwater and surface water exchange and interact with landscape fluxes of nitrogen (Minnesota Department of Natural Resources, Division of Ecological Services, 2003).
- **Figure 2: Schematic of the Cape Cod groundwater system.** This diagram gives regional hydrologic context (A) to individual groundwater flow-through lakes like Snake Pond, as shown in (B). Groundwater entering the lake is generally poor in labile carbon and high in inorganic N as NO₃⁻ from anthropogenic groundwater pollution. We sampled the groundwater recharge, or outflow side of the lake, where oxidation of organic matter depletes the recharging water of oxygen, depicted by the red box.
- **Figure 3: Map of Massachusetts and Snake Pond.** (A). Cape Cod is a 100-km-long peninsula that extends into the Atlantic Ocean. (B) Snake Pond, with sampling site shown on the south shore. Map units are in km. Map Projection is UTM, Zone 19T.
- **Figure 4: Site picture from Snake Pond.** View is looking northeast, with the injection ring installed in the pond sediments offshore in the center frame.
- **Figure 5: Schematic of injection ring**. A 55-cm diameter plastic drum with open ends is inserted into the lakebed sediments to 22 cm-depth. Downward 'recharge' flow is induced by experimentally elevating the hydraulic head in the injection ring (shown in the schematic as dH). Four steel piezometers (USGS MINIPOINT design) are inserted into the sediments and water is pumped from them at ~2.5 mL/min, so as not to disrupt the hydraulic flow field. In-line from the piezometers are dissolved O₂ and electrical conductivity flow-through sensors.
- **Figure 6: Schematic of Tracer Additions at Snake Pond.** Before the experiments, water from the lake was pumped into a 1.89 m³ holding tank. Using a series of pumps and float switches (FS) to maintain steady water levels, water was pumped into an intermediate bucket and then into the injection ring. Tracers were added using a peristaltic pump at a rate of ~3 mL/min.
- **Figure 7: Breakthrough curves for extracting residence time.** Specific conductivity was measured at 9.5 and 14.5 cm depth within the injection ring sediments. Panel (A) is for the onset of the experiments, and panel (B) is for the transition from high flux rate to low flux rate, corresponding with a replacement of the injection ring water (Cl⁻ labeled) with fresh lake water, Points along breakthrough curves are for the median time of arrival for the conductivity plume for each depth, in cm. For the injection: 0.53 h at 9.5 cm and 0.79 h at 14.5 cm. For the flush: 0.29 h at 9.5 cm and 0.53 h at 14.5 cm.
- **Figure 8: Conceptual Diagram of Snake Pond Experimental Modifications.** The three natural controls on SWI N processing are microbial community composition, porewater reactant chemistry, and hydrologic transport. By confirming with a ¹⁵NO₃- tracer that a microbial community capable of N transformations was present, Experiments 2-4 interrogated how changing reactant chemistry changes N removal, and Experiment 5 tested the hypothesis that hydrologic residence time is a key control.

- **Figure 9: Particle size distribution for shallow Snake Pond cores.** 8 cores were collected on 7/26/2016 and sampled at 2 cm depth. The 10th percentile and 50th percentile particle sizes are shown for each core.
- **Figure 10: Particle size distribution for a deep core from Snake Pond.** A core was collected on 7/8/2016 to 11 cm depth. Depth intervals are shown, with the 10th percentile and 50th percentile particle sizes for each interval.
- Figure 11: Loss on Ignition results from Snake Pond core. A core collected on 7/9/2016, sampled at 2 cm intervals up to 11 cm depth. (A) % mass lost on ignition, sorted by particle size greater than and less than 500 μ m. (B) Percent LOI converted to mass loss per cm³.
- Figure 12: Concentration profiles with depth below the sediment-water interface for Snake Pond. Concentrations (C) are shown at steady state (~24 h) and expressed as C/Cmax or δ^{15} N/ δ^{15} N_{max}. The five experiments are described in Table 1. Species shown: NO₃-, O₂, DOC, δ^{15} N₂, and N₂O (symbol legend in figure). Error bars are for the standard deviation of three replicates at each depth, when available; some error bars are within the size of the plotted point.
- **Figure 13: Biogeochemical flux rates in the Snake Pond experiments.** Rates of O₂, NO₃, DOC measured as NPOC, N₂, and N₂O, across the five experiments (Table 1). For the ambient profile (A), rate is calculated between 0 and 18 cm depth. For gases (O₂, N₂, and N₂O), rates are between 9.5 and 19.5 cm depth. For NO₃⁻ and DOC, rates are calculated between 9.5 and 19.5 cm for Experiments 1-2, and between 0 and 19.5 cm for Experiments 3-5. Rates are calculated as in Section 2.2.5. Error bars are based off the standard deviation of the concentrations of 3 samples at each depth.
- Figure 14: Maps of Massachusetts, the Ipswich River Watershed, and Sawmill Brook. (A) Study region within Massachusetts, USA with the (B) Ipswich River Watershed, showing the study site at Sawmill Brook and the nearest USGS stream gage (01101500) on the Ipswich River at South Middleton, MA. (C) Topographic map of the Sawmill Brook study reach and site (marked with star). Map units are kilometers. Datum is UTM zone 19T.
- **Figure 15: Detailed Plan-view Site Map of Sawmill Book.** Stream level and banks were surveyed. The two injection ring locations are shown as 'Ring US' (upstream) and 'Ring DS' (downstream) (see Figure 5 for ring details). The groundwater (GW) and background (ambient) locations were sampled for groundwater and SWI porewater samples, respectively. The SWI ambient samples were taken at sediment depths of 2.5, 5, 7.5, 10, 15, 20 cm depths, and the groundwater sample was taken at 60 cm depth. The site labeled as stage (Figure 14) shows the location of our in-stream pressure logger. Map units are meters. Coordinates are for UTM zone 19T.
- **Figure 16: Site picture from Sawmill Brook.** View is looking east, downstream, with ring US in the foreground and ring DS in the background. Additional equipment not described herein, such as the orange wiring seen in the image, are associated with a concurrent geophysical (electrical resistivity imaging) study.

 45
- **Figure 17: Schematic of Tracer Addition at Sawmill Brook.** Before the experiments, water from the stream was pumped into two holding tanks. ¹⁵NO₃⁻ was added to both tanks, and NaCl

to only one. Using a series of pumps and float switches (FS) to maintain steady water levels, water was pumped into an intermediate bucket and then into the injection ring. An aerator was in the intermediate bucket to keep water oxygenated during sometimes long residence times in the bucket at low flux rates. There was no aerator in the holding tank.

48

Figure 18: Conceptual Diagram of Sawmill Brook Experimental Modifications. The three major natural controls on SWI Function on N are microbial community composition, porewater reactant chemistry, and hydrologic transport conditions. By confirming with a ¹⁵NO₃- tracer that a microbial community capable of N transformations was present and seeking to isolate the role of reactant chemistry on N removal, Experiments 1-4 systematically changed hydrologic flux, with two experiments exploring an oxic or anoxic regime, to observe changes in N removal as a result of changes in hydrologic controls.

Figure 19: Stream stage and chemical conditions during sampling at Sawmill Brook. (A) Stage monitored at the site on Sawmill Brook over the study dates. Sampling periods of the four experiments are shown by red bars, with the commencement of each injection as the beginning of the bar and the end of sampling for that experiment as the end of the bar. Experiment order was 2 m/d, 3 m/d, 0.8 m/d, 1.2 m/d. Total conductivity (TC; not temperature corrected) from the site surface water is also shown, with points showing spot-checks of TC with a handheld probe. (B) NO₃- concentrations in the stream, shown by connected lines, and concentrations in the tank water ("T"), Ring US ("U") and Ring DS ("D"). Boxplots on the right show the median and interquartile range for samples collected in the stream, tanks, and rings. Whiskers are to the minimum and maximum. Points are outliers. (C) DOC concentrations as shown in panel C. (D) Oxygen (O₂) saturation and concentration are shown for the surface water from the two SWI rings. The boxplot shows O₂ during the sampling periods (red boxes). (E) Temperature as monitored at the stream stage site and within the two SWI rings.

Figure 20: Concentration over depth and residence time from Sawmill Brook experiments. Concentrations of O₂, NO₃⁻, and DOC over flowpath length (A) and over porewater residence time (B). Symbols denote data from Rings US and DS. The color of each line and point denotes the flux rate (see inset legend in the lower left panel), where lighter shade denotes the lower flux rates. Error bars are the standard deviation of concentration when repeated samples were possible.

Figure 21: Removal rates for O₂, NO₃⁻, and DOC from the Sawmill Brook Experiments. Symbols denote ring US or DS. Error bars are based on the standard deviation of concentrations used in the rate calculations, where multiple samples are available. More negative values indicate increasing removal rates. Positive values indicate accumulation along the flowpath.

Figure 22: ¹⁵N tracer conditions of N₂ and concentrations of N₂O from Sawmill Brook **Experiments.** ¹⁵N isotopic enrichment of N₂ and concentrations of N₂O over flowpath length (A) and over porewater residence time (B). Symbols denote data from Rings US and DS. The color of each line and point denotes the flux rate, where lighter shade denotes the lower flux rates. Error bars are the standard deviation of concentration when repeated samples were possible. 58

Figure 23: Production rates of N₂ and N₂O from Sawmill Brook Experiments. Symbols denote ring US or DS. Error bars are based on the standard deviation of concentrations used in

the rate calculation,	where multiple samples are available.	Positive values indicate accumulation
along the flowpath.		59

- **Figure 24: Residence time over flux rate in the Sawmill Brook experiments.** Residence time is shown at 20 cm depth, or the bottom of the SWI flowpath, for each flux rate experiment.
- Figure 25: Concentrations over Damköhler number for O₂ from Sawmill Brook Experiments. Concentrations of O₂, NO₃-, N₂O, and δ^{15} N₂ over the Damköhler number for oxygen removal (DaO2), calculated for each ring in each experiment.
- Figure 26: Removal rates over Removal Velocities for O₂ (left) and NO₃ (right) from Sawmill Brook Experiments. Removal rates are reported as in Figure 21 and calculated in Section 2.2.5 and Removal velocities are calculated as in Section 3.2.5. Blue lines are linear regression lines. Circles are from ring DS and triangles are from ring US.

Figure 27: Conductivity Breakthrough Curves from the Sawmill Brook Experiments. Data are plotted as electrical conductivity over time for the first three experiments, for both 10 and 20 cm depth on the injection (A) and flush (B) phases of the high-conductivity injections. Time is normalized to the beginning of injection or flush. Red lines mark the initial concentration and plateau; the orange line marks the median concentration between those two, and the green line marks the time of median arrival time, which was used to calculate velocities as in Table 9.

KEY TO ABBREVIATIONS

SWI – Sediment-water interface N - NitrogenN_R – Reactive Nitrogen NO_3^- – Nitrate N₂ – Di-nitrogen gas N₂O – Nitrous oxide gas $NH_3 - Ammonia$ C – Carbon DOC - Dissolved Organic Carbon POC – Particulate Organic Carbon NPOC – Non-Purgeable Organic Carbon DO – Dissolved Oxygen Cl⁻ – Chloride SO_4^{2-} – Sulfate USGS – United States Geological Survey US EPA – United States Environmental Protection Agency SIF – Stable Isotope Facility, University of California Davis °C – Degrees Celsius PVC-Polyvinyl-ChlorideHDPE – High Density Polyethylene

EC- Electrical Conductivity

VHG – Vertical Head Gradient

CHAPTER 1: INTRODUCTION

Anthropogenic inputs of reactive nitrogen to landscapes have steadily increased since the beginning of the 20th century following the advent of industrial nitrogen fixation for fertilizer production and the proliferation of nitrogen fixing crops, resulting in an up to 20-fold increase in fluxes of nitrogen to the ocean (Howarth et al., 1996). Nitrate (NO₃-) loading in surface waters is now considered one of the top global threats to ecosystems and humanity (Rockström et al., 2009; Steffen et al., 2015). Fortunately for the world's oceans, only about 25% of anthropogenic reactive nitrogen (N_R) inputs to the continents is exported by rivers to the oceans, with the balance either sequestered or removed (Howarth et al., 1996; Boyer et al., 2006). Freshwater ecosystems perform a critical ecosystem service by contributing to this N_R retention and removal: the freshwater continuum is estimated to remove ~50% of N_R that enters water bodies before export to the oceans (Galloway et al., 2004). Lakes and rivers are estimated to contribute a similar proportion of anthropogenic N_R removal (Seitzinger et al., 2006). The dominant removal pathway of N_R in freshwaters is denitrification, the microbially-mediated anaerobic reduction of dissolved inorganic N as NO₃⁻ to di-nitrogen (N₂) and nitrous oxide (N₂O) gases (Payne, 1973; Tiedje et al., 1983). Most denitrifiers are facultative aerobes and thus are thought to only perform denitrification when oxygen (O₂) becomes limiting (Tiedje et al., 1984; Mosier et al., 2002), though studies have shown that this process can occur in predominantly oxic soil environments (Robertson and Kuenen, 1984; Lloyd et al., 1987; Robertson and Tiedje, 1987; Lloyd, 1993). The sediment-water interface (SWI), an important ecotone between surface and groundwater ecosystems (Boulton et al., 1998; Boano et al., 2014) (Figure 1), is a hospitable environment for denitrifying microbes. The mixing of these two waters in the SWI and aerobic respiration of DOC results in the depletion of O₂ supplies, with NO₃- supplied by in situ

nitrification or by external surface-water or groundwater inputs. Studies have focused on both fluvial (Marzadri *et al.*, 2011; Zarnetske *et al.*, 2011a, 2012; Harvey *et al.*, 2013) and lacustrine (Whitmire and Hamilton, 2005; Burgin and Hamilton, 2008; Smith *et al.*, 2015; Stoliker *et al.*, 2016) settings to examine the role of the SWI in NO₃⁻ removal and denitrification. Despite research covering a range of ecosystems and impact levels, questions remain regarding the relative impact of external chemical versus physical conditions on SWI biogeochemical function. In other words, the relative importance of reaction and transport controls to NO₃⁻ removal and denitrification in the SWI remains poorly understood.

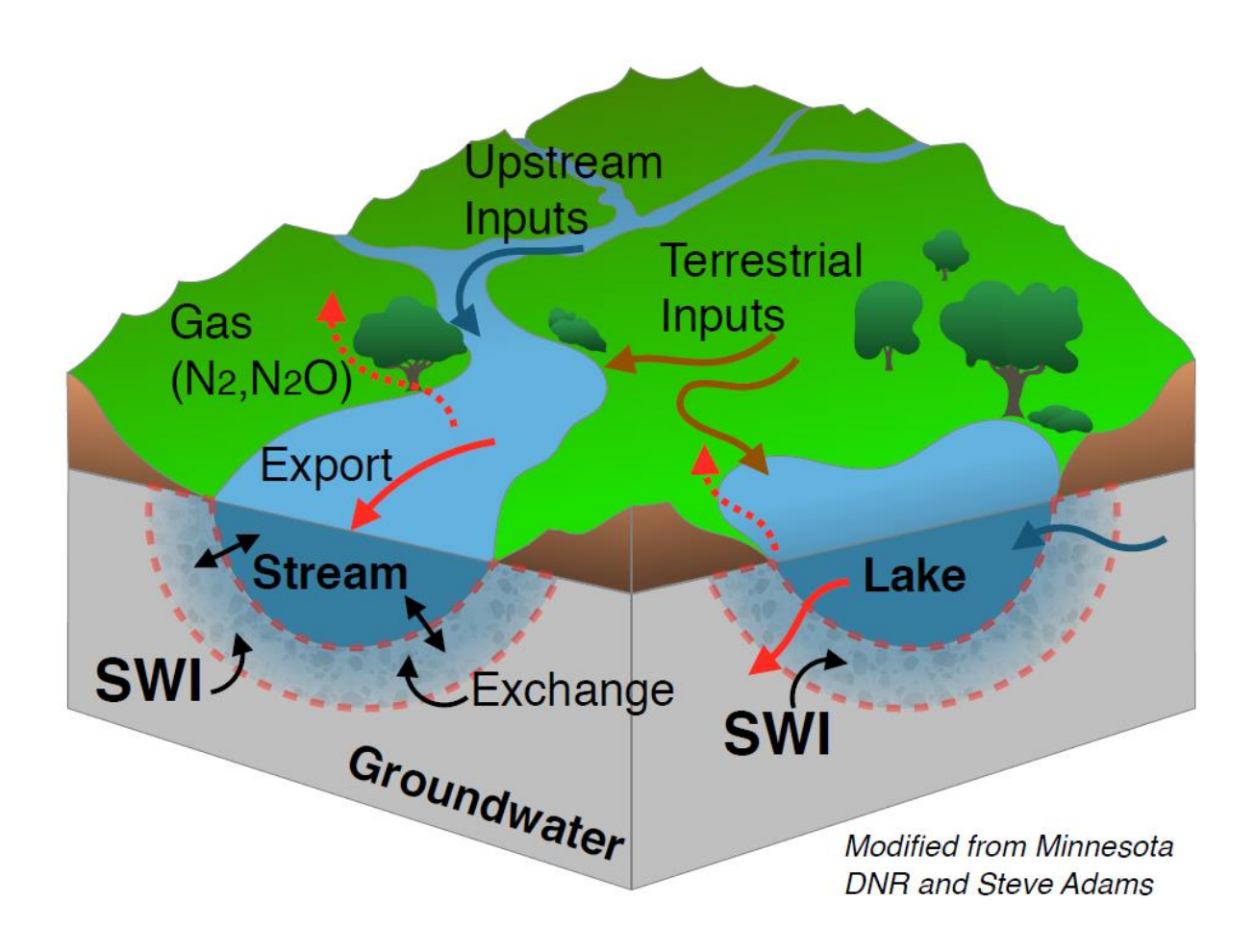


Figure 1: Diagram of the sediment-water interface (SWI). In streams and lakes, groundwater and surface water exchange and interact with landscape fluxes of nitrogen (Minnesota Department of Natural Resources, Division of Ecological Services, 2003).

Many NO₃ removal pathways in the SWI, including denitrification, are controlled by multiple concurrent factors, including the availability and lability of electron donors such as DOC (Baker et al., 1999; Zarnetske et al., 2011b); NO₃-concentrations (Mulholland et al., 2008); SWI flowpath length (Quick et al., 2016); microbial community composition and abundance (Storey et al., 1999; Farrell et al., 2013; Stoliker et al., 2016); and physical residence times that in turn are a product of stream-bed morphology and composition and hydrologic conditions (Cardenas, 2008). Though not often discussed in SWI studies, these controls are interrelated, since hydrodynamics result in a distribution of flowpath lengths and residence times (Briggs et al., 2014b; Marzadri et al., 2014) governing the transport of reactants to resident microbes and of reaction products downstream or down-gradient. Some previous studies have suggested as much interrelatedness, and hypothesize that hydrologic conditions would be among the most dominant controls on SWI function (Ocampo et al., 2006; Gu et al., 2007; Stoliker et al., 2016). However, relatively few studies have performed controlled manipulative experiments exploring SWI function in a field setting to assess the relative influence of biogeochemical versus hydrological controls.

This thesis explores the magnitude of major controls on SWI NO₃⁻ cycling by systematically regulating both hydrologic and biogeochemical conditions in real SWIs. The experiments are centered around a series of controlled variable-head hydrologic manipulation experiments, examining the removal of NO₃⁻ from infiltrating surface-water along an isolated SWI flowpath. The first set of experiments (described in Chapter 2) were conducted in Snake Pond, MA (Figure 3) during the summer of 2016. This site was chosen to provide a hydrologically stable environment to test these new methods, while also leveraging an environment of interest to other N_R studies in the region (Barbaro *et al.*, 2013; Smith *et al.*,

2015). This study also directly addressed hypotheses proposed by Stoliker *et al.* (2016) on the role of hydrologic variation in controlling N export from lakes. The Snake Pond study sought to address the following main research questions: 1) how do changing concentrations of DOC and NO₃⁻ influence NO₃⁻ removal in the SWI; and 2) how does hydrologic variability (as invoked by manipulating pressure head) change residence times along a SWI flowpath and the removal of O₂, DOC, and NO₃⁻? The second set of experiments described in Chapter 3 was conducted in Sawmill Brook, a tributary of the Ipswich River, MA (Figure 14). Following the Snake Pond experiments, the study design focused on examining the scaling nature of SWI processing of NO₃⁻ with varying hydrologic residence times, reexamining question 2 described above. While the transition to a fluvial environment posed additional logistical challenges, this study had high relevance to studies comparing N_R removal and denitrification at the same site to streams across the conterminous United States (Wollheim *et al.*, 2005; Mulholland *et al.*, 2008; Beaulieu *et al.*, 2011).

In these two studies, I find that NO₃⁻ concentration and labile DOC abundance both stimulate increased NO₃⁻ removal and denitrification (Mulholland *et al.*, 2008; Zarnetske *et al.*, 2011b), but that hydrologic residence time primarily controls the NO₃⁻ removal rate (Stoliker *et al.*, 2016) more than the abundance of NO₃⁻ or labile DOC. The experiments also specifically examine how these hypothesized controls influence the abundance of two respective end products of denitrification – N₂O and N₂ gases. The nitrogen gas end-products of denitrification are of particular interest because N₂O is a potent greenhouse gas (Forster *et al.*, 2007) and also a strong contributor to recent depletion of stratospheric ozone (Ravishankara *et al.*, 2009), while N₂ is relatively inert. Increased emissions of N₂O from freshwater environments as a result of anthropogenic NO₃⁻ loading contribute significantly to global anthropogenic emissions

(Galloway *et al.*, 2004; Beaulieu *et al.*, 2011). In addition to evaluating controls on NO₃⁻ removal, this research examines how the proposed controls affect the conversion of NO₃⁻ to N₂O versus N₂, ultimately affecting the relative amounts of these gases being released from the SWI. These findings will inform future conceptual- and process-based modeling efforts to study NO₃⁻ cycling in streams and lakes.

Additionally, while not directly part of the scope of the proposed experiments, this research also addresses the likely prominence of less-mobile porosity (e.g., diffusion dominated mass-transfer) in the oxygenated zone of the study SWI sediments (Briggs *et al.*, 2015). This less-mobile porosity may be an important location for SWI denitrification (Briggs *et al.*, 2015). Finally, data from these experiments will be beneficial to future numerical flow and transport models, by enhancing understanding of NO₃⁻ removal in the SWI and generating parameterization and validation data sets.

CHAPTER 2: EXPERIMENTAL MODIFICATIONS OF REACTANT AND HYDROLOGIC CONTROLS ON NITROGEN PROCESSING: RESULTS FROM FLOW-THROUGH LAKEBED SWI SEDIMENTS

2.1. Introduction

Excess reactive nitrogen (N_R) in surface waters is considered one of the top global threats to aquatic ecosystems (Vitousek et al., 1997; Steffen et al., 2015), and freshwater ecosystems perform a critical ecosystem service by removing about 25% of anthropogenic N before it is transported to the oceans (Howarth et al., 1996; Boyer et al., 2006; Seitzinger et al., 2006). Many processes governing N concentrations in freshwater systems take place within sedimentwater interfaces (SWIs) (Boulton et al., 1998; Boano et al., 2014). Though the role of SWIs in N processing are often studied in the context of fluvial systems (Zarnetske et al., 2011a, 2012; Harvey et al., 2013), surface-groundwater exchanges in lakes also create the potential for N processing (Chen et al., 1972; Cherkauer et al., 1992; Rysgaard et al., 1993; van Luijn et al., 1996; Kidmose et al., 2015; Lewandowski et al., 2015; Smith et al., 2015), particularly in groundwater flow through lakes with strong advective exchange (Rosenberry et al., 2015). SWIs are disproportionately important to N cycling in freshwater systems due to long exposure timescales, mixing of organic and inorganic solutes, and high microbially active sediment surface area (McClain et al., 2003; Zarnetske et al., 2012; Abbott et al., 2016). The main process for "permanent" N removal is denitrification, the microbially mediated anaerobic reduction of dissolved inorganic N as nitrate (NO₃⁻) to di-nitrogen (N₂) and nitrous oxide (N₂O) gases (Tiedje et al., 1983). While N₂ is inert, N₂O – a product of incomplete denitrification – is a potent greenhouse gas (Beaulieu et al., 2011) that has also been implicated in the depletion of stratospheric ozone (Forster et al., 2007; Ravishankara et al., 2009). Both biogeochemical and

physical conditions may dictate how much and what form of N is ultimately exported from freshwater systems (Zarnetske *et al.*, 2012).

The biogeochemical functioning of the SWI with respect to N is dictated by a hierarchy of conditions: 1) transport or exchange of surface waters across the SWI, 2) sufficient N and associated electron acceptors in the SWI waters, and 3) the presence of a microbial community within the SWI capable of removing N_R. N-modifying communities are consistently shown to be ubiquitous in SWI sediments (Sobczak et al., 1998; Findlay and Sinsabaugh, 2003; Stoliker et al., 2016), suggesting that their presence is not a limiting factor and that the resident community will readily process N in the order of the most energetically favorable reactions (Storey et al., 1999; Burgin and Hamilton, 2007; Burgin et al., 2011). Biogeochemical controls on N processing are important, as NO₃⁻ concentrations influence both NO₃⁻ removal and N₂ and N₂O production (Mulholland et al., 2008; Beaulieu et al., 2011; Quick et al., 2016). Both the quantity and quality (lability) of dissolved organic carbon (DOC) are potential limiting reactants for denitrification (Sobczak et al., 2003; Zarnetske et al., 2011b). Key to the understanding of overall SWI function in N processing is that parcels of water entering the SWI experience a distribution of residence times and flowpaths (Marzadri et al., 2014; Briggs et al., 2015), and longer residence times result in longer contact times between reactants and microbial communities (Findlay, 1995; Zarnetske et al., 2012). Longer SWI residence times and higher oxygen (O₂) removal rates enhance rates of NO₃ removal (Thomas et al., 2001; Zarnetske et al., 2012). Physics ultimately regulates the delivery of solutes to SWI microbial communities as well as solute residence/exposure timescales. This physical transport limitation would occur when short residence times constrain the exposure of solutes to microbes even if there is abundant NO₃ and labile DOC in the water.

The interaction between lakes and groundwater affect water chemistry and N cycling in the water column. This is important to water managers trying to alleviate excess N pollution. Many studies have focused on groundwater flow-through lakes (Born *et al.*, 1974, 1979; Anderson and Munter, 1981; Winter *et al.*, 1998; Winter, 1999); a specific classification of lake common in glacio-fluvial terrains where the lake intersects an aquifer with discharge and recharge zones located along the up-gradient and down-gradient sides of the lake shore, respectively (Figure 2). These lakes are significant in the regional groundwater budget in highly populated and economically valuable regions such as Cape Cod, MA, USA, where approximately 25% of the total groundwater flux passes through lakes (Walter and Whealan, 2004; Walter and Masterson, 2011), and the U. S. Environmental Protection Agency estimates billions of \$USD will be spent in the coming years to mitigate N_R pollution in lakes, rivers, and coastal bays (US EPA, 2016).

For these groundwater flow-through lakes in particular, a previous study showed that the potential for N transformations at the SWI was not limited by microbial community or functional group presence – all groups were found to be ubiquitous – and instead other environmental variables such as availability of DOC and water residence time may control N removal at the SWI (Stoliker *et al.*, 2016). For example, it is expected that changes in lake stage and the adjacent groundwater table create a dynamic hydraulic gradient across lakebed sediments, resulting in variable flowpath orientation and porewater velocities and residence times (Winter, 1999), which in turn affect the N-processing function of the SWI.

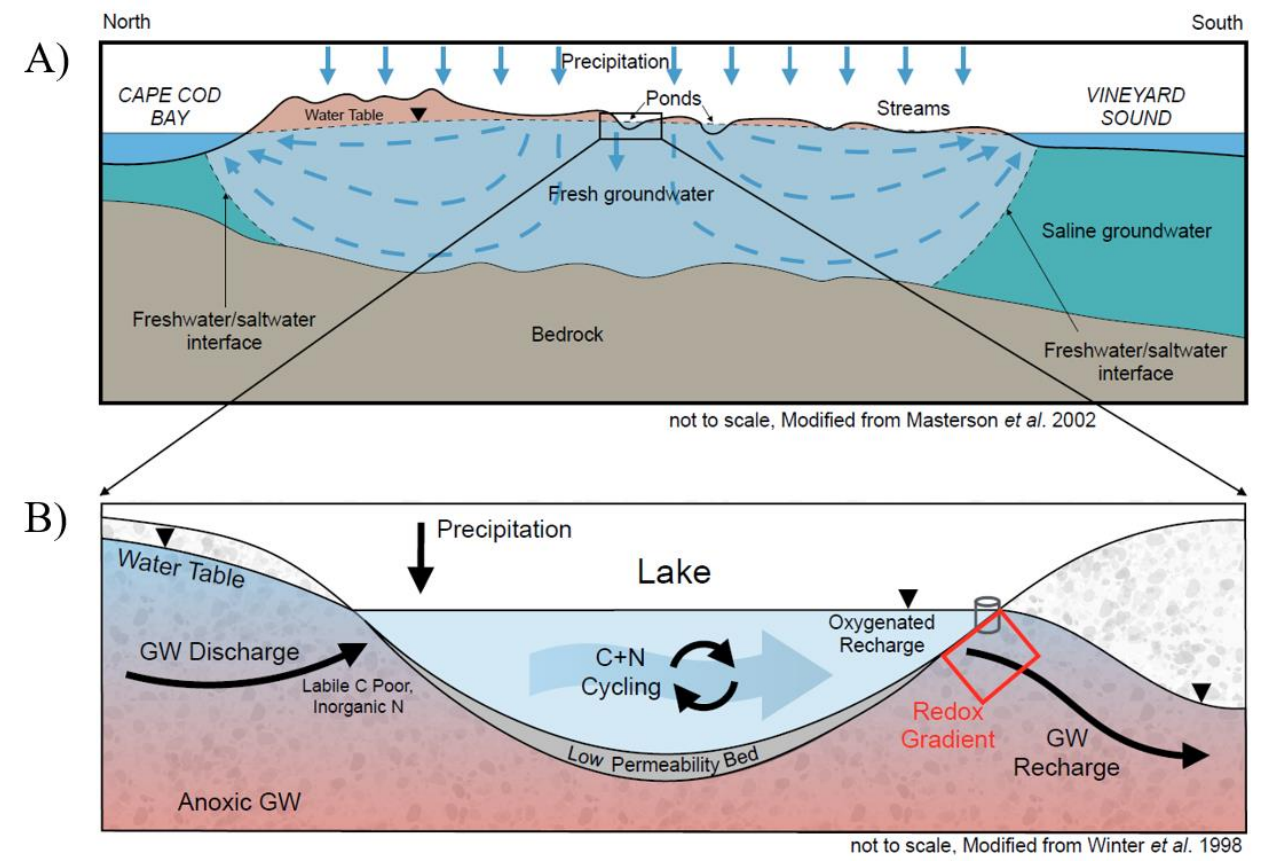


Figure 2: Schematic of the Cape Cod groundwater system. This diagram gives regional hydrologic context (A) to individual groundwater flow-through lakes like Snake Pond, as shown in (B). Groundwater entering the lake is generally poor in labile carbon and high in inorganic N as NO₃⁻ from anthropogenic groundwater pollution. We sampled the groundwater recharge, or outflow side of the lake, where oxidation of organic matter depletes the recharging water of oxygen, depicted by the red box.

The objective of this research was to characterize how changing reactant and hydrologic conditions concomitantly influence the fate of NO₃⁻ passing through the SWI of flow-through lakebed sediments. Using a novel field method of induced vertical recharge through lakebed sediments, we specifically explored how NO₃⁻ and labile DOC availability influenced microbial respiration rates (e.g. oxygen removal rates) and how changing the system residence time by reducing the hydraulic gradient would affect these rates. We hypothesized that labile carbon supply would limit denitrification, and that reducing the hydraulic gradient would increase removal of N and C. We also directly addressed previous hypotheses about how seasonal

changes in N and C availability and hydraulic gradient through sediments affect biogeochemistry and N pollution (Stoliker *et al.*, 2016).

2.2. Materials and Methods

2.2.1. Site Description

Snake Pond is a 33-hectare kettle lake on the Cape Cod Peninsula in Sandwich,

Massachusetts, USA (Figure 3). This peninsula consists of several intersecting glacial moraines with outwash plain deposits extending to the south (Mather *et al.*, 1942). The aquifer is composed of permeable sands and gravels (Masterson *et al.*, 1996), and like many of the lakes on Cape Cod, Snake Pond is a groundwater flow-through lake with no surface-water inlets or outlets (Winter *et al.*, 1998). The lake is adjacent to the Joint Base Cape Cod, which has contaminated regional groundwater with N_R (LeBlanc *et al.*, 1991; Smith *et al.*, 1991; Repert *et al.*, 2006; Barbaro *et al.*, 2013). Snake Pond is attractive for studies involving solute manipulation: being near the regional groundwater high point (Massachusetts Division of Fisheries and Wildlife, 1993), natural total dissolved solutes are relatively low and stable (Ahrens and Siver, 2000). Therefore, in addition to residence time, potential limitations on net N removal imposed by dissolved N and C availability could readily be tested. The study was conducted in July 2016, with the study site located at the southern, naturally recharging, side of the lake (Figure 4) in a gravel-cobble substrate (Figure 9), about 3 m from the shoreline in shallow water.

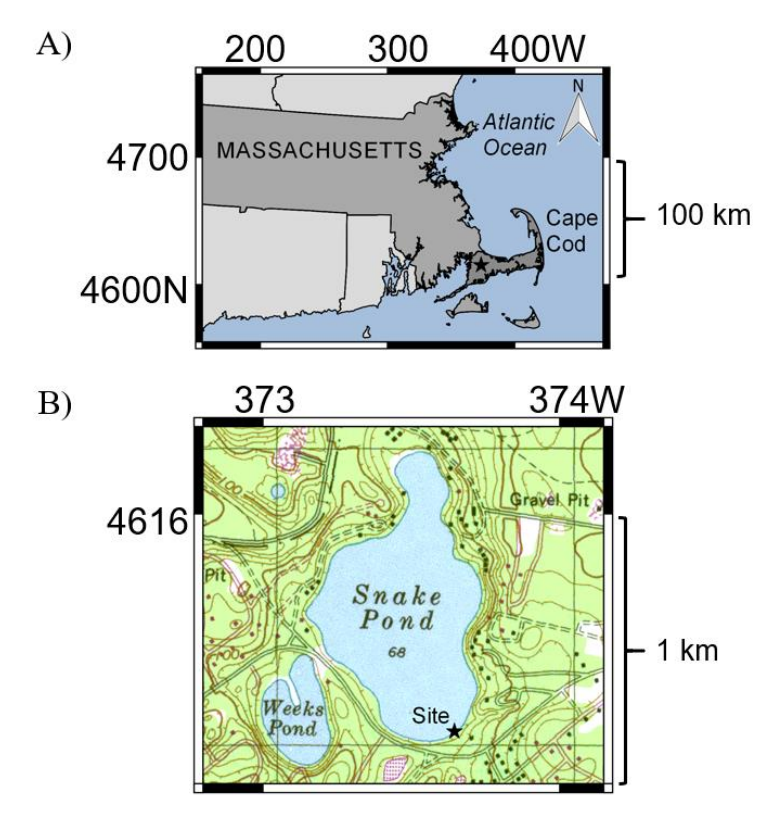


Figure 3: Map of Massachusetts and Snake Pond. (A). Cape Cod is a 100-km-long peninsula that extends into the Atlantic Ocean. (B) Snake Pond, with sampling site shown on the south shore. Map units are in km. Map Projection is UTM, Zone 19T.



Figure 4: Site picture from Snake Pond. View is looking northeast, with the injection ring installed in the pond sediments offshore in the center frame.

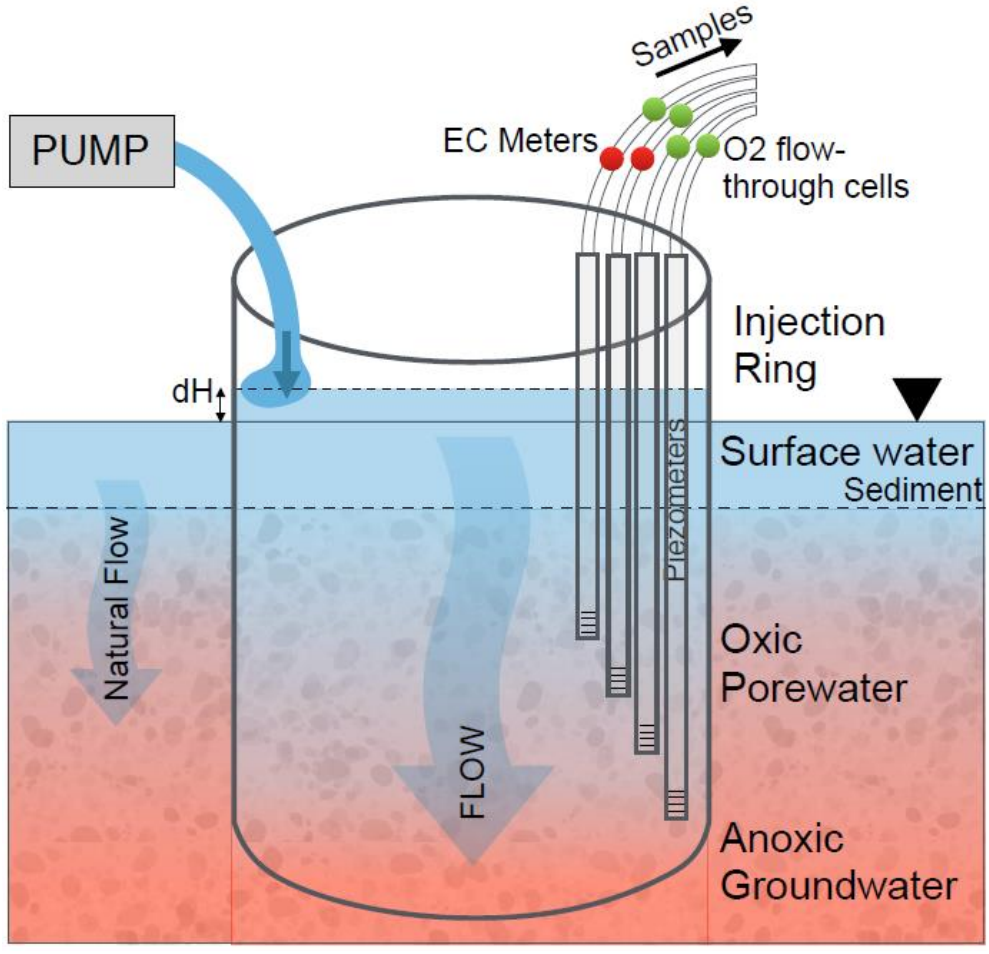


Figure 5: Schematic of injection ring. A 55-cm diameter plastic drum with open ends is inserted into the lakebed sediments to 22 cm-depth. Downward 'recharge' flow is induced by experimentally elevating the hydraulic head in the injection ring (shown in the schematic as dH). Four steel piezometers (USGS MINIPOINT design) are inserted into the sediments and water is pumped from them at ~2.5 mL/min, so as not to disrupt the hydraulic flow field. In-line from the piezometers are dissolved O₂ and electrical conductivity flow-through sensors.

2.2.2. Experimental Setup

The studied lake sediments were isolated from the surrounding environment using a 55-cm-diameter polyvinyl-chloride (PVC) barrel, which was installed in the lakebed and driven to a depth of 22 cm, also serving to ensure vertical flow (Figure 5). Water from the lake was pumped into a 1.89 m³ holding tank located on the shore, where it was mixed with sodium chloride (NaCl) salt to bring the total conductivity of the water from \sim 60 to 550 μ S/cm.

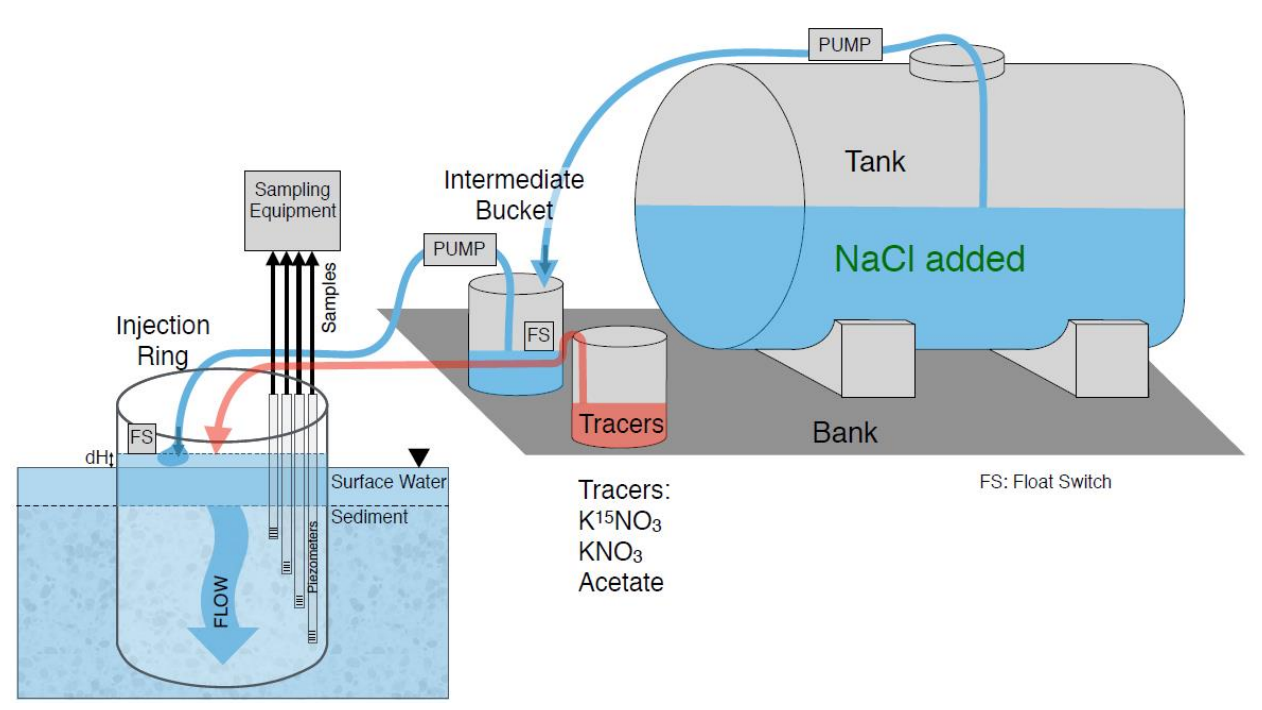


Figure 6: Schematic of Tracer Additions at Snake Pond. Before the experiments, water from the lake was pumped into a 1.89 m³ holding tank. Using a series of pumps and float switches (FS) to maintain steady water levels, water was pumped into an intermediate bucket and then into the injection ring. Tracers were added using a peristaltic pump at a rate of ~3 mL/min.

Using an intermediate bucket and a series of float switches (Figure 6) to maintain a constant water level within the PVC injection ring, water was pumped from the holding tank to the intermediate bucket and into the ring to enhance and control the natural recharge rate (Table 1) by precisely manipulating the vertical hydraulic gradient (Scruggs *et al.*, 2016). The flux rates were chosen so that these experiments could be directly compared to previous SWI-related studies in Ashumet Pond (Bussey and Walter, 1996; Walter and LeBlanc, 1997; McCobb *et al.*, 2003; Rosenberry *et al.*, 2013; Santelli *et al.*, 2014; Smith *et al.*, 2015; Stoliker *et al.*, 2016), which is about 4.8 km to the south and has similar hydrologic and geologic characteristics, and where downwelling seepage rates have been reported to be as high as 1.7 m/d (Harvey *et al.*, 2015). A combination of measured water flux rates and specific conductivity (SpC) breakthrough curves (Figure 7) was used to determine vertical flowpath residence times in the various

experiments. A second series of breakthrough curves was obtained as the high conductivity water was pushed out by new fresh lake water added at the beginning of Experiment 4 (see next section). This was done to match the injection breakthrough curve at approximately the same flux, before flux was reduced by lowering the hydraulic head in the ring, which was performed for Experiment 5.

Ambient porewater samples were collected about 5 m away from the injection rings at a similar distance from the shore. Also adjacent to the injection rings, iButton thermal data loggers (model DS1922L, Maxim Integrated, CA, USA) were installed at a depth spacing of 0.03 m up to 0.11 m. Ambient vertical downwelling flux was calculated using a diurnal signal amplitude attenuation-based model run by VFLUX2, as in Briggs *et al.* (McCallum *et al.*, 2012; Briggs *et al.*, 2014a; Irvine *et al.*, 2015).

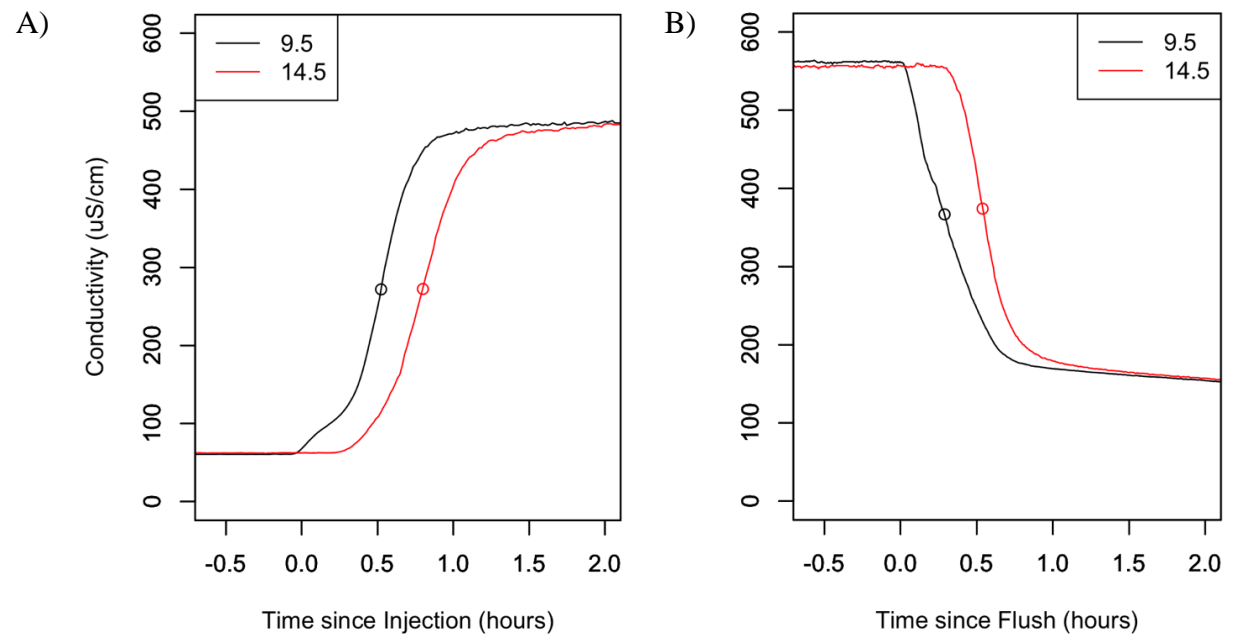


Figure 7: Breakthrough curves for extracting residence time. Specific conductivity was measured at 9.5 and 14.5 cm depth within the injection ring sediments. Panel (A) is for the onset of the experiments, and panel (B) is for the transition from high flux rate to low flux rate, corresponding with a replacement of the injection ring water (Cl⁻ labeled) with fresh lake water, Points along breakthrough curves are for the median time of arrival for the conductivity plume for each depth, in cm. For the injection: 0.53 h at 9.5 cm and 0.79 h at 14.5 cm. For the flush: 0.29 h at 9.5 cm and 0.53 h at 14.5 cm.

2.2.3. N, C, and Residence Time Manipulations

Five different experiments were conducted, with sequential reactant additions followed by an increase in residence time. Sampling of porewater was conducted roughly 24 hours after the beginning of each experiment to allow solute concentrations to reach steady-state.

Conservative tracer and dissolved oxygen (O₂) profiles at depth were examined to ensure steady-state flow conditions and that dissolved O₂ concentrations had stabilized at the time of sampling. Reactants and tracers were drawn from 20 L tanks at about 3 mL/min using a peristaltic pump and added to the recharging lake water within the injection ring (Figure 6). Each reactant addition involved adding the new reactant or tracer to the injection ring following previous additions. A summary of modifications and expected results are as follows (see also Figure 8 and Table 1):

- Ambient Profile: The goal was to assess N, O₂, and C processing in the native lakebed sediments under the background downwelling rates (~0.12 m/d).
- Experiment 1: The goal was to assess N processes and biogeochemical conditions under increased downwelling rates (1.2 m/d) relative to the Ambient Profile, introducing a $^{15}\text{NO}_3$ tracer to track ^{15}N denitrification products.
- Experiment 2: The goal was to assess available NO₃⁻ limitation on N processing. We added a NO₃⁻ amendment, where the original addition of ¹⁵N in the first modification was calculated to achieve about 5 atomic percent (atom %) ¹⁵NO₃⁻ in this experiment.
- Experiment 3: The goal was to assess available labile DOC limitation on N processing when NO_3^- is abundant. We added labile DOC (as acetate), at the same time as the ^{15}N and NO_3^- amendments.

Experiment 4: The goal was to assess N processing when NO₃⁻ and DOC are abundant, under anoxic conditions. This also concluded the salt injection (see previous section). The injection ring water was replaced with new lake water and the NaCl addition ceased. New lake water was pumped into the intermediate bucket and injection ring. To achieve the same concentrations in the recharging water as the previous experiment, a slug of solutes was mixed with the fresh lake water, and all three amendments (¹⁵N, NO₃⁻, C) were pumped into the injection ring throughout the experiment just as in Experiment 3. The acetate addition rate was increased to eliminate DOC limitation and stimulate O₂ depletion at depth.

Experiment 5: The goal was to assess the effect of increased residence time when NO₃ and DOC are abundant. The hydraulic head was reduced to just above average lake level, to achieve a downward flux of approximately 0.92 m/d.

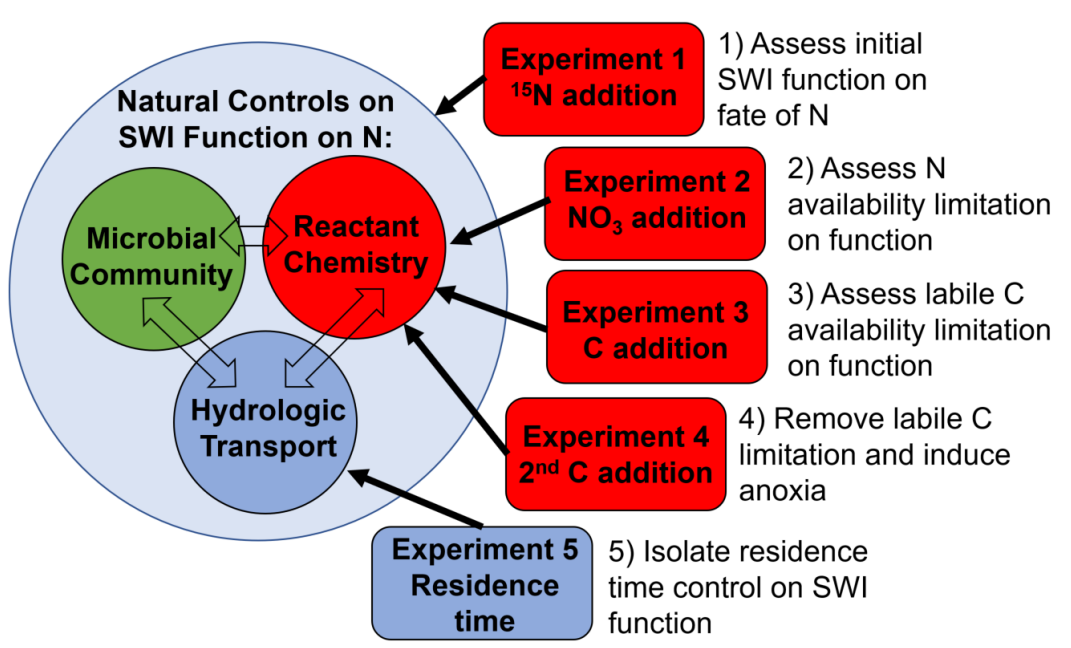


Figure 8: Conceptual Diagram of Snake Pond Experimental Modifications. The three natural controls on SWI N processing are microbial community composition, porewater reactant chemistry, and hydrologic transport. By confirming with a ¹⁵NO₃- tracer that a microbial community capable of N transformations was present, Experiments 2-4 interrogated how

changing reactant chemistry changes N removal, and Experiment 5 tested the hypothesis that hydrologic residence time is a key control.

Table 1: Details of the Snake Pond experiments. Details are provided on the addition of reactants and changing flux rates. Concentrations of the reactant tanks are reported, as well as the measured pump rate from the tank into the surface water of the injection ring. The addition rate is the concentration in the addition tank multiplied by the pump rate. The hydraulic flux through the ring is also reported for each experiment, either directly measured or interpolated.

Experiment	Abbrev	Details	Pump Rate	Addition Rate	Hydraulic Flux
	iation		(mL/min)	(µmol/h)	Rate (m/d)
Ambient	Amb	Outside injection	NA	NA	0.12
Conditions		ring			
Experiment 1:	15N	51.3 mg/L K ¹⁵ NO ₃	2.90	87 ¹⁵ NO ₃ -	1.2
¹⁵ N Addition		(99% purity)			
Experiment 2:	NO ₃	1,474 mg/L KNO ₃	2.90	87 ¹⁵ NO ₃ -	1.267
NO ₃ - Addition			2.95	2600 NO ₃ -	(interpolated)
Experiment 3:	N+C	615 mg/L NaAcO	2.90	87 ¹⁵ NO ₃ -	1.356
Acetate Addition			2.95	2600 NO ₃	(interpolated)
			3.08	2800 C	
Experiment 4:	N++C	1714 mg/L NaAcO	2.90	87 ¹⁵ NO ₃ -	1.45
2 nd Acetate			2.95	2600 NO ₃ -	
Addition			3.08	7800 C	
Experiment 5:	N++C,	All added	2.90	87 ¹⁵ NO ₃ -	0.92
Increased	R_{T}		2.95	2600 NO ₃	
Residence Time			3.08	7800 C	

2.2.4. Porewater Sampling and Laboratory Methods

Sampling at depth was achieved using four stainless steel MINIPOINT samplers, similar to the USGS MINIPOINT system (Harvey *et al.*, 2013), installed in the lakebed sediments within the ring. These had an outer diameter (OD) of 3.2 mm, a screened interval 10 mm long, with 3 individual slits ~0.5 mm in width. Samplers were driven to depths of 9.5, 14.5, 19.5, and 24.5 cm below the lakebed. 3.2-mm OD tubing was attached to the end of each MINIPOINT and the two shallowest lines were fed through two electrical conductivity (EC) micro flow-through cells (Amber Science, OR, USA). EC was converted to SpC at 25°C automatically by the micro flow-cell control units using sensor-specific calibrations performed at the beginning of the experiment. Flow-through cells equipped with fiber-optic O₂ microsensors attached to a FireStingO2 Optical

Oxygen Meter (Pyro Science, Germany) were in-line with the tubing from the MINIPOINTs. Ambient porewater data were also collected outside the injection ring approximately 5 m away at the same distance from shore. For these ambient data, MINIPOINT samplers were driven to depths of 1.5, 7, 12, and 18 cm below the lakebed. During Experiments 1-2, concentrations of the reactants were not measured in the downwelling surface water, however, mass balance calculations based on the reactant addition rates and downwelling water flux indicates that changes between surface and 9.5 cm depth for all solutes in these two experiments were negligible.

From the onset of each experimental modification and reactant addition, about 24 hours passed before sampling took place. Triplicate water samples were obtained in a closed system using peristaltic pumps (Cole-Parmer, IL, USA) and syringes, followed by immediate filtration through a 0.7-µm glass-fiber filter and 0.2-µm cellulose-acetate filter into acid-washed amber high-density polyethylene (HDPE) bottles (Nalgene, NY, USA). Water samples were chilled on site and frozen the evening following collection. For dissolved gas samples, 1.6 mm OD tubing directly from the pump was placed into the bottom of a 12-mL glass Exetainer (Labco, United Kingdom) and filled for two full volumes. Samples were preserved with 120 µL of 50% w/v zinc chloride solution. Preserving a convex meniscus, the tubing was removed, and the cap was screwed on to prevent any air bubbles in the sample. Gas samples were stored at room temperature in the dark and later shipped to the Stable Isotope Facility (SIF) at the University of California, Davis, for isotope (15N) analysis of dissolved gases (N₂ and N₂O). Water samples were later separated into groups for ¹⁵N analysis of NO₃-, which were shipped frozen to the SIF, and for anion, carbon, and nutrient analysis, which were kept chilled at 4°C during shipment and prior to analysis at Michigan State University.

At the SIF, the sealed 12-mL glass Exetainers had 4 mL of sample water replaced with a helium headspace, which was then allowed to equilibrate with the remaining 8 mL of sample. Stable isotope ratios of nitrogen (15N) in N2 and N2O from the equilibrated headspace gas were measured using a ThermoScientific GasBench + Precon gas concentration system interfaced to a ThermoScientific Delta V Plus isotope-ratio mass spectrometer (Bremen, Germany). Nitrate in water samples was converted to N2O by the bacterial denitrification assay and 15N ratios were measured as stated above for N2. At Michigan State University, anions were measured with a Dionex ICS-2100 Ion Chromatography System (ThermoScientific, MA, USA), including chloride (Cl⁻), nitrite (NO2⁻), nitrate (NO3⁻), and sulfate (SO4²⁻). Non-purgeable Organic Carbon (NPOC) and Total Dissolved Nitrogen were measured using a TOC-L total organic carbon analyzer (Shimadzu, Japan) using catalytic oxidation at 720°C followed by gas chromatographic measurement of CO2 and chemiluminescence measurement of NO. Samples were also shipped to the USGS in Reston VA for analysis of NH3 using a Seal AQ2 Discrete Analyzer (Seal Analytical, WI, USA) using method EPA-103-A Rev 10.

2.2.5. Calculations

After inserting the injection ring into the lakebed, the recharge flux was increased from the ambient downwelling flux of 0.12 m/d to 1.2 m/d. Flux rate increased to 1.5 m/d over the course of the experiments (Table 1), due to dropping lake stage and changes in the hydraulic gradient between the elevated head in the ring and the lake stage. Median arrival times of the Cl-labeled lake water at 9.5 and 14.5 cm-depths were estimated from SpC breakthrough curves and median porewater velocities were calculated by subtracting the median time of arrival at 9.5 cm from the time at 14.5 cm and dividing by the known separation distance of 5 cm. Velocities for Experiments 2 and 3 were interpolated, assuming a linear increase in velocity and flux over time.

Porosity was calculated by dividing the flux by the porewater velocity, resulting in an effective porosity of 30%. Porewater velocities for Experiment 5, with increased residence times, were calculated by assuming the same porosity and dividing the flux of 0.92 m/d by the porosity. Residence times at each depth for each experiment were then calculated by dividing the depth by the calculated porewater velocity for that experiment.

Removal rates were calculated as the linear regression of concentration over time as in Lansdown *et al.* (2015):

$$R_u = \frac{c_2 - c_1}{\tau_2 - \tau_1} \tag{1}$$

 R_u is the removal rate in μ mol/L/h, C is concentration in μ mol/L and τ is the residence time in hours (h) at a given depth. Concentrations were retrieved directly from the analytical instruments described in Section 0.

For calculations of denitrification rates (N_2 and N_2O production), rates were based on a linear isotopic mixing model (Ostrom *et al.*, 2002; Harvey *et al.*, 2013). The SIF provided data for concentrations and ^{15}N enrichment (as $\delta^{15}N$ relative to air) of N_2 and N_2O gases from the equilibrated helium headspace of the 12-mL Exetainers. The concentration of gas in the original liquid sample was calculated as the total mass in the system divided by the liquid volume:

$$C = \frac{m_H + m_L}{V_L} \tag{2}$$

Where C is the original dissolved gas concentration in the liquid sample, V_L is the vessel liquid volume of 8 mL, m_H is the reported mass of N_2 or N_2O in the final equilibrated vessel headspace, and m_L is the mass remaining in the liquid, which can be calculated based on the headspace mass:

$$m_L = C_L * V_L = \left(P * B_H * \frac{m_H}{V_H}\right) * V_L$$
 (3)

Where C_L is the equilibrated vessel liquid concentration, P is the atmospheric pressure with units of atmospheres, V_H is the vessel headspace volume of 4 mL, and B_H is the Bunsen solubility coefficient for headspace equilibration within the vessel (units of atm⁻¹). The Bunsen solubility coefficient for N_2 and N_2O are calculated as a function of equilibrium temperature (T_{eq}) in units of Kelvin (Weiss, 1970; Weiss and Price, 1980; Table 2):

$$B_H = a^{(b) + (c * \frac{100}{Teq}) + (d * \ln(\frac{Teq}{100})) + (e * (\frac{Teq}{100})^2)} * f$$
 (4)

Table 2: Parameter values for calculation of Bunsen solubility coefficients for N₂ and N₂O gasses in water. Values from Weiss (1970) and Weiss and Price (1980).

Parameter	а	b	С	d	е	f
Value in	2.7182818	-59.6274	85.7661	24.3696	0	1
B_{H-N_2}						
Value in	2.7182818	-165.8806	222.8743	92.0792	-1.48425	0.0821
B_{H-N_2O}						* 273.15

Isotopic enrichment of N_2 and N_2O gases was reported by SIF as $\delta^{15}N$ relative to air. To conduct a ^{15}N mass balance, the isotopic mole fraction (X_{15_N}) was calculated to determine the proportion of reported N_2 and N_2O mass that originated from the added $^{15}NO_3^-$ tracer. First $\delta^{15}N$ was converted to the ratio (R) of $^{15}N/^{14}N$, by standardizing against the natural abundance ratio of ^{15}N in the environment ($R_S = 0.0036764$) (Ostrom *et al.*, 2016), then the ratio was transformed into a fraction:

$$R = \left(\frac{\delta 15N}{1000} + 1\right) * R_S \tag{5}$$

$$X_{15_N} = \frac{R}{1+R} \tag{6}$$

In the isotopic mixing model, the N composition of porewater sampled at depth i is a mixture of the porewater advected from depth i-1 and the mass and composition of products of denitrification (C_dX_d) between these depths:

$$C_{(i-1)}X_{(i-1)} = C_iX_i + C_dX_d (7)$$

where C is concentration and X is the isotopic mole fraction of 15 N. The mass of the product can be solved for by assuming that the isotopic enrichment of the denitrification product (X_d) is equivalent to the enrichment of the 15 N labeled NO₃- source at depth i-1:

$$C_d = \frac{(C_{(i-1)}X_{(i-1)} - C_iX_i)}{X_d}.$$
 (8)

The denitrification rate can be calculated as in the previous section by dividing the mass of the product by the difference in residence times between the two depths i-1 and i:

$$R_d = \frac{c_d}{\tau_i - \tau_{(i-1)}} \,. \tag{9}$$

For the ambient profile, rates are calculated between 0 and 18 cm depth. For gases (O₂, N₂, and N₂O), rates are between 9.5 and 19.5 cm depths. For NO₃⁻ and DOC, rates are calculated between 9.5 and 19.5 cm for Experiments 1-2, and between 0 and 19.5 cm for Experiments 3-5.

2.2.6. Sediment Characterization

An 11-cm deep core was collected proximal to but outside of the injection ring during the sampling (7/9/2016), and later 8 shallow (~3 cm deep) cores were collected from the surface sediments surrounding the site (on 7/26/2016). Methods of coring and analysis followed Harvey *et al.* (2013) with only a few exceptions. Cores were collected by pushing a clear polycarbonate cylinder (nominally 4.8 cm internal diameter and 1.6 mm wall) that had been sharpened at one end into the lakebed. Cores were capped with butyl rubber stoppers and removed from the lakebed. After removal the cores were immediately extruded, sectioned into 1 or 1.5-cm increments, bagged, placed on ice, and returned to the laboratory. Cores were wet sieved to remove fines from sand and gravel and dried at 60 degrees C to constant weight. Porosity was determined using dry weight and bulk volume of each core increment assuming a grain density of 2.65 g/cm³. The grain size distribution was determined by dry sieving samples through 17000, 4000, 1000, 500, 250, 125, and 63 µm diameter sieves on a Gilson Model SS-3 shaker and

weighing each size fraction. The secondary axis of pebbles larger than 17000 μm were measured individually. Characteristic grain sizes of gravel, sand, and fines were determined with reference to a 4000 μm maximum as indicators of the median grain size (D₅₀) and the diameter of the tenth percentile weight fraction (D₁₀). These grain size metrics characterize the finer sediment that fills in between the pebbles, increasing granular surface area and decreasing the hydraulic conductivity of the bulk streambed sediment. The 11-cm deep core was analyzed for particulate organic carbon (POC) in sediments less than 4000 μm by combusting samples at 550 degrees C in a muffle furnace for 24 hours to determine weight fraction after loss on ignition (LOI). The core was divided into 1-2 cm intervals and sieved to particle sizes less than and greater than 500 μm. Mass loss was calculated by multiplying the % LOI by the sediment density to obtain mass loss in grams of organic matter per cm³.

2.3. Results and Discussion

2.3.1. Sediment Characterization

Sediments at the sampling site were medium and coarse sands with small contributions of fines below 0.5 mm in diameter (Figure 9). Gravel and pebbles also made up a small portion of the sediments. Sediments had a polydisperse nature, with moderate to poor grading. There was generally high variability in sediment characteristics observed within the 8 shallow cores collected in July. Slight coarsening was observed with depth within the cores (Figure 10). POC was on average 0.43 weight % of the total sediment, with a larger proportion (0.58 wt. %) as LOI on particles <500 μ m (Figure 11). Particles >500 μ m were 0.35 wt. % of the sediment but showed a larger percent decrease from 0 to 11 cm (-34%) than total POC (-15%).

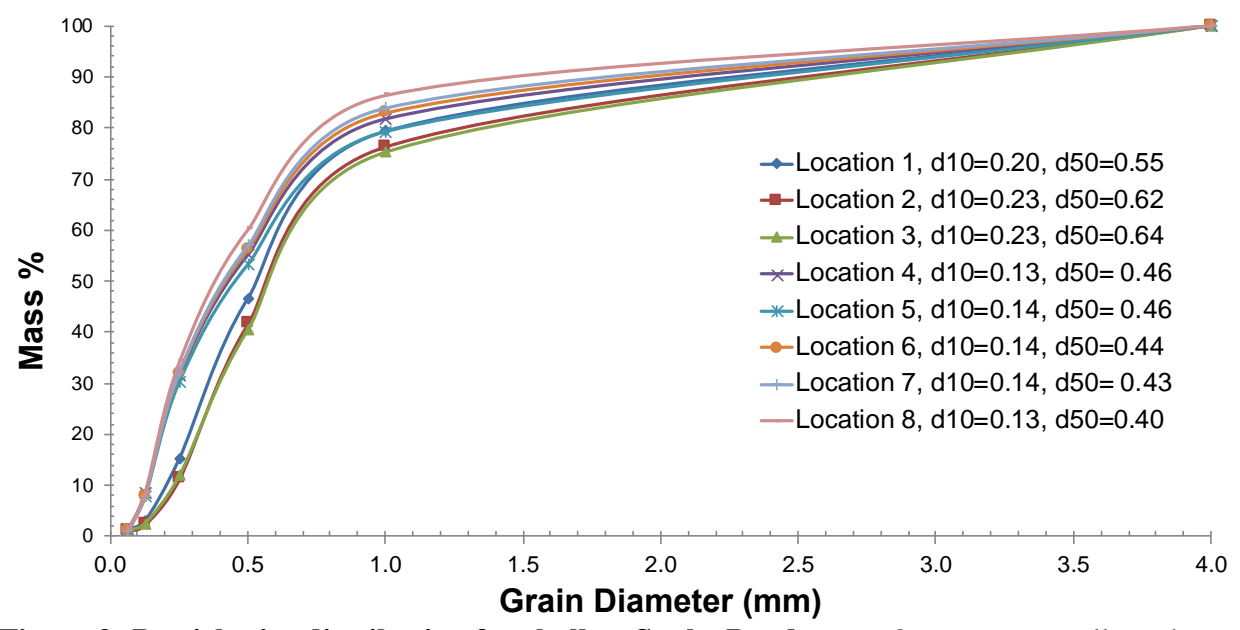


Figure 9: Particle size distribution for shallow Snake Pond cores. 8 cores were collected on 7/26/2016 and sampled at 2 cm depth. The 10th percentile and 50th percentile particle sizes are shown for each core.

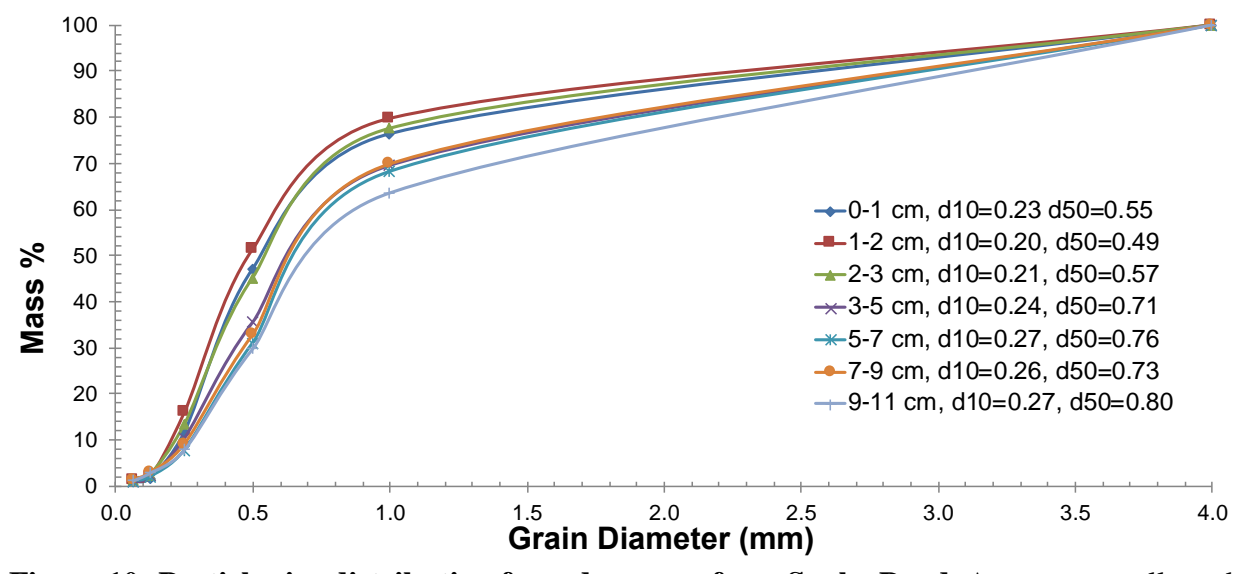


Figure 10: Particle size distribution for a deep core from Snake Pond. A core was collected on 7/8/2016 to 11 cm depth. Depth intervals are shown, with the 10th percentile and 50th percentile particle sizes for each interval.

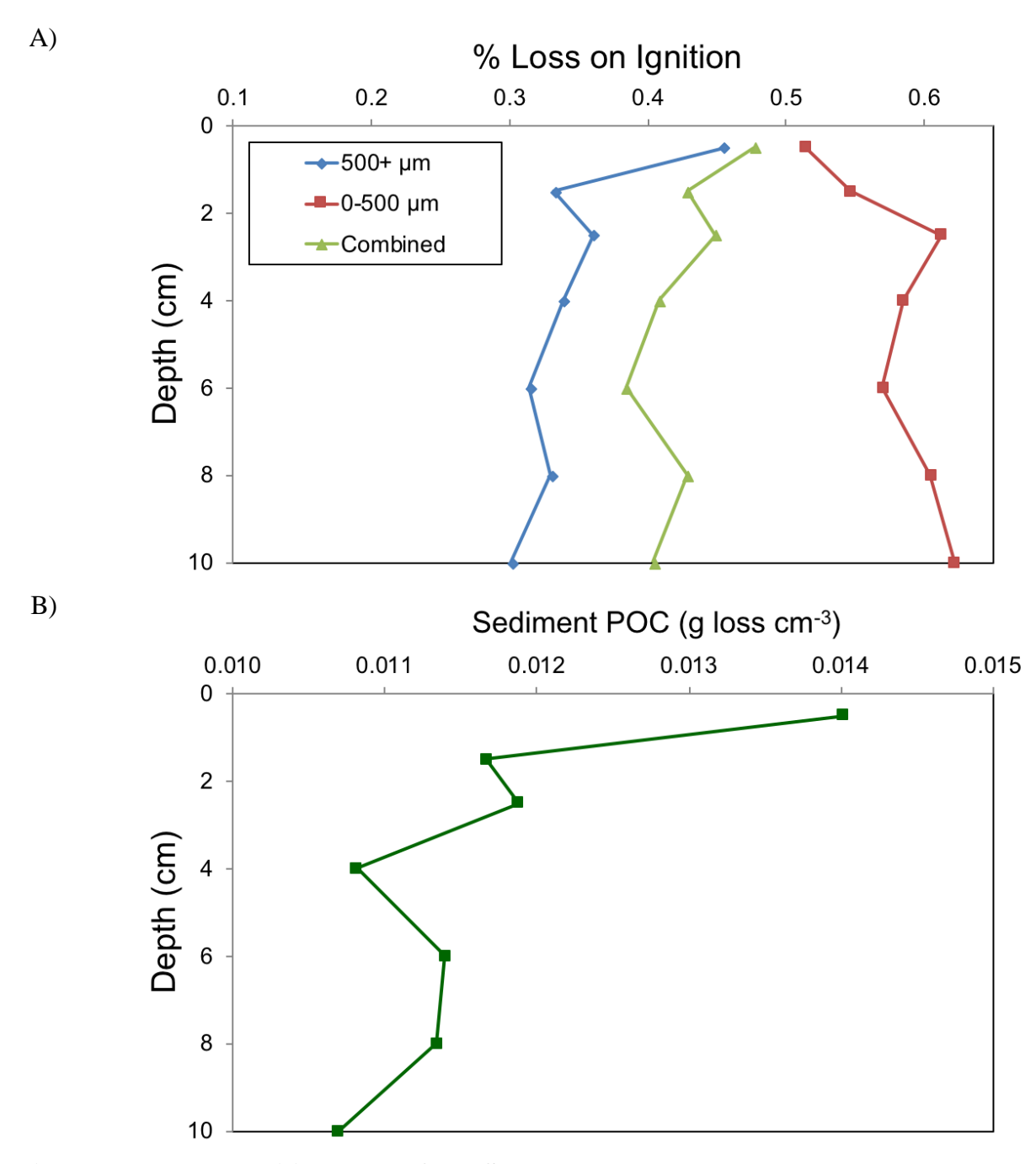


Figure 11: Loss on Ignition results from Snake Pond core. A core collected on 7/9/2016, sampled at 2 cm intervals up to 11 cm depth. (A) % mass lost on ignition, sorted by particle size greater than and less than $500 \, \mu m$. (B) Percent LOI converted to mass loss per cm³.

2.3.2. Hydrologic and Chemical Setting

Ambient local downwelling rates were 0.12 m/d adjacent to the experimental ring, as determined by temperature modeling. This modeling used an in-situ measurement of thermal

diffusivity of 0.13 m²/d, which was derived from changes in paired diurnal signal amplitude and phase with depth (Luce *et al.*, 2013; Briggs *et al.*, 2014a; Irvine *et al.*, 2015). Ambient dissolved O₂ data showed anoxic or virtually anoxic (<63 μmol O₂/L; Rosamond *et al.*, 2012) conditions at shallow depths beneath the sediment surface, reaching a concentration of 11 μmol O₂/L at 7 cm below the sediment surface (Figure 12). Ambient NO₃⁻ concentrations were low (<1.3 μmol NO₃/L), but patterns with depth suggested a small zone of nitrification as well as a zone of net NO₃⁻ removal below the oxic-anoxic transition.

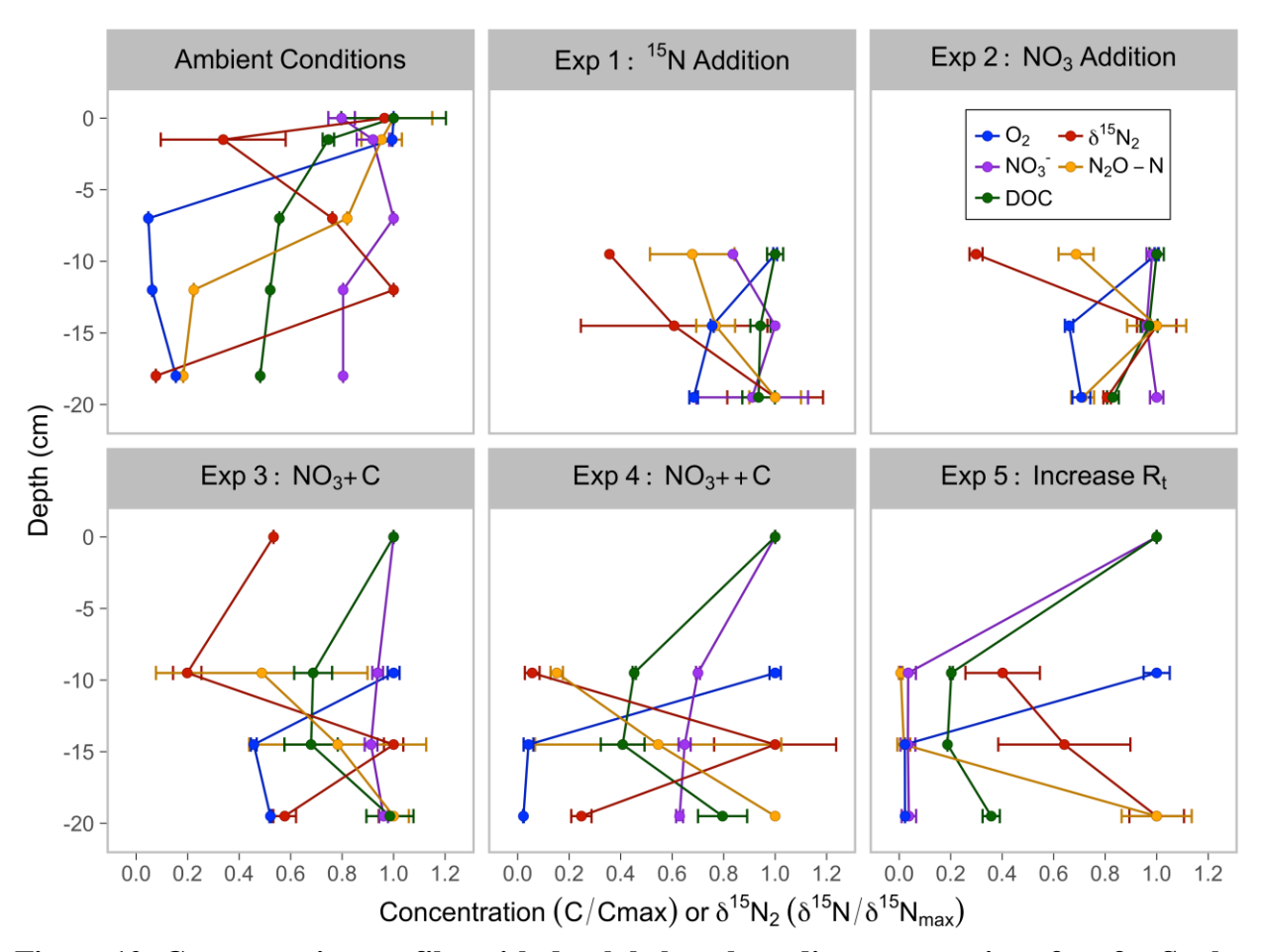


Figure 12: Concentration profiles with depth below the sediment-water interface for Snake Pond. Concentrations (C) are shown at steady state (~24 h) and expressed as C/Cmax or δ^{15} N/ δ^{15} N_{max}. The five experiments are described in Table 1. Species shown: NO₃-, O₂, DOC, δ^{15} N₂, and N₂O (symbol legend in figure). Error bars are for the standard deviation of three replicates at each depth, when available; some error bars are within the size of the plotted point.

Concentrations of NH₃ were below detection (<1.43 µmol NH₃/L) for almost all samples, and thus nitrification was unlikely to contribute significantly to N cycling unless it was closely coupled with denitrification. Removal rates of DOC (between 0-18 cm depths) were low compared to the later experiments, at 10.6 µmol DOC/L/h, with concentrations reducing to about half from 0 to 18 cm depth (Figure 12). These ambient chemical profiles demonstrate the presence of microbial populations performing aerobic respiration, as rates of O₂ and DOC removal were similar, but 8 times greater on average than the 1:1 O₂:C molar ratio predicted by the expected stoichiometric relationship (Findlay and Sobczak, 1996). This could be explained if respiration was utilizing particulate organic carbon (POC) in the sediments (Sawyer, 2015; Quick *et al.*, 2016), which is consistent with the decreased POC content with depth in our sediment cores (Figure 11).

2.3.3. Experimental Outcomes

Downwelling conditions were maintained within the injection ring for the duration of the experiments. Analysis of data from the 24.5 cm depth MINIPOINT piezometer indicated that it was too close to the bottom of the 1-dimensional flow field generated by the experimentally raised hydraulic head, and that our conservative and reactive tracers were being diluted by ambient groundwater. For this reason, data from the 24.5 cm depth are not discussed.

The onset of our experiments corresponded with an increase in downwelling flux from an estimated 0.12 m/d to 1.2 m/d and with the addition of $^{15}NO_3$ - to serve as a tracer for denitrification. During Experiment 1, the increased downwelling rate caused the shallow anoxic (<63 µmol O_2 /L) zone that was present in the ambient sediments to move deeper (Figure 12). The sampling depth at 9.5 cm remained consistently oxic through Experiments 1-5, with an average O_2 concentration of 216 µmol O_2 /L. Despite the reduced efficacy of O_2 removal in

Experiment 1, dropping from 85% removal at 18 cm under ambient conditions to 27% removal at 19.5 cm, O₂ removal rates increased by 620% relative to ambient conditions (Figure 13), suggesting that ambient conditions had been transport-limited in terms of O₂ supply. Removal of DOC also decreased from 52% efficacy to 6.4%, despite a 180% increase in DOC removal rate.

During Experiment 1, production of N₂O was also observed, presumably from the reduction of the added ¹⁵NO₃⁻ tracer. Concentrations of N₂O at 19.5 cm depth were 9.18 nmoles N₂O-N/L. The production of N₂O in Experiment 1 indicates that N₂O escaped during the sequential reduction of NO₃⁻ to N₂ in denitrification (Firestone and Davidson, 1989; Baulch *et al.*, 2011). Sediments were observed to be bulk-oxic (i.e., dissolved O₂ was detected in bulk samples), so the source of this denitrification byproduct can be attributed local anoxic microzones embedded in the sediment matrix (Triska *et al.*, 1993; Harvey *et al.*, 2013; Briggs *et al.*, 2015; Sawyer, 2015).

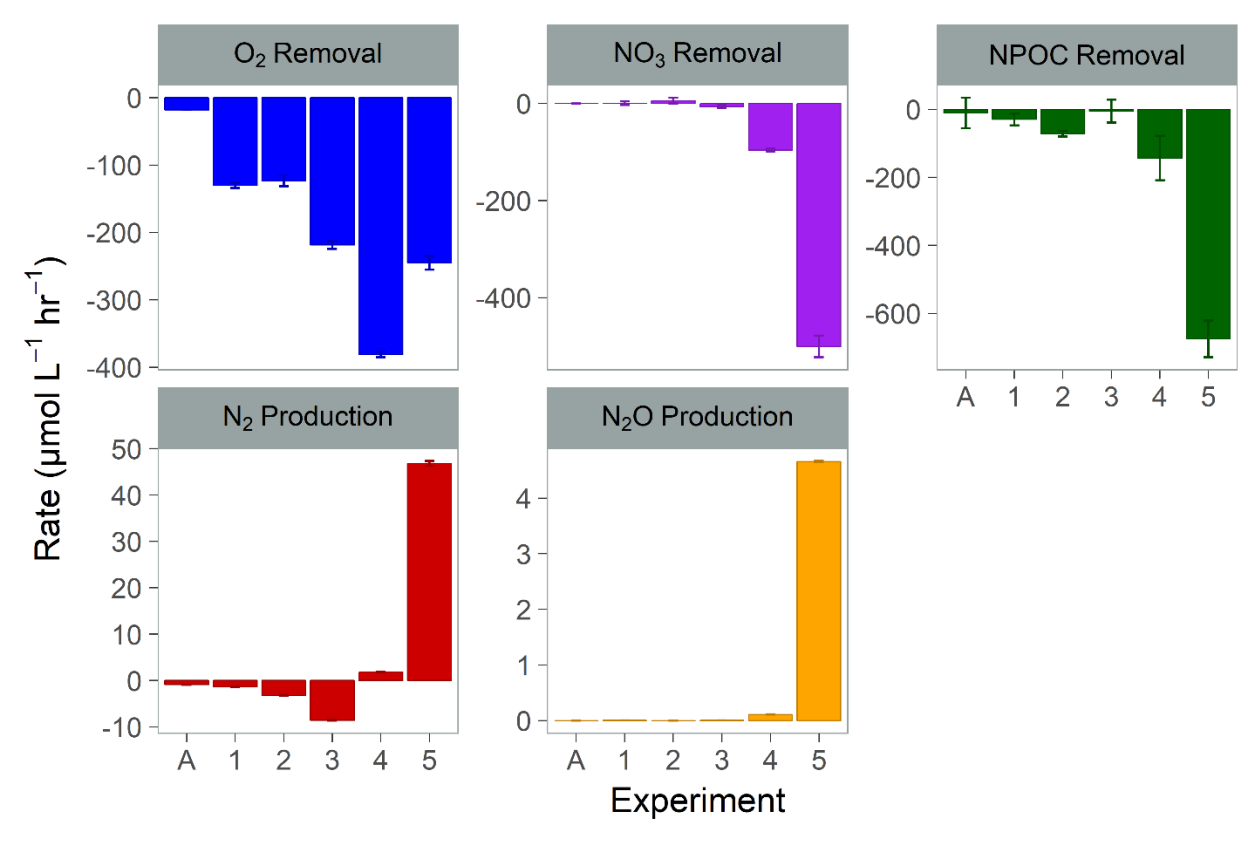


Figure 13: Biogeochemical flux rates in the Snake Pond experiments. Rates of O₂, NO₃, DOC measured as NPOC, N₂, and N₂O, across the five experiments (Table 1). For the ambient profile (A), rate is calculated between 0 and 18 cm depth. For gases (O₂, N₂, and N₂O), rates are between 9.5 and 19.5 cm depth. For NO₃⁻ and DOC, rates are calculated between 9.5 and 19.5 cm for Experiments 1-2, and between 0 and 19.5 cm for Experiments 3-5. Rates are calculated as in Section 2.2.5. Error bars are based off the standard deviation of the concentrations of 3 samples at each depth.

In Experiment 2, downwelling lake water was amended with NO₃⁻, bringing NO₃⁻ from a background concentration of 1.04 μmol/L to approximately 142 μmol/L. This NO₃⁻ addition had little effect on O₂ removal or denitrification (Figure 12), suggesting organic carbon, and more likely the availability of labile DOC, was a more important limitation on denitrification.

Increased NO₃⁻ concentrations corresponded with an increase in the peak N₂O concentration (at 14.5 cm) in the sediments by 110%, in agreement with previous studies showing correlations between dissolved NO₃⁻ and N₂O concentrations (Firestone and Davidson, 1989; Beaulieu *et al.*, 2011; Quick *et al.*, 2016). In Experiment 2, DOC removal between the 9.5-19.5 cm depths also

increased by 140% (Figure 13), with the greatest removal rates of DOC for both Experiments 1 and 2 taking place between the depths of 14.5 and 19.5 cm. Still, there was a slight mismatch between the depth intervals of maximum O₂, NO₃-, and DOC removal (Figure 12).

Consequently, in the subsequent experiments (Experiments 3-4) we tested if denitrification in our interrogated sediments was limited by DOC.

In Experiment 3, downwelling lake water was amended with labile DOC in the form of acetate (Baker et al., 1999; Zarnetske et al., 2011b; Kurz et al., 2017), bringing DOC from a background concentration of approximately 250 µmol /L to approximately 370 µmol /L (+47%). Following this labile DOC addition in Experiment 3, rates of O₂ removal (9.5-19.5 cm) increased by 77%, and NO₃⁻ removal (0-19.5 cm) increased to 6.36 μmol/L/h, confirming DOC limitation of respiration and NO₃⁻ removal. Even with the addition of both NO₃⁻ and acetate, conditions remained oxic throughout the sediments in Experiment 3. Under these and subsequent experimental conditions, the majority of NO₃ and DOC removal took place along flowpaths in the first 9.5 cm beneath the sediment surface, whereas the highest O₂ removal occurred between 9.5 and 14.5 cm. The removal rate of DOC (0-19.5 cm) in Experiment 3 decreased by 93%, but this was largely caused by an apparent signal of DOC 'production' or 'liberation' at the deepest depth intervals, between 14.5 and 19.5 cm (Figure 12). Net DOC production has previously been observed in alluvial aquifers, but at much longer residence times than those in our study (Helton et al., 2015). In Experiment 3 the sediments had transitioned away from having any nitrification signal, conditions remained oxic, and N₂ production was too low to be detectable by our methods. N₂O production rates (9.5-19.5 cm) were not observed to be different from Experiment 2. The increase in NO₃ removal was not accompanied by an increase in the proportion of denitrification accounted for by N₂O, which was only 0.04%.

The acetate addition in Experiment 4 produced an 82% increase in DOC concentrations (to 680 μmol C-DOC/L) in the downwelling lake water. The goal of inducing more anoxia was achieved for the first time in Experiment 4, where the anoxic zone shifted upwards toward the SWI to 14.5 cm, driven by a 74% increase in the O₂ removal rate (0-19.5 cm). In Experiment 4, the sampling depths straddled the bulk oxic-anoxic transition between 9.5 and 14.5 cm-depth. During Experiment 4 NO₃⁻² concentrations increased in the injectate from 160 to 250 μmol/L (+54%) as a function of the shift in injection rate due to a constant experimental water level within the ring and naturally changing lake stage. Thus, Experiment 4 was not solely a DOC manipulation.

The 86% increase in labile DOC supply in Experiment 4 yielded a 1400% increase in NO₃⁻ removal (0-19.5 cm) and 2700% increase DOC removal rate (0-19.5 cm). Concentrations of DOC decreased by 20% from surface water to 19.5 cm depth. (Figure 13). At 14.5 cm depth, the percent removal of DOC from the surface water concentration increased from 32% in Experiment 3 to 59% in Experiment 4. Concentrations of DOC continued to exhibit apparent productionat depth, suggesting that the true DOC removal rate was higher especially up to 14.5 cm depth. Removal of O₂ also continued to outpace removal of DOC, with >60% of O₂ removal unaccounted for in the removal of DOC. This suggests that over the duration of our experiments local POC continued to be an important electron donor in aerobic respiration. This is supported by the presence of POC in our sediment cores (Figure 11), and by observations of strong retention of DOC in shallow sediments of Ashumet Pond (Harvey *et al.*, 2015). While this labile DOC addition demonstrated that an increased supply of acetate promotes NO₃⁻ removal, it did not have a strong effect on denitrification rates.

In Experiment 4, the N_2 production rate (9.5-19.5 cm) increased to 1.8 μ mol N_2 -N/L/h, but only represented 1.9% of the observed NO_3^- removal. In contrast, the N_2O production rate (9.5-19.5 cm) increased by almost 4400%, representing 5.7% of total denitrification ($N_2 + N_2O$). Most clearly shown in Experiment 4 was a spatial offset between NO_3^- removal and denitrification (Figure 12), with most of the ^{15}N gas accumulating further along the downwelling flowpath. Concentrations of NO_3^- were low where the highest denitrification rate was observed.

In Experiment 5, where residence times were increased by the reduced flux, O₂ concentrations only decreased another 5% from surface water conditions when compared to Experiment 4 because O₂ was already close to being entirely depleted at depth (Figure 12). Like the case in Experiment 4, and due specifically to the manipulated flux rate and enhanced concentration of the flux from the reactant drip tanks, measured NO₃⁻ and DOC concentrations increased in the lake water to 800 μmol NO₃⁻/L (+220%) and to 1600 μmol DOC/L (+135%). Under these increased residence time conditions in Experiment 5, NO₃⁻ removal (0-19.5 cm) increased by another 420% to 500 μmol/L/h. The removal rate for DOC (0-19.5 cm) also increased by 370% to 680 μmol/L/h (77% removal at 19.5 cm depth) (Figure 13), with a maximum rate of DOC removal occurring along the first 9.5 cm of flowpath. At 14.5 cm depth, the percent removal of DOC from the surface water concentration increased from 59% in Experiment 4 to 85% in Experiment 5 (Figure 12).

Once longer residence time conditions were introduced (Experiment 5), denitrification also increased markedly by 2500% to a rate (9.5-19.5 cm) of 47 µmol N₂-N/L/h, and N₂O production (9.5-19.5 cm) increased by 4100% to a net rate of 4.66 µmol N₂O-N/L/h. Therefore, under reactant-replete conditions (Experiments 1-4), measured NO₃⁻ removal rates were strongly transport-limited. This scenario can be translated to the downwelling sediments of Ashumet

Pond, where this transport limitation is likely a significant control on N export. Increased denitrification rates are a result of the sediment becoming anoxic once NO₃⁻ and DOC additions occurred (Experiment 4). Specifically, the O₂ removal rates increased with subsequent acetate additions, suggesting increased aerobic processing of DOC that depleted the O₂ (Hedin *et al.*, 1998). So in the presence of conditions favorable to anoxia, the net NO₃⁻ removal becomes a function of residence (or exposure) time in the SWI, as suggested by theory and reviews of previous studies (Zarnetske *et al.*, 2012; Abbott *et al.*, 2016). In Experiment 5, N₂ production increased to represent 9.4% of the observed NO₃⁻ removal, and N₂O production increased to represent 9.1% of total NO₃⁻ removal. N₂O production accounted for 0.93% of NO₃⁻ removal, in agreement with previous observations in aquatic sediments (Beaulieu *et al.*, 2011).

Taken together, the results of these experiments demonstrate that while NO₃⁻ and DOC concentrations are important limiting factors for denitrification and specifically N₂O production (Bernhardt and Likens, 2002; Mulholland *et al.*, 2008; Zarnetske *et al.*, 2011b), residence time is the most important control on N₂O production. Despite higher percent increases in reaction rates for NO₃⁻ and DOC between Experiments 3 and 4, this experimental increase in residence times during Experiment 5 showed the largest magnitude of increases in reaction rates (Figure 13), as well as for denitrification from ambient conditions. Quick *et al.* (2016) showed in their column experiments that N₂O accumulation peaks at an intermediate residence time such that oxygen is depleted, and sediments are bulk-anoxic, but where N₂O does not become the most energetically favorable electron donor to then produce N₂.

Only 9.5% of NO_3^- removal could be accounted for in production of N_2 and N_2O in this study. In other studies in lakes, this proportion can vary widely from 63 to 100% (Chen *et al.*, 1972; Rysgaard *et al.*, 1993); and in one study of streams, up to 87% of $^{15}NO_3^-$ added in

sediment incubations could be accounted for by biological assimilation (Lansdown et al., 2012). Sulfur (S) oxidation-driven reduction of N could also be evidenced by the observed increasing SO₄²- concentrations with depth (Table 4). Burgin and Hamilton (2008)(Burgin and Hamilton, 2008) observed, in a review of studies, that S-driven NO₃ reduction to N₂ accounted for on average 25% of NO₃⁻ removal in streams, and 45% in lakes. The SO₄²- concentrations in our SWI may indicate NO₃⁻ being reduced to N₂ while sulfide is oxidized to SO₄²-, because SO₄²concentrations increased with depth in all our experiments. Still, based on the observed SO₄²increases, the S-driven NO₃ reduction pathway could only account for 33%, 3.7%, and 3.5% of NO₃ removal in the Experiments 3, 4, and 5, respectively. Further, the stoichiometry of this Sreaction during Experiment 4, based on observed SO₄²- production, could predict almost 97% of N₂ production. Predicted N₂ production by this reaction under increased residence times (Experiment 5) could account for 19% of the total observed N₂ production. Consequently, the ¹⁵N-NO₃- tracer would have still produced ¹⁵N₂ by this S-based reaction, and it may not be possible to differentiate this S-driven pathway of N₂ production from dissimilatory N reduction via denitrification.

In addition, there was a net increase of NO₂⁻ to 25 μmol/L at 19.5-cm depth, while in Experiment 4 NO₂⁻ concentrations only increased to 13 μmol/L (Table 4). These concentration increases of NO₂⁻ corresponded to nitrate reduction rates of 12 and 3.7 μmol/L/h occurring between the sediment surface and 19.5 cm depth for Experiments 4 and 5, respectively. For Experiments 4 and 5, taking into account recovery of N end-products as N₂, N₂O, and NO₂⁻, 86 and 89% of NO₃⁻ removal must be accounted for by some other pathway, such as biological assimilation.

The initial ambient conditions and the results of Experiments 1-4 suggest that low background concentrations of NO₃⁻ and DOC created reactant limitations for denitrification. However, it is not until the transport timescales are manipulated that it becomes apparent that this SWI system is also limited by rates of hydrological transport. Importantly, the largest increase in overall biogeochemical function of these sediments with respect to NO₃⁻ and DOC removal and denitrification was observed with the experimentally increased residence times.

2.3.4. Residence Time Controls N Cycling

Our results agree with previous findings that denitrification is limited by labile DOC supply (Baker *et al.*, 2000b; Zarnetske *et al.*, 2011b; Quick *et al.*, 2016). In this study we also address the role that residence time plays in the biogeochemical function of a system receiving water with the same initial concentrations and ratios of DOC and NO₃⁻ flowing through a fixed SWI volume at different rates. The likelihood that a SWI flowpath will transition from net nitrification to net denitrification increases after the residence time increases to the point where dissolved O₂ is depleted and anoxia can develop, often represented in a Damköhler number framework for O₂ (Zarnetske *et al.*, 2012; Briggs *et al.*, 2014b; Marzadri *et al.*, 2014). The Damköhler framework acknowledges that at longer residence times denitrification becomes more likely, but it is incomplete in capturing other limitations, such as reactant limitations, on denitrification.

A complicating factor is that at longer residence times, the DOC source is also more likely to be exhausted, especially the labile forms as they are removed preferentially, concentrating the more recalcitrant DOC compounds along longer flowpaths (Zarnetske *et al.*, 2011b; Lansdown *et al.*, 2015; Quick *et al.*, 2016). This increases the likelihood of DOC limitation of the second half of the denitrification reaction and would increase the likelihood of

more N₂O reduction relative to N₂ production because additional carbon electron donors are needed to get from N₂O to N₂ (Hedin *et al.*, 1998; Quick *et al.*, 2016). These dynamics between N₂O versus N₂ production are indicated in our second acetate addition (Experiment 4) and increased residence time (Experiment 5) experiments. Here we observed increased proportions of N₂O production representing total denitrification and NO₃⁻ removal relative to the N₂, corresponding with an over 4000% increase in total N₂O production (Figure 13). Similar to the results of Experiment 5, Lansdown *et al.* (2015) found that residence time was a principal control on denitrification and NO₃⁻ in deep stream sediments, where their deeper sediments accounted for 81% of observed subsurface NO₃⁻ removal in their study.

Denitrification products containing tracer ¹⁵N were observed in the SWI even at depths where bulk oxic conditions were present, (Experiments 1-3). These observations imply the presence of anoxic microzones embedded in bulk oxic pore waters that facilitate denitrification, a process long proposed to occur in unsaturated soils (Reddy and Patrick, 1975; Sexstone *et al.*, 1985; Kravchenko *et al.*, 2017) and in stream sediments (Triska *et al.*, 1993; Zarnetske *et al.*, 2011a; Harvey *et al.*, 2013; Lansdown *et al.*, 2014, 2015). The heterogeneity in sediment porosity characteristics common in SWI environments can result in a broad distribution of residence times along the flowpaths, with smaller throated pores having longer residence times and creating pore volumes more likely to become anoxic (Briggs *et al.*, 2015). Given the nature of the sediments observed in our SWI (Figure 12, Table 4), there are certainly a distribution of more- and less-connected pore volumes. Briggs *et al.* (2015) modeled anoxic microzones across a range of changing hydrologic flow rates and O₂ removal rates and showed that small portion of porosity (3-5%) was consistently anoxic, with slower flow rates and shorter threshold time to anoxia, resulting in the highest proportion of microzones. Along with physical sediment grain

heterogeneity, buried POC has also been shown to result in localized anoxic zones (Kravchenko *et al.*, 2017), and enhanced microbial activity (Sobczak *et al.*, 1998). Recognition that denitrification rates and residence times can be highly variable across small spatial scales (Harvey *et al.*, 2013; Lansdown *et al.*, 2015) further emphasizes the potential importance of microzone contribution to total flowpath denitrification, especially N₂O production, which was observed in our study.

This study is one of the first field demonstrations of the dynamic biogeochemical functioning of groundwater flow through lake SWI sediments (as represented by N and C removal and denitrification rates). It also clearly shows that the functioning of these SWIs can be dramatically changed by altering hydraulic gradients and thus residence times (Stoliker *et al.*, 2016). Consequently, any environmental factor that changes local or regional hydraulic flux (e.g., seasonal- or management-induced variable lake stage or regional water table) will change the biogeochemical function of the SWI and impact the abundance of NO₃⁻ and N₂O mass moving through and out of these important inland waters. This dependence has been observed in comparable studies done in rivers, where it has been demonstrated that changing river stage changes the fate of NO₃⁻ in the SWI of a river (Gu *et al.*, 2008).

2.4. Conclusions

Past studies in groundwater flow-through lakes have shown that there is not a fundamental microbial limitation on the transformation of N_R in these coupled surface and groundwater systems because denitrifiers are ubiquitously distributed and facultatively aerobic (Stoliker et al., 2016). Consequently, the controls on the fate of N_R in SWIs have been hypothesized to be primarily via limitations on the supply and reactant exposure timescales. Here we directly tested this hypothesis in the SWI of a lake and show that while labile carbon limitations are important, the overall net effect of physical transport timescales is a more dominant control on the fate of N_R . Future studies can explore the optimal condition of multiple reactants and multiple residence times by conducting more field- and lab-based residence time manipulation experiments. Overall, we established that the transport limitation interacts with the reaction limitation, including increasing the anoxic domain and volume where denitrification can occur. Consequently, the fate of N_R in these coupled lake and groundwater systems will vary primarily with hydrological processes that regulate hydraulic gradients driving surfacegroundwater exchanges, and thus the transport timescales of reactants through lake SWIs. To investigate the scaling nature of transport timescales and SWI N processing, a follow-up study was conducted and is described in Chapter 3.

CHAPTER 3: EXPERIMENTAL MODIFICATIONS OF HYDROLOGIC FLUX AND RESIDENCE TIME REVEAL CONTROLS ON NITROGEN PROCESSING IN THE SEDIMENT-WATER INTERFACE OF A HEADWATER STREAM

3.1. Introduction

Human activity has dramatically altered the global nitrogen (N) budget, impacting nearly all aquatic ecosystems on the planet (Vitousek et al., 1997). This N manipulation is caused principally by the conversion of atmospheric N_2 to N-based fertilizers through the Haber-Bosch process, but also by altering atmospheric NO_x concentrations and thus N deposition through the burning of fossil fuels (Galloway et al., 2004). There is large uncertainty around the global fluxes of anthropogenic reactive N (N_R) from landscapes to the oceans, but freshwater ecosystems are highlighted as both important transporters and sinks of N (Schlesinger et al., 2006). The proportion of anthropogenic N_R inputs to landscapes that is ultimately removed by freshwater ecosystems before reaching the oceans has been estimated to range from 8-50% (Howarth et al., 1996; Galloway et al., 2004; Boyer et al., 2006; Seitzinger et al., 2006). Despite this uncertainty, most of this transformation likely occurs in headwater streams (Peterson et al., 2001; Thomas et al., 2001; Bernhardt and Likens, 2002; Seitzinger et al., 2002). Headwater streams make up the majority of river network length (Downing et al., 2012), and have the highest proportion of sediment contact area to surface flow area (Anderson et al., 2005; Gardner and Doyle, 2018). Consequently, a key locus of N transformations in smaller rivers and streams is the sediment water interface (SWI): often called the hyporheic zone, which is the zone of exchange between stream water and groundwater (Boulton et al., 1998; Boano et al., 2014).

The SWI is a dynamic ecotone that provides many ecosystem services, including its role in denitrification, or the microbially-mediated reduction of oxidized forms of N, most abundantly present as nitrate (NO₃-), to N₂ gas (Duff and Triska, 1990; Triska *et al.*, 1993). While the

denitrification process is inhibited in the presence of dissolved oxygen, SWIs with significant stream water exchange and oxygenation have nonetheless been shown to become anoxic and create significant sinks of N (Findlay, 1995; Harvey et al., 2013). A byproduct of the denitrification reaction is nitrous oxide (N₂O), which is an intermediary product of the reduction of NO₃, and which can then be further reduced to N₂. The fraction of denitrified N_R that is released as N₂O in sediments has been reported to be ~1% (Mulholland et al., 2008; Beaulieu et al., 2011), however streams and rivers have been shown to account for 10-20% of the recent increase in atmospheric N₂O concentrations due to anthropogenic activity (Seitzinger and Kroeze, 1998; Kroeze et al., 1999; Beaulieu et al., 2011). This is of concern because N₂O is a strong greenhouse gas, with 300 times the warming potential as CO₂ (Forster et al., 2007), and in addition it is a significant contributor to atmospheric ozone depletion (Ravishankara et al., 2009; Syakila and Kroeze, 2011). It has also been shown that N₂O emission rates are higher in headwater streams relative to large rivers (Seitzinger and Kroeze, 1998; Marzadri et al., 2017), and though the causes for this are yet to be revealed, recent modeling suggests it can be attributed to SWI processing of landscape N_R (Marzadri *et al.*, 2017).

A key challenge in upscaling understanding of SWI function to entire fluvial networks, specifically the contribution of SWI to N processing rates and NO₃-, N₂, and N₂O export from headwaters, is the unique and dynamic interplay of reaction chemistry and hydrodynamics in the SWI (Triska *et al.*, 1993; Zarnetske *et al.*, 2012; Lansdown *et al.*, 2015; Liu *et al.*, 2017). Adding to the complexity of efforts to characterize large-scale N processing in stream SWIs is that sediment conditions and stream flows can be extremely heterogeneous in space and time (Marzadri *et al.*, 2014). Consequently, studies attempting to characterize SWI functions such as N processing face difficulty in characterizing individual controls in natural settings because the

mixing of reactants (e.g., nutrients, oxidants) between surface and groundwaters is fundamentally dependent on the direction and magnitude of exchange flows (Triska *et al.*, 1990, 1993; Brunke and Gonser, 1997; Zimmer and Lautz, 2014; Danczak *et al.*, 2016), For example the physical exchange flow between streams and the SWI have been documented to vary up to 5 orders of magnitude, and the fraction of total stream discharge passing through the SWI can be very high relative to surface flow depending on substrate and sediment depths (Boulton *et al.*, 1998; Anderson *et al.*, 2005; Tonina *et al.*, 2016). This flow variability can be further divided among variability of flowpath length and residence times during both steady-state and variable flow conditions (Wörman *et al.*, 2002; Anderson *et al.*, 2005; Kaufman *et al.*, 2017). The large range in fluxes and residence times in the SWI can be contrasted with documented changes in nutrient and reactant chemistry rates and timescales across catchments, which typically only vary 1-2 orders of magnitude (McGuire *et al.*, 2014; Abbott *et al.*, 2018; Ruhala *et al.*, 2018). These large ranges in controls on biogeochemical reaction rates in the SWI are rarely reconciled in field observations or experiments.

There have been significant efforts by multiple disciplines to explore and model the function of the SWI across a range of spatiotemporal scales, but significant questions remain from this large body of research as to whether reactive versus hydrologic (transport) controls are most important to the fate of NO₃⁻ in streams (Sophocleous, 2002; Cardenas, 2015).

Consequently, there is a need for novel field investigation techniques that can estimate the relative importance of these controls to the fate of NO₃⁻. Based on the documented range of variability in physical transport and reaction rate controls across stream SWIs that have been studied (Zarnetske *et al.*, 2012), we hypothesize that physical parameters (hydrologic exchange timescales) are the master control on SWI biogeochemical function in N processing. To test this

hypothesis, we used a novel field method of controlled vertical exchange of known surface water chemistry through the SWI of a headwater stream that carries anthropogenically increased NO₃⁻ concentrations. Using ¹⁵N-NO₃⁻ as a tracer, we monitored the transformation of stream water NO₃⁻ as it passed through SWI flowpaths. We hypothesized that under stable biogeochemical inputs, changing the SWI recharge flux rate, and thus porewater residence times, would result in substantial changes in aerobic respiration (as indicated by oxygen removal) and NO₃⁻ removal through the SWI. This study attempts to bridge results from controlled lab experiments on stream sediments (Quick *et al.*, 2016; Liu *et al.*, 2017) with more natural, but less well constrained, insitu studies of NO₃⁻ processing (Zarnetske *et al.*, 2011a; Lansdown *et al.*, 2015). Specifically, this study was conducted in a natural headwater stream SWI setting, but experimentally constrained NO₃⁻ tracer and flow conditions made it more feasible to assess how systematically changing hydrologic residence time controls biogeochemical functioning of the SWI using NO₃⁻ as a reactive solute.

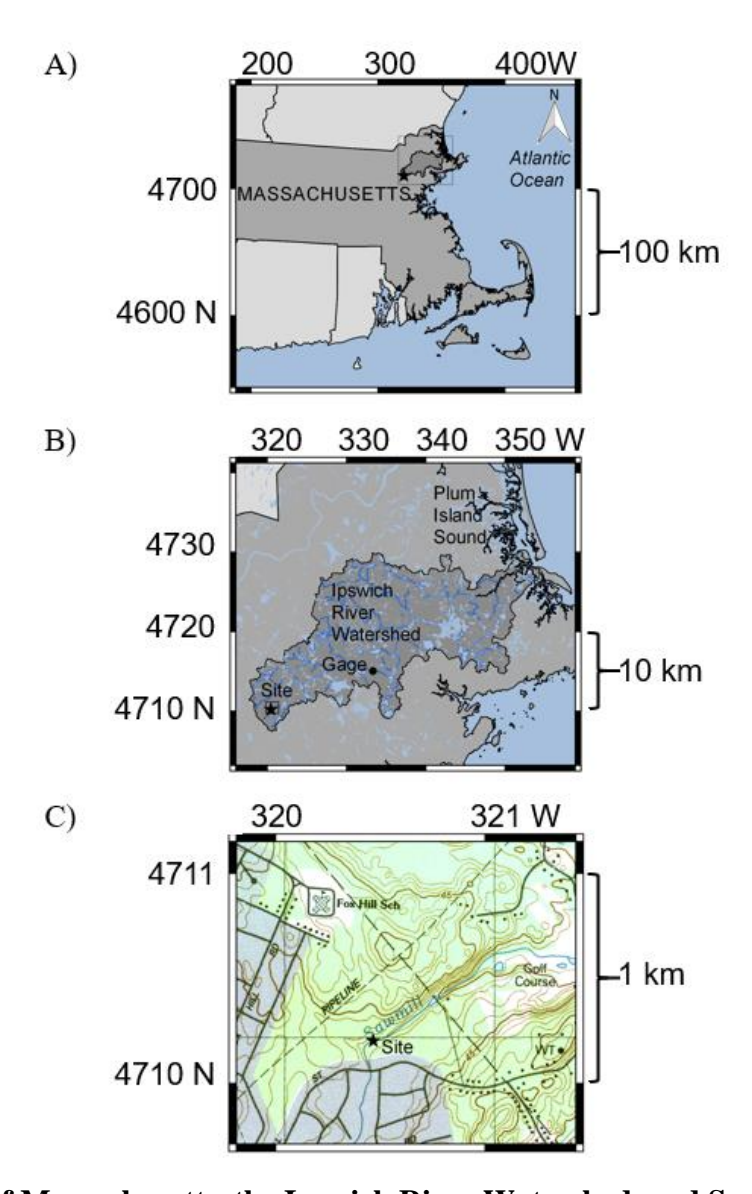


Figure 14: Maps of Massachusetts, the Ipswich River Watershed, and Sawmill Brook. (A) Study region within Massachusetts, USA with the (B) Ipswich River Watershed, showing the study site at Sawmill Brook and the nearest USGS stream gage (01101500) on the Ipswich River at South Middleton, MA. (C) Topographic map of the Sawmill Brook study reach and site (marked with star). Map units are kilometers. Datum is UTM zone 19T.

3.2. Materials and Methods

3.2.1. Site Description

The study reach and SWI experimental site are located in Sawmill Brook, which is a first order tributary to the Ipswich River, in Burlington, Massachusetts (Figure 14). The Ipswich River drains a watershed of 404 km² composed of mixed forest and urban land uses, and is underlain by Pleistocene glacial deposits (Carlozzi *et al.*, 1975; Briggs *et al.*, 2010). This watershed has been previously investigated for N_R removal in streams because there is significant N_R contamination from the surrounding heavily urbanized headwaters (Williams *et al.*, 2004). The site at Sawmill Brook (Figure 15) drains a 4.1 km² watershed with 72% urban/residential land use, and 25% impervious surface cover (Wollheim *et al.*, 2005).

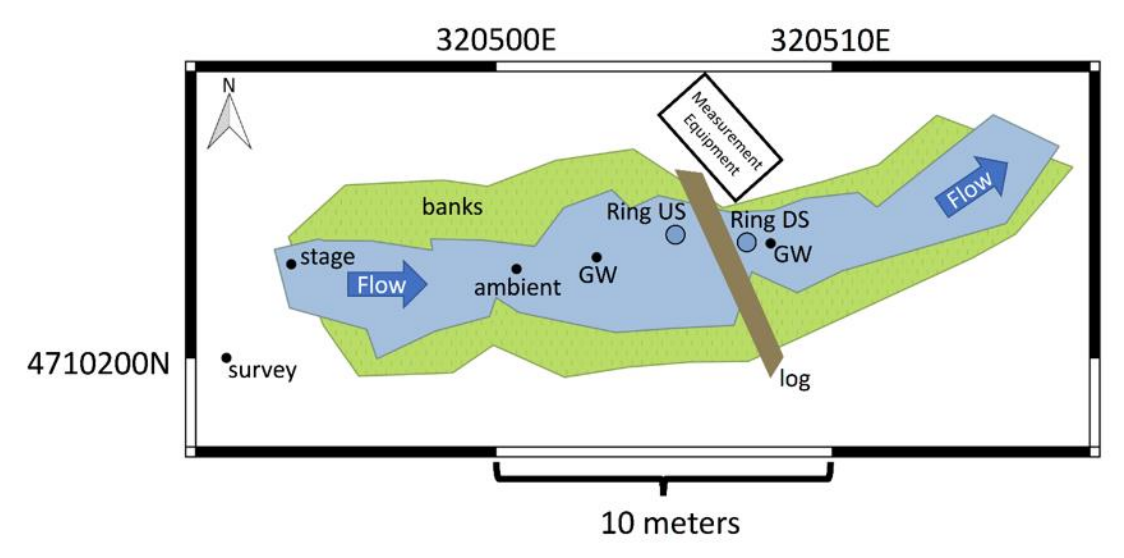


Figure 15: Detailed Plan-view Site Map of Sawmill Book. Stream level and banks were surveyed. The two injection ring locations are shown as 'Ring US' (upstream) and 'Ring DS' (downstream) (see Figure 5 for ring details). The groundwater (GW) and background (ambient) locations were sampled for groundwater and SWI porewater samples, respectively. The SWI ambient samples were taken at sediment depths of 2.5, 5, 7.5, 10, 15, 20 cm depths, and the groundwater sample was taken at 60 cm depth. The site labeled as stage (Figure 14) shows the location of our in-stream pressure logger. Map units are meters. Coordinates are for UTM zone 19T.



Figure 16: Site picture from Sawmill Brook. View is looking east, downstream, with ring US in the foreground and ring DS in the background. Additional equipment not described herein, such as the orange wiring seen in the image, are associated with a concurrent geophysical (electrical resistivity imaging) study.

This location was selected in part because it allowed us to conduct our SWI manipulation experiments in a stream that is relevant to previous extensive stream N studies, including the Lotic Intersite Nitrogen eXperiments II (LINX II), which were conducted there between 2003 and 2005 (Mulholland *et al.*, 2008, 2009; Hall Jr *et al.*, 2009).

The stream channel was highly incised into native glacial deposits (Figure 16). Two dominant benthic sediment types were present at the site: 1) eroded sand and clay from the native surficial till, with high amounts of organic debris, and 2) deposits of road sand carried from road crossings upstream (see Figure 16). Due to the high percentage of impervious surface in the catchment, the stream is very flashy. A large precipitation event of approximately 75 mm on the evening of July 12 caused a fast response in the stream of approximately 0.46 m in stage (Figure 19), but the stage returned to close to base level within 6 h.

3.2.2. Experimental Setup

The methods for this study are consistent with those presented in Chapter 2 and are only slightly modified for the stream SWI setting of this study. Hence, they are briefly reviewed here with highlights of the key differences between Chapter 2 approach and this study. Our study took place from July 10 – 18, 2017. The studied stream sediments were isolated from the surrounding environment using two open ended 55-cm-diameter polyvinyl-chloride (PVC) barrels, which were installed in the stream bed and driven to a depth of 20 cm; ensuring vertical 1-directional flow (Figure 5). Individual sites were located by verifying downwelling or neutral flow from the stream to the groundwater, using a large 55-cm-diameter steel seepage meter (Rosenberry and LaBaugh, 2008). They were also selected to target the two benthic sediment types, with the upstream injection ring (Ring US) placed in the organic-rich sands, and the downstream injection ring (Ring DS) placed in the road sand deposits. The two rings were 2.1 meters apart (Figure 15). Immediately before the experiments were conducted, stream water was pumped into 1.9-m³ and 1.1-m³ holding tanks located on the stream bank (Figure 17). In both tanks, stream water was mixed with K¹⁵NO₃ (99% purity) to create the NO₃ injectate enrichment of 5 atom-percent ¹⁵N, assuming a background concentration of 96 µmol NO₃-/L (W. Wollheim, personal communication). In only one tank, stream water was also mixed with sodium chloride (NaCl) to bring the total conductivity of the water from a background of approximately 1000 µS/cm to approximately 2000 µS/cm. This NaCl concentration was required to accurately observe breakthrough curves of the higher conductivity water moving through the sediments and thereby characterize hydrologic flow conditions during the experiments. Using two intermediate buckets and a series of float switches, we were able to maintain a constant water level and hydrologic flux rate within each PVC injection ring (Figure 5, Figure 17). The water was pumped from each

holding tank to the intermediate bucket and into the ring to enhance and control the rate of downwelling of surface water through the SWI within the ring. In this way, we were able to systematically create a range of stable hydrologic flux rates and resulting hydrologic residence times under which to conduct tracer experiments to test our hypotheses (Figure 18). An aerator was placed in the intermediate buckets to keep water oxygenated during what were sometimes long residence times in the bucket at low flux rates. There was no aerator in the tank.

Initially, the hydraulic conditions in the ring were sustained with a hydraulic flux set to 3 m/d, which was repeatedly confirmed by monitoring the injection rate through the intermediate bucket (Figure 17). Flux rates were modified over four experiments (Table 3), from 2 m/d (Experiment 1, July 11) to 3 m/d (Experiment 2, July 14), then 0.8 m/d (Experiment 3, July 15), and finally to 1.2 m/d (Experiment 4, July 16), which represents four realistic and systematic changes in SWI residence times, respectively. The storm event on July 12 briefly delayed the experiments, and stream conditions were allowed to stabilize before experiments resumed. During each experiment, high conductivity water from the NaCl-labelled tank was injected, until porewater conductivity up to 20 cm depth within the injection ring stabilized, and then the water in the ring was immediately evacuated and quickly filled with lower conductivity water, which then continued to flow into the ring at the same flux rate, allowing for assessment of two conductivity breakthrough curves at each flux rate. A combination of measured injection ring flux rates and specific conductivity (SpC) breakthrough curves was used to determine vertical flowpath residence times throughout the experiments, with the porewater velocity for each experiment was derived from the average of the injection and flux curves (detailed below in Section 3.2.5).

 Table 3: Details of the Sawmill Brook Experiments.
 The measured hydraulic flux through the

ring is reported for each experiment.

Experiment	Flux Rate	Injection time and	Experiment
Zaperment	(m/d)	Sampling time	Duration (h)
	(III/G)	(Y-M-D H:M)	Duration (ii)
Experiment 1	2.0	2017-07-11 19:35	17.6
1		2017-07-12 13:10	
Experiment 2	3.0	2017-07-14 13:15	19.4
•		2017-07-15 08:40	
Experiment 3	0.8	2017-07-15 09:45	27.4
_		2017-07-16 13:10	
Experiment 4	1.2	2017-07-16 21:30	12.3
•		2017-07-17 09:45	

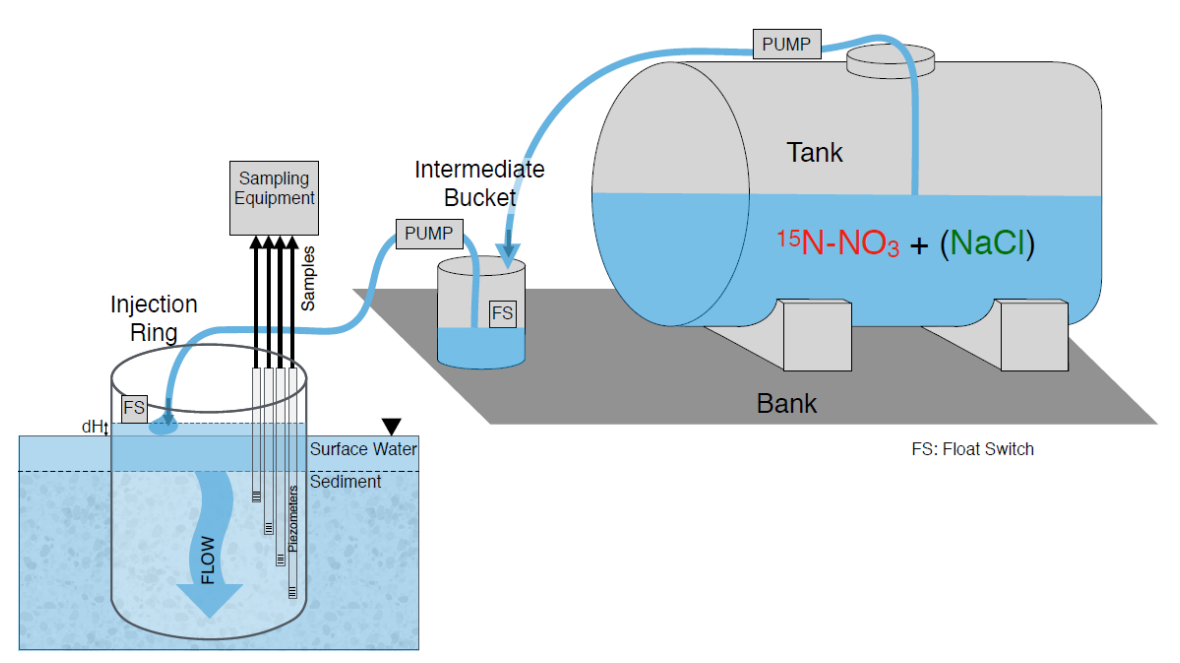


Figure 17: Schematic of Tracer Addition at Sawmill Brook. Before the experiments, water from the stream was pumped into two holding tanks. ¹⁵NO₃ was added to both tanks, and NaCl to only one. Using a series of pumps and float switches (FS) to maintain steady water levels, water was pumped into an intermediate bucket and then into the injection ring. An aerator was in the intermediate bucket to keep water oxygenated during sometimes long residence times in the bucket at low flux rates. There was no aerator in the holding tank.

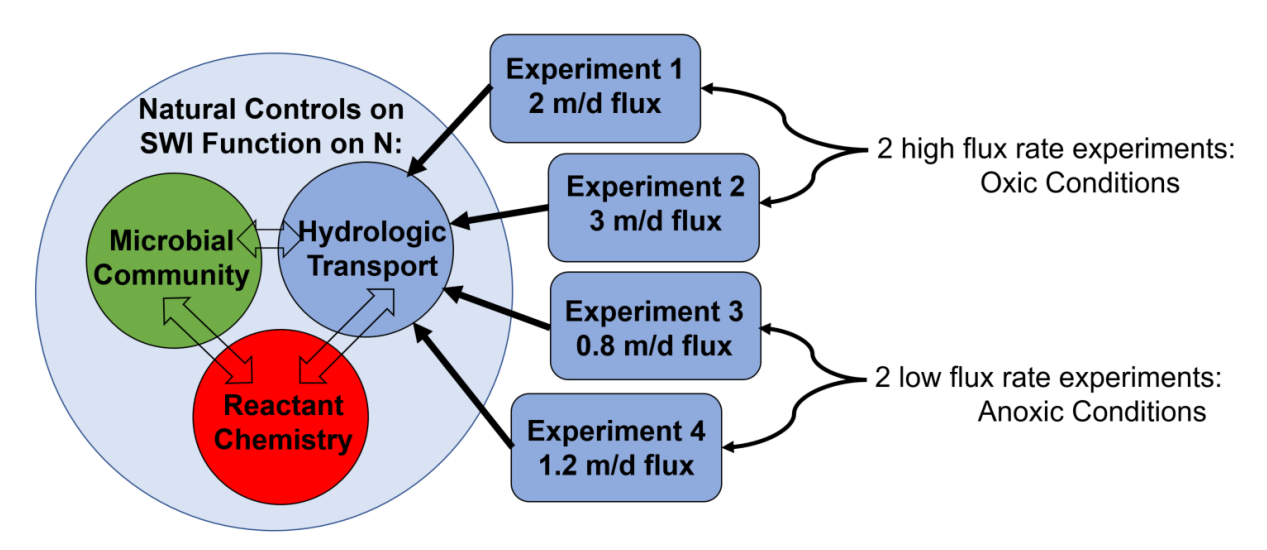


Figure 18: Conceptual Diagram of Sawmill Brook Experimental Modifications. The three major natural controls on SWI Function on N are microbial community composition, porewater reactant chemistry, and hydrologic transport conditions. By confirming with a ¹⁵NO₃⁻ tracer that a microbial community capable of N transformations was present and seeking to isolate the role of reactant chemistry on N removal, Experiments 1-4 systematically changed hydrologic flux, with two experiments exploring an oxic or anoxic regime, to observe changes in N removal as a result of changes in hydrologic controls.

Site stream flow conditions were monitored with a Levelogger pressure-temperature datalogger (Solinst, ON, Canada). The datalogger was suspended in the stream water column at the location indicated in Figure 15. This logger provided high-resolution information on stage, but also stream-water total conductivity (TC) and temperature. Measurements of TC and temperature were also spot-checked and validated using a OrionStar handheld probe (ThermoScientific, MA, USA).

3.2.3. Porewater Sampling Methods

Measurement of dissolved oxygen (O₂) concentration and temperature within the ring water was accomplished by two MiniDOT loggers (Precision Measurement Engineering, CA, USA) suspended beneath the surface. Porewater sampling methods were identical to those presented in Section 0. Briefly reviewed here, porewater sampling at depth was achieved using four stainless steel minipoint samplers, similar to the USGS MINIPOINT system utilized by

Harvey *et al.* (2013). These had an outer diameter (OD) of 3.2 mm, a screened interval 10 mm long, with 3 individual slits 0.4-0.7 mm in width. The samplers were driven to depths of 5, 10, 15, and 20 cm below the stream sediments within each ring. 3.2-mm OD tubing was attached to the end of each minipoint, and the 10 and 20 cm sample depths were fed through two electrical conductivity (EC) micro flow-through cells (Amber Science). EC was converted to SpC at 25°C automatically by the micro flow-cell control units using sensor-specific calibrations performed at the beginning of the experiment. Flow-through cells equipped with fiber-optic oxygen microsensors attached to a FireStingO2 Optical Oxygen Meter (Pyro Science, Germany) were inline with the tubing from the 10 and 20 cm MINIPOINTs.

For each experiment, porewater sampling took place once the lower conductivity flush was at steady-state (i.e., reaching a stable lower conductivity 'plateau' on the breakthrough curve). Water sampling was accomplished in a closed system by peristaltic pumps (Cole-Parmer, IL, USA), and water was collected in syringes, followed by immediate filtering through a 0.7 μm glass fiber filter and 0.2 μm cellulose acetate filter into acid washed amber HDPE bottles (Nalgene, NY, USA). Water samples were chilled at 4°C on site and then frozen within 8 h of collection. For dissolved gas samples, 1.6 mm OD tubing directly from the pump was placed into the bottom of a 12 mL glass Exetainer (Labco, United Kingdom) and over-filled for two full volumes before collecting the sample volume. These gas samples were preserved with 120 μL of 50% w/v zinc chloride solution. Preserving a convex meniscus, the tubing was removed, and the cap was screwed on to prevent any air bubbles in the sample. Gas samples were stored at room temperature in the dark, and later shipped to the Stable Isotope Facility (SIF) at the University of California, Davis, for isotope (15N) analysis of dissolved gases (N2 and N2O). Water samples were later separated into groups for 15N analysis of NO3⁻, which were shipped frozen to the SIF,

and for nutrient, anion, and carbon analysis, which were never frozen but kept chilled at 4°C during shipment and prior to analysis at Michigan State University.

3.2.4. Laboratory Analyses

Stable isotope ratios of nitrogen (¹⁵N) in gas were measured using a ThermoScientific GasBench + Precon gas concentration system interfaced to a ThermoScientific Delta V Plus isotope-ratio mass spectrometer (Bremen, Germany). Nitrate in water samples was converted to N₂O by the bacteria denitrification assay and ¹⁵N ratios were measured as stated above. Anions were measured by a Dionex ICS-2100 Ion Chromatography System (ThermoScientific, MA, USA), producing concentrations for chloride (Cl⁻), nitrite (NO₂⁻), nitrate (NO₃⁻), and sulfate (SO₄²⁻). Non-purgeable Organic Carbon (NPOC), and Total Nitrogen (TN), were measured using a TOC-L total organic carbon analyzer (Shimadzu, Japan) catalytic oxidation at 720°C followed by gas chromatographic measurement of CO₂ and chemiluminescence measurement of NO.

3.2.5. Calculations of Residence Time and Reaction Rates

The SpC was measured at 10 and 20-cm depth within each of the two injection rings. For each of the four experiments, flux was varied, and the injection of higher conductivity water resulted in one breakthrough curve, and the following flush of lower conductivity water resulted in a second (see Figure). Median porewater velocities (see Table 9) for each injection/flush were calculated by subtracting the two median times of arrival and dividing by the separation distance. The average of the injection/flush velocities for both 10 and 20 cm sampling depth for each ring was used as the velocity to calculate residence time at 5, 10, 15, and 20-cm depths for each experiment.

Solute removal rates were calculated as the linear regression of change of concentration over median residence time, as in Section 2.2.5. Rates, unless otherwise specified, are calculated

between surface water (0 cm) and the 20 cm depth. Calculations of denitrification rates are outlined in Section 2.2.5. For each ring and experiment, residence time with depth was also transformed using the O_2 removal rates to calculate Damköhler numbers, consistent with the method of Zarnetske *et al.* (2012), which help illustrate if the SWI potential for bulk oxic or anoxic (<63 μ mol O_2/L) conditions is limited by transport or reaction timescales. For each ring and experiment, the removal velocity of O_2 (V_{O_2}) was calculated as the slope of the linear regression of the natural log of O_2 concentration over time. The removal velocity is equivalent to the 1st order decay constant k. For each depth, Damköhler values (Da_{O_2}) were calculated by multiplying the residence time (τ) at each depth by the O_2 removal velocity:

$$Da_{O_2} = \tau * V_{O_2} \tag{10}$$

 Da_{NO_3} was calculated by the same method, using a linear regression of the log of NO_3^- concentration over time to calculate the NO_3^- removal velocity.

3.3. Results

3.3.1. Hydrologic and Chemical Setting

Stream water chemistry remained relatively steady across the experimental periods (Figure 18). Concentrations of NO₃⁻ and DOC were on average 67 ± 8 μmol NO₃/L and 490 ± 80 μmol DOC/L (Figure 19) during the experimental periods. Background stream-water conductivity was approximately 1000 μS/cm. Stream Cl⁻ concentrations were strongly correlated with stream water TC (R²>0.99), suggesting that variation in TC was largely due to the variable influence of road salt application as NaCl in the watersheds (Kaushal *et al.*, 2018). Concentrations of Cl⁻ in stream water were on average 8000 μmol/L, as opposed to groundwater concentrations of 1400 μmol/L, providing a good contrast between the two waters exchanging through the SWI at the site. Groundwater contained an average of 21 ± 2 μmol NO₃/L and 355 ±

52

44 μmol DOC/L. The storm event on July 12 resulted in a large increase of stream stage, corresponding with dilution of both stream-water TC and NO₃⁻, and an increase in DOC, and concentrations slowly returned to the pre-event conditions, while stage recovered much faster (Figure 19). Removal of stream water to fill the tanks before mixing injectate for the remaining experiments was delayed until stream stage and chemistry returned to previous conditions. This is reflected in the concentrations of the tank water being highly stable, relative to the stream water (boxplots: Figure 19).

Concentrations of the tank water that was injected into the rings were on average 77 ± 5 μ mol NO₃-/L and 450 \pm 70 μ mol DOC/L, suggesting that after mixing with our tracers, the injectates were representative of background chemistry measured in the stream during the experimental periods (Figure 19). Tank concentrations of water drawn from the stream did not change considerably before and after the storm. Shifts in the concentrations of NO₃ were minimal between the holding tanks and surface water in the injection rings. Nitrate concentrations within the surface water of the rings were on average $76 \pm 4 \,\mu\text{mol/L}$. An increase in DOC concentrations was observed from the tanks to the ring surface water, with an average ring concentration of $520 \pm 100 \,\mu\text{mol DOC/L}$. The higher carbon concentrations could have been due to leaching of carbon from leaves and woody debris captured within the rings at the sediment-water interface, which was more prevalent in Ring US. Concentrations of dissolved O₂ in the injection ring water were on average $220 \pm 40 \,\mu\text{mol/L}$ (Figure 19), and stayed above 200 umol/L during the sampling periods (red bars: Figure 19) except for in ring US during Experiment 4 (flux 1.2 m/d), when the concentration dropped to 140 µmol/L. This was due to a temporary overnight failure of the aerator system within the intermediate bucket that kept the injection water oxygenated.

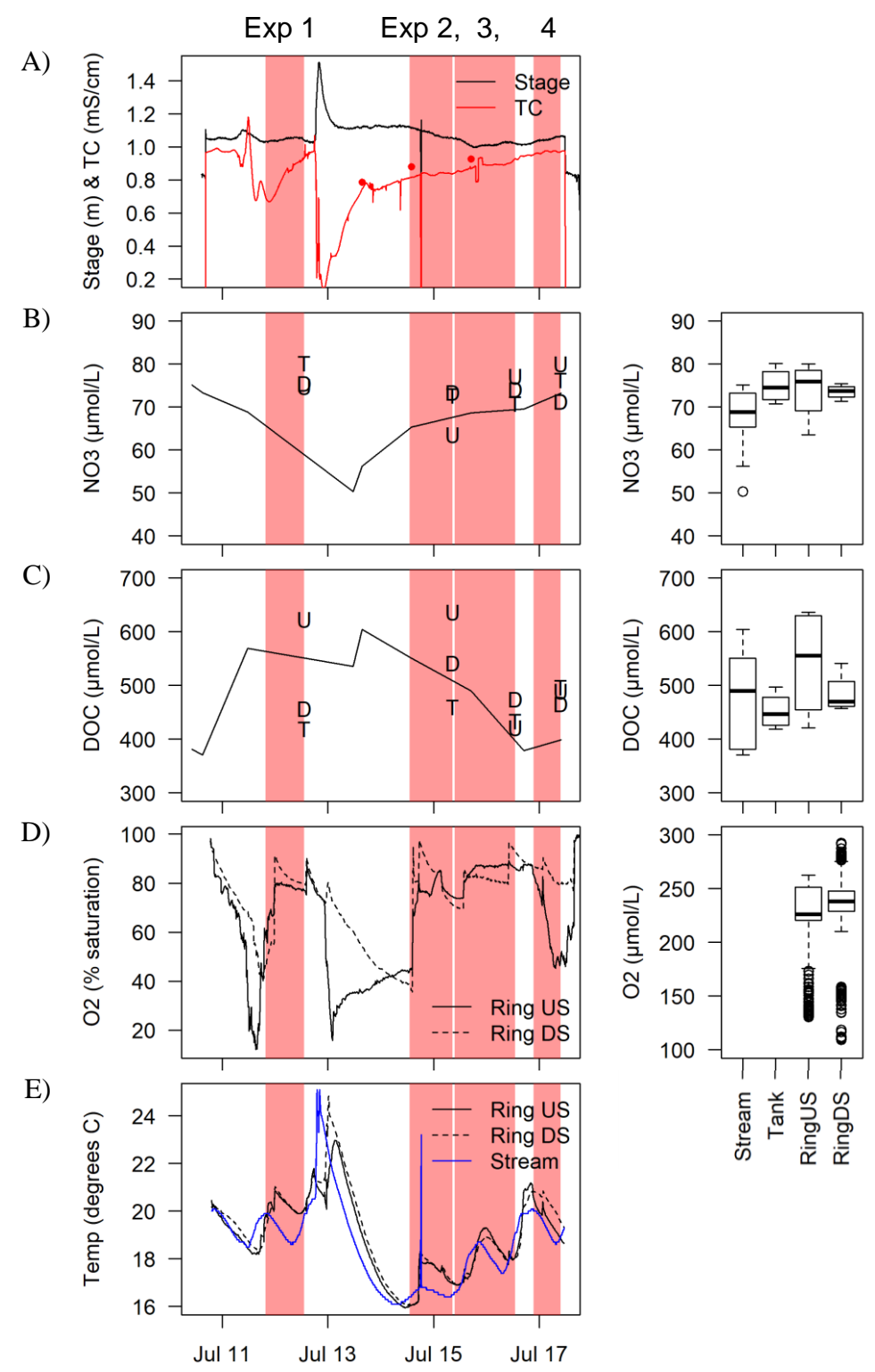


Figure 19: Stream stage and chemical conditions during sampling at Sawmill Brook. (A) Stage monitored at the site on Sawmill Brook over the study dates. Sampling periods of the four experiments are shown by red bars, with the commencement of each injection as the beginning of the bar and the end of sampling for that experiment as the end of the bar. Experiment order was 2 m/d, 3 m/d, 0.8 m/d, 1.2 m/d. Total conductivity (TC; not temperature corrected) from the

site surface water is also shown, with points showing spot-checks of TC with a handheld probe. (B) NO₃⁻ concentrations in the stream, shown by connected lines, and concentrations in the tank water ("T"), Ring US ("U") and Ring DS ("D"). Boxplots on the right show the median and interquartile range for samples collected in the stream, tanks, and rings. Whiskers are to the minimum and maximum. Points are outliers. (C) DOC concentrations as shown in panel C. (D) Oxygen (O₂) saturation and concentration are shown for the surface water from the two SWI rings. The boxplot shows O₂ during the sampling periods (red boxes). (E) Temperature as monitored at the stream stage site and within the two SWI rings.

3.3.2. Solute Removal with Depth

During each of the four hydrologic flux rate experiments, Rings US and DS showed similar behavior. The O₂ concentrations at all depths during Experiments 1-2 (higher fluxes of 3 and 2 m/d) remained greater than 50 μmol O₂/L (Figure 20). During Experiments 3-4 (lower fluxes of 1.2 and 0.8 m/d) porewaters were anoxic (<63 μmol O₂/L) at 5 cm and deeper, except for in ring DS at 0.8 m/d flux, where the 5 cm concentration was 28 μmol O₂/L but was 0.0 μmol O₂/L at 10 cm and deeper. Removal of NO₃- showed similar trends to O₂, with an average percent removal of 33% of the injection concentration for Experiments 1-2, and 79% for Experiments 3-4. Concentrations of DOC did not suggest strong removal, and concentrations increased by 34% on average from the injection concentration. Removal of DOC was only seen for the 3 m/d flux rate (Experiment 2), with 19% removal on average for the two rings.

When accounting for changing residence times with hydrologic flux, the linear removal rates of O₂ between 0 and 20 cm depths showed similar behavior between Experiments 1 and 2 and between Experiments 3 and 4 but increased with increasing residence times. Depth-integrated removal rates of O₂ decreased from 112 during Experiments 1-2 to 70.6 µmol O₂/L/h during Experiments 3-4 (Figure 21), but O₂ depletion occurred at very shallow depths in Experiments 3-4, and O₂ removal rates between 0 and 5 cm were 78% higher in Experiments 3-4. There were slight differences between rings US and DS, with 38% higher O₂ removal rates on average for ring DS than US for each flux rate. Removal rates of NO₃- were 7.7% higher for

Experiments 3-4 than Experiments 1-2 (Figure 21). In contrast to the trend between the two rings for O₂ removal, ring US had NO₃⁻ removal rates that were 47% higher than those in ring DS for each flux experiment, and the difference was most pronounced during Experiments 1-2 (i.e., shorter residence times), with 76% higher values than in ring DS on average, than for Experiments 3-4 (i.e., longer residence times), at only 29% higher than in ring DS (Figure 21).

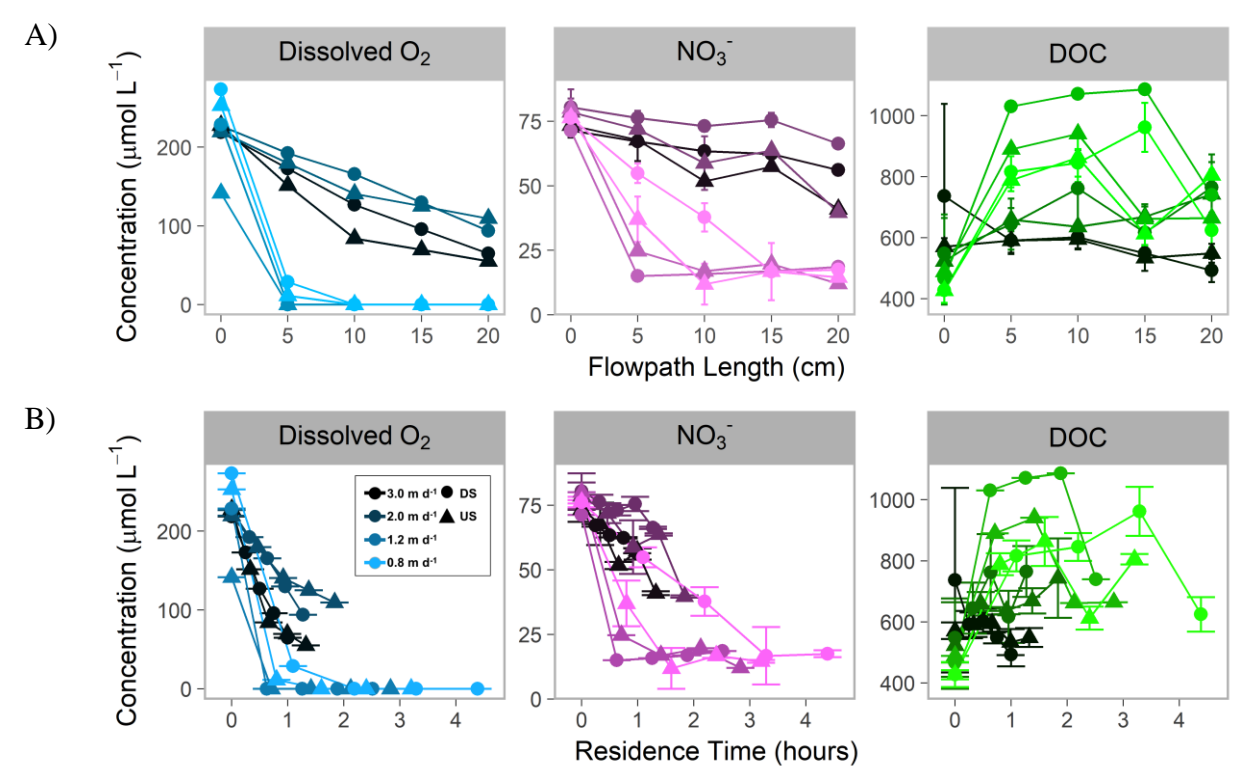


Figure 20: Concentration over depth and residence time from Sawmill Brook experiments. Concentrations of O₂, NO₃⁻, and DOC over flowpath length (A) and over porewater residence time (B). Symbols denote data from Rings US and DS. The color of each line and point denotes the flux rate (see inset legend in the lower left panel), where lighter shade denotes the lower flux rates. Error bars are the standard deviation of concentration when repeated samples were possible.

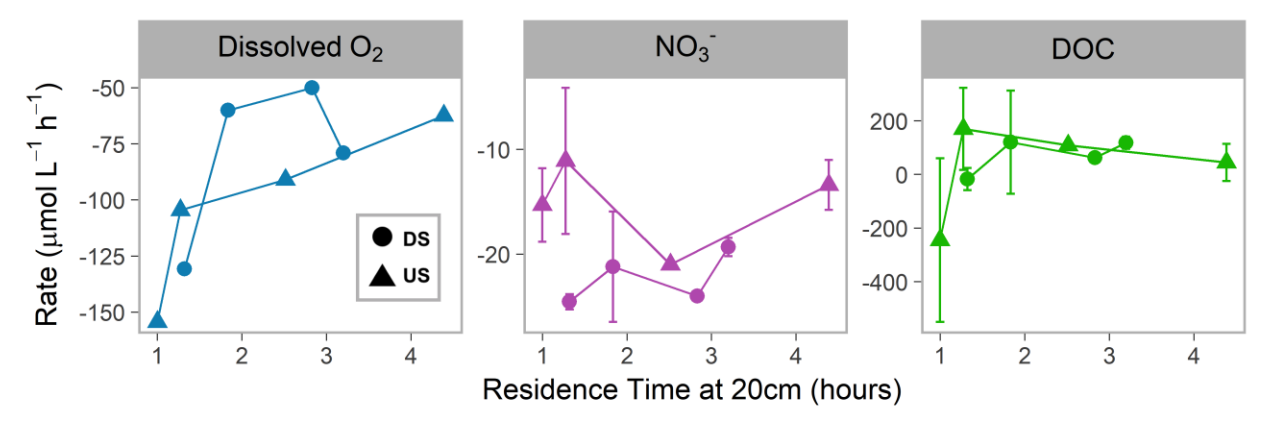


Figure 21: Removal rates for O₂, NO₃⁻, and DOC from the Sawmill Brook Experiments. Symbols denote ring US or DS. Error bars are based on the standard deviation of concentrations used in the rate calculations, where multiple samples are available. More negative values indicate increasing removal rates. Positive values indicate accumulation along the flowpath.

The NO₃⁻ tracing showed evidence for denitrification during each hydrologic flux rate experiment. The N_2 concentrations were on average $450 \pm 60 \mu mol N_2/L$, which would be predicted by water in equilibrium with the atmosphere at a pressure of 1 atm and a water temperature of 30°C (Weiss, 1970). Temperature measurements within the injection ring water, however, suggested that average temperature was 19.4 ± 2.4 °C during daytime hours (Figure 19). Temperatures during evening hours were warmer on average, at 20.4 ± 2.9 °C. There was no notable difference in temperature between the two rings (average difference 0.18 ± 0.45 °C). Water temperatures in the tanks were not monitored but are expected to have varied on a diel cycle, resulting in the potential for slight degassing, especially of O₂ and N₂, from tanks. However, O₂ concentrations measured continuously in the injection rings indicated that the aerators in the intermediate buckets and mixing upon entering the injection rings kept water stable and sufficiently oxygenated (229 \pm 31 μ mol O₂/L). Along each SWI flowpath, the N₂ concentrations increased on average 2.2%, however, in one instance, the concentration was observed to decrease by 11% in ring DS during Experiment 1 (2 m/d flux), and was observed to increase by 14% in ring US during Experiment 2 (3 m/d flux; Figure 22).

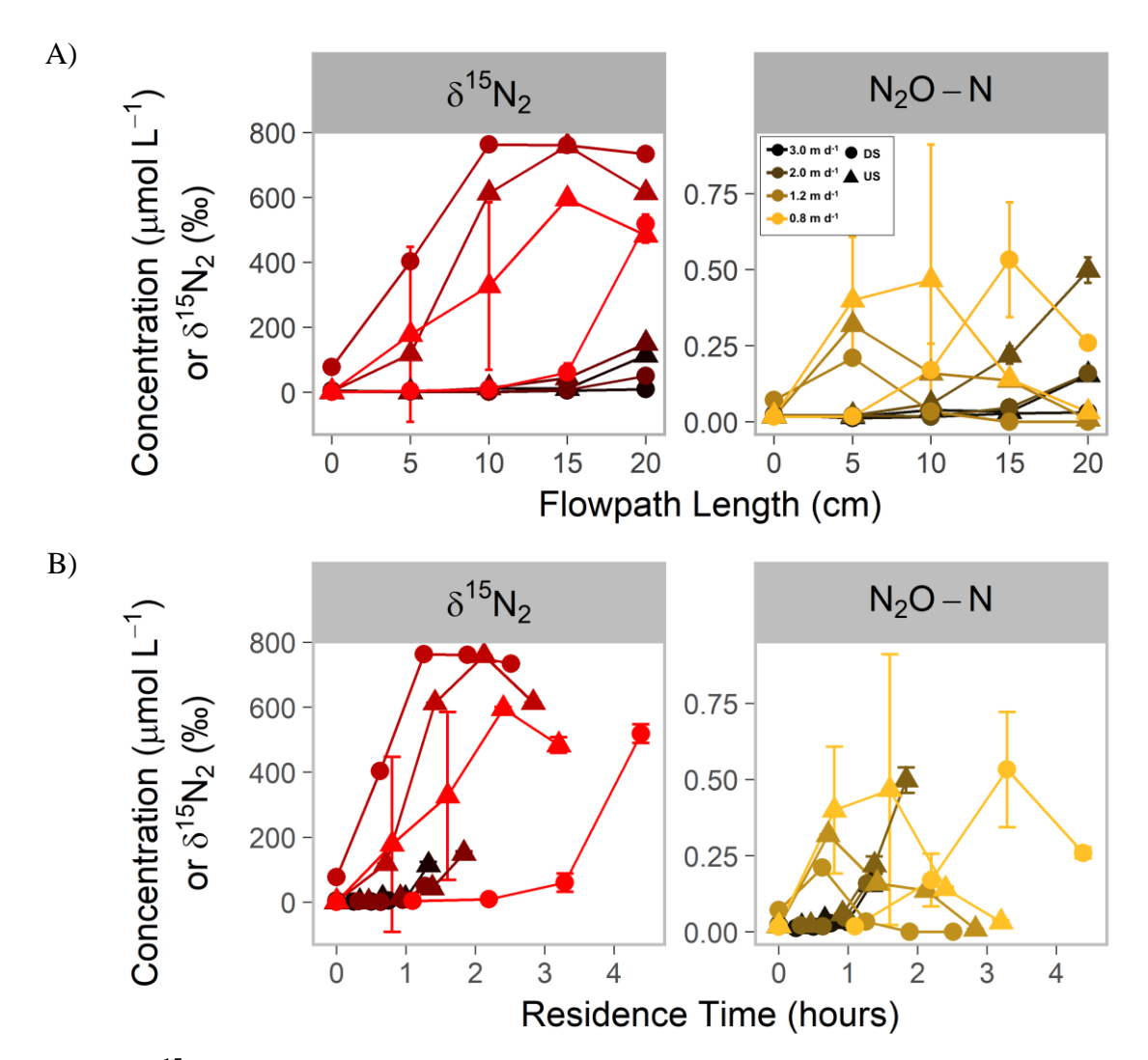


Figure 22: ¹⁵N tracer conditions of N₂ and concentrations of N₂O from Sawmill Brook Experiments. ¹⁵N isotopic enrichment of N₂ and concentrations of N₂O over flowpath length (A) and over porewater residence time (B). Symbols denote data from Rings US and DS. The color of each line and point denotes the flux rate, where lighter shade denotes the lower flux rates. Error bars are the standard deviation of concentration when repeated samples were possible.

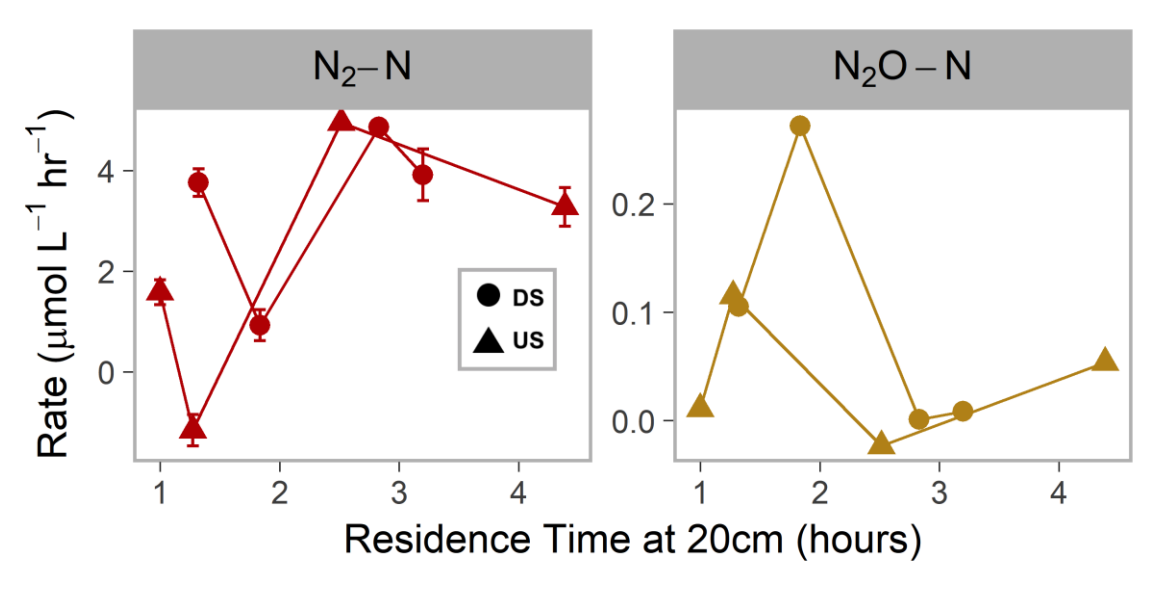


Figure 23: Production rates of N_2 and N_2O from Sawmill Brook Experiments. Symbols denote ring US or DS. Error bars are based on the standard deviation of concentrations used in the rate calculation, where multiple samples are available. Positive values indicate accumulation along the flowpath.

Despite relatively small changes in total dissolved N_2 mass, enrichment of $^{15}N_2$ was observed along each flowpath, especially for Experiments 3-4 (long residence times), with enrichment increasing to 0.494 atom % on average; higher than for Experiments 1-2 with an average of 0.374 atom %, which is closer to natural abundance of ^{15}N . In ring US for Experiments 1-2, $^{15}N_2$ was present at 20 cm depth with an abundance of 0.408 and 0.421 atom %, respectively (Figure 22). The same decrease in total N_2 mass along the flowpath for ring DS during Experiment 1 was reflected during the same experiment in a 6.8% decrease in $^{15}N_2$ mass. During Experiment 2 for both rings and Experiment 1 only for ring US, $^{15}N_2$ mass increased by 14% on average from 0 to 20 cm. The increase was larger for Experiments 3-4 for both rings, by 60% on average. These increases in $^{15}N_2$ mass are reflected in denitrification rates, which were on average 1.3 μ mol N_2 -N/L/h for Experiments 1-2, and 4.3 μ mol N_2 -N/L/h for Experiments 3-4 (Figure 23).

The N₂O concentrations increased with depth for all experiments (Figure 22).

Concentrations of N₂O closely mirrored ¹⁵N-N₂O enrichment patterns, which generally increased

from 1 to 7.5 atom % for most experiments, with the exception of ring DS during Experiment 2 (3 m/d flux) enrichment only rose to about 5 atom %, and during Experiment 4 (1.2 m/d flux) where enrichment decreased with depth from over 7 to below 1 atom % (Figure 22). Concentrations of N₂O were higher in ring US than ring DS for each experiment by 2.4-fold on average, and peak concentrations for each experiment were 4.9-fold higher on average in ring US. Concentrations of N₂O increased with depth for all experiments, between 0 and 20 cm, by 7fold on average. This increase with depth was greater for ring US, at a 7.9-fold average increase, than ring DS at a 6.1-fold average increase. Despite this, for Experiment 4 (1.2 m/d flux) in both rings, total N₂O concentrations decreased from 0 to 20 cm, however ¹⁵N-N₂O enrichment suggested that for ring US in Experiment 4 there was still net N₂O production via reduction of the injected ¹⁵NO₃- tracer. Production of N₂O via denitrification was highest for ring US in Experiment 1 at a rate of 0.27 µmol N₂O-N/L/h (Figure 23). For Experiments 2-4 for all rings and Experiment 1 only in ring DS, the N₂O production rate was on average $0.039 \pm 0.054 \,\mu\text{mol}$ N₂O-N/L/h. Rates were higher in ring US than in ring DS, at 2.3- and 9.5-fold higher for Experiments 1 and 2 (2 m/d and 3 m/d fluxes), respectively. The N₂O production rates for Experiments 3-4 were not substantially different between the two rings (5.8% difference on average). N₂O production rates were much lower during Experiments 1-2 than during 3-4, at 0.01 ± 0.06 and 0.13 ± 0.11 µmol N₂O-N/L/h, respectively. Although N₂O production rates were small, there were distinct patterns with depth for N₂O. For Experiments 1-2, the highest N₂O concentrations with depth for each experiment were at 20 cm. The ¹⁵N-N₂O enrichment peaked at 5 cm-depth for Experiment 4 (1.2 m/d flux), and at either 10 or 15 cm-depth for Experiment 3 (0.8 m/d flux). For specific 5 cm depth intervals within each of the injection rings, the maximum N₂O production rates were not substantially different between the averages of Experiments 1-2

and 3-4 (1.3% different). For Experiments 1-2, 5 cm interval production rates were highest in the deeper portion of the sediments, while the highest rates were in the shallowest depth interval for Experiments 3-4. The N₂O removal rates showed larger differences between Experiments 1-2 and 3-4, with the largest 5 cm-interval removal rates 27-fold higher on average for the Experiments 3-4 than for the Experiments 1-2.

Production of N_2 accounted for 14% of NO_3^- removal on average for Experiments 1-4, and production of N_2O accounted for 0.4% of NO_3^- removal on average. For production of N_2O , this percentage was higher in Experiments 1-2 (0.7%) than in Experiments 3-4 (0.09%), whereas for production of N_2 the reverse was true. During Experiments 1-2 production of N_2 accounted for 5% of NO_3^- removal, but this increased to 22% on average for Experiments 3-4. The proportion of NO_3^- removal accounted for by total denitrification ($N_2 + N_2O$) increased from 6% to 22% on average from Experiments 1-2 to Experiments 3-4. The estimated proportion of NO_3^- removal unaccounted for by denitrification then ranged from 75% (Experiment 3 ring DS) to 94% (Experiment 1 ring US).

3.3.3. Scaling by Residence Time

Residence times with depth for each experiment were calculated by assuming a uniform porewater velocity through the sediments for each experiment in each ring, which is possible given the constrained flow field within the ring. That velocity was calculated from the average of the injection and flush breakthrough curves of high conductivity water at both 10 and 20 cm depth in each ring. The total residence time of each ring, as the residence time from 0 to 20 cm depth, increased with decreasing flux rate. For ring US, total residence time increased approximately linearly with decreasing flux rate, while for ring DS total residence time increased exponentially with decreasing flux rate. For ring US, total residence times increased from 1.3 h

at 3 m/d flux to 3.2 h at 0.8 m/d flux, while for ring DS total residence times increased from 1.0 h to 4.4 h (Figure 24). A 3.7-fold decrease in flux resulted in a 2.5-fold increase in residence times in ring US, but in a 4.4-fold increase in ring DS. Assuming seepage flux is directly proportional to porewater velocity by a factor of the porosity, this exponential increase in residence times would be expected for a uniform porosity: as flux approaches zero, residence times will approach infinity.

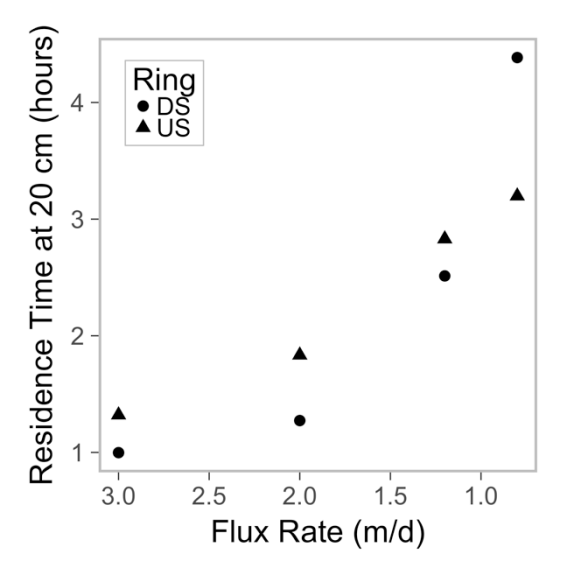


Figure 24: Residence time over flux rate in the Sawmill Brook experiments. Residence time is shown at 20 cm depth, or the bottom of the SWI flowpath, for each flux rate experiment.

In Experiments 1-2, with porewater residence times up to 2 h, O₂ concentrations remained in the oxic range (>16 μmol/L), whereas in Experiments 3-4, anoxia was achieved at residence times as early as 0.7 h (Figure 20). O₂ did not show a threshold response where after the same specific residence time, concentrations were fully anoxic (as in Briggs *et al.*, 2015). For NO₃-, removal was governed by different removal velocities (see Section 3.2.5) and increased with increasing porewater residence times. Concentrations of ¹⁵N-N₂ increased with residence time. Concentrations of N₂O and ¹⁵N-N₂O were higher at intermediate residence times, generally around 1 to 3 h, but for some experiments concentrations peaked earlier and decreased along the

flowpath, and, for ring DS during Experiment 3, concentration peaked at 3.3 h and then decreased only by half at 4.4 h.

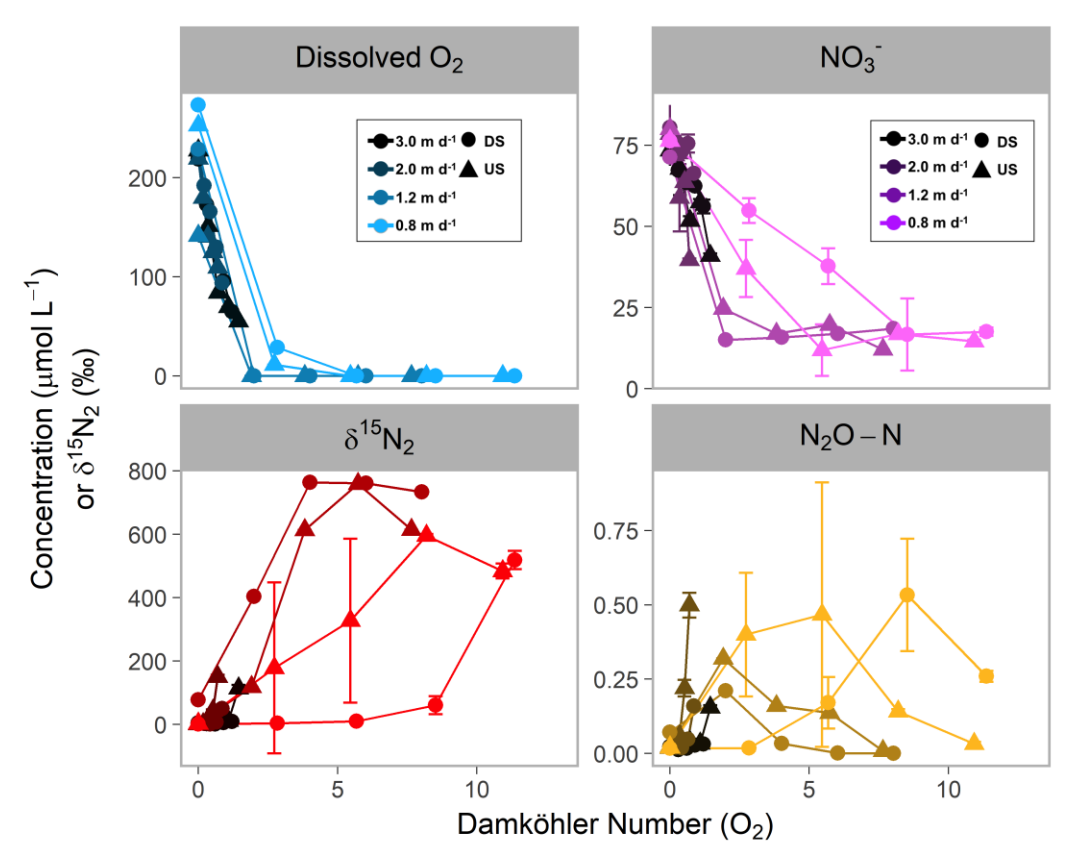


Figure 25: Concentrations over Damköhler number for O₂ from Sawmill Brook Experiments. Concentrations of O₂, NO₃⁻, N₂O, and δ^{15} N₂ over the Damköhler number for oxygen removal (Da_{O_2}), calculated for each ring in each experiment.

The Damköhler number (Da_{O_2}) was used as a nondimensional approach to scale residence times by the O_2 removal velocity, using Equation 10. The Da_{O_2} approach more clearly illustrates the threshold patterns in N processing rates. Average O_2 removal velocity was 3.5-fold higher for Experiments 3-4 than for Experiments 1-2. This resulted in compression of the O_2 concentrations for Experiments 1-2 in early Da_{O_2} space (Figure 25), with values up to 1.5, while Experiments 3-4 extended into Da_{O_2} values from 7.5 to 11.5. The O_2 concentrations, when scaled by Da_{O_2} , show a characteristic removal pattern, meaning that anoxia occurs after a

specific Da_{O_2} threshold. Da_{O_2} =1 means O_2 supply and demand timescales are in unity and larger values indicate conditions conducive to anoxia (Zarnetske *et al.*, 2012). Anoxia occurred at a threshold Da_{O_2} value =1.9, beyond which $^{15}N_2$ enrichment increased the most, along with decreases in NO_3^- concentrations. Removal velocities for NO_3^- were also calculated (Figure 26). Although removal velocities represented by a first-order reaction k value are generally thought to be more representative of biogeochemical processes in the SWI (Hedin *et al.*, 1998; Zarnetske *et al.*, 2012), we found that removal rates for NO_3^- as calculated by Lansdown *et al.* (2015) were appropriate representations of SWI function. The relationship between O_2 removal rates and removal velocities was less clear, hence examining the data in Da_{O_2} space.

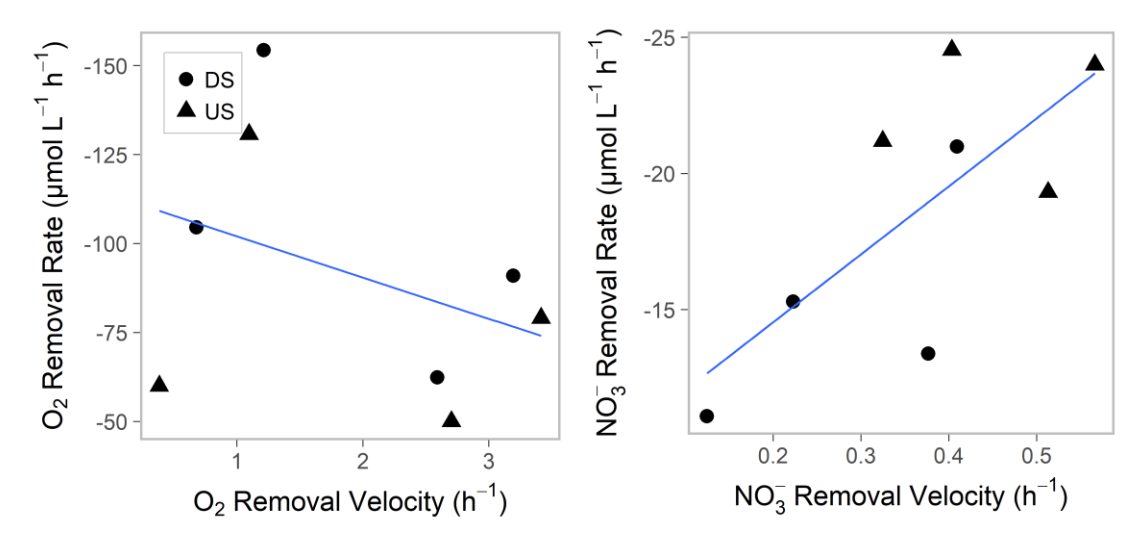


Figure 26: Removal rates over Removal Velocities for O₂ (left) and NO₃⁻ (right) from Sawmill Brook Experiments. Removal rates are reported as in Figure 21 and calculated in Section 2.2.5 and Removal velocities are calculated as in Section 3.2.5. Blue lines are linear regression lines. Circles are from ring DS and triangles are from ring US.

Resulting Da_{NO_3} values ranged from 0.16 to 0.59 for the Experiments 1-2, and from 1.03 to 1.65 for Experiments 3-4. The N₂O concentrations did not show a relationship to Da_{O_2} or Da_{NO_3} , as for each experiment the peak N₂O concentration occurred at an intermediate Da_{O_2} ranging from 0.7 to 8.5. The average peak N₂O concentration in both rings for Experiment 1 was

6% higher than the average peak concentration for Experiment 3, and the outflow was 3.4-fold higher in Experiment 1 versus Experiment 3. Thus, under the conditions of Experiment 1, with shorter residence times, there was a daily export of 948 μ mol N₂O-N/d per ring, which is 8.5-fold greater than the export for Experiment 3, which had the longest residence times.

3.4. Discussion

3.4.1. Biogeochemical Reaction Rates in the SWI Controlled by Residence Time

Our study shows that the biogeochemical function of the stream SWI, especially for NO₃⁻ removal, is controlled by residence time when reactant concentrations in input water are stable. Decreasing SWI hydrologic fluxes by 73% resulted in longer residence times, which increased removal of O₂ and NO₃ and increased rates of production of denitrification end-products (Figure 21, Figure 23). This same increase in NO₃ removal and denitrification rates with increasing residence times has been previously observed in laboratory perfusion column studies (Gu et al., 2007; Bourke et al., 2014; Liu et al., 2017), where controlled manipulations of hydrologic flux were paired with stable simulated river water influx chemistry. In our study, the removal rates of NO₃⁻ increased with increasing residence times as predicted by previous experimental and modeling studies (Hedin et al., 1998; Marzadri et al., 2011; Zarnetske et al., 2012; Quick et al., 2016). Unlike these previous studies that were unable to fully decouple biogeochemical (Hedin et al., 1998; Zarnetske et al., 2012) and hydrologic variability or conduct their work in field settings (Marzadri et al., 2011; Quick et al., 2016; Liu et al., 2017), we were able to clearly confirm and quantify the impact of variable residence time on the fate of O_2 and NO_3 in a stream SWI.

Overall, concentrations of NO₃⁻ decreased consistently once entering the SWI, showing no threshold response related to co-occurring oxic conditions. Removal of NO₃⁻ was greatest in

shallow sediment intervals (Figure 20), supporting previous findings in other SWI sediments that indicated that the very uppermost sediment interval is the most reactive for NO_3^- (Inwood *et al.*, 2007; Harvey *et al.*, 2015). Concentrations of O_2 and NO_3^- both showed declines with depth that were characteristic of a 1st order removal reaction, but the removal velocity was not constant across our experiments (Figure 20, Figure 26). Nitrate removal was consistently enhanced by increased residence times. Removal rates of NO_3^- , production rates of N_2 , and the proportion of removed NO_3^- explained by production of denitrification end-products (N_2 and N_2O) also increased when the SWI sediments were fully anoxic below 5 cm, which occurred during Experiments 3-4 (fluxes of 0.8 and 1.2 m/d). The proportion of NO_3^- removal accounted for by $N_2 + N_2O$ production increased with residence times, from 6% to 22% on average from Experiments 1-2 to Experiments 3-4. Still, up to 94% of the NO_3^- removal was unaccounted for by denitrification end-products across the experiments, suggesting alternative pathways for removal of NO_3^- in the SWI.

Biological assimilation may account for a large proportion of observed NO₃⁻ removal during our experiments. Our findings that most of NO₃⁻ removal was unaccounted for by denitrification has also been observed in most other studies in streams. For example, Lansdown *et al.* (2012) found that up to 87% of ¹⁵NO₃⁻ removal observed during sediment incubations could be accounted for by biological assimilation. Mulholland *et al.* (2008) also found that, across 72 streams, the total stream reach denitrification accounted for less than 16% of total NO₃⁻ removal at over half of their sites. Even controlled mesocosm studies, where there is a large degree of control and precision for the N budgets, have found that denitrification could not account for 40-70% of NO₃⁻ removal (Stelzer *et al.*, 2015). It is possible that once NO₃⁻ was assimilated into biomass, that N could be re-mineralized and ultimately denitrified (Seitzinger *et*

al., 2002; Hall Jr *et al.*, 2009). In addition, certain sulfur bacteria are known to be able to take up and store NO₃⁻ for later use in dissimilatory metabolic transformations (Burgin and Hamilton 2007). Unfortunately, measuring all these different N pools was outside of the scope of this work because this study was focused more on the complete N_r removal pathway of denitrification. Lastly, Wollheim *et al.* (2005) also show that at Sawmill Brook study site that, despite high N_R loading, 65-85% of N_R is retained in the catchment. Our study suggests, that the SWI of Sawmill Brook is effective at removing NO₃⁻, but that only a small fraction of the removal is likely due to immediate and direct denitrification in the top 20 cm of the SWI.

3.4.2. Role of Anoxic Microzones and POC

Interestingly, we documented large fluxes of both denitrified N₂ and N₂O from our studied sediments where porewater O₂ concentrations were bulk-oxic (>50 µmol O₂/L), adding to the growing list of studies documenting this phenomenon of anaerobic microbial metabolism occurring in bulk oxic conditions, as specifically related to leaf particulates in soils (Kravchenko *et al.*, 2017, 2018), and further implicating anoxic microzones as important denitrification sites in stream sediments (Triska *et al.*, 1993; Zarnetske *et al.*, 2011a; Harvey *et al.*, 2013; Briggs *et al.*, 2015; Kravchenko *et al.*, 2017). We also confirmed results from studies suggesting that N₂O emissions would peak at intermediate residence times in sediments (Firestone and Tiedje, 1979; Firestone *et al.*, 1980; Quick *et al.*, 2016; Liu *et al.*, 2017). Not only did N₂O concentrations peak at intermediate residence times in each depth profile (Figure 22), but N₂O production rates were also highest at intermediate system residence times, as in the 2 m/d flux rate experiments (Figure 23). During Experiment 1 (2 m/d flux rate), N₂O production represented the largest percentage of NO₃⁻ removal of any of the experiments, at 1.2%. In contrast, N₂ production was the highest proportion of NO₃⁻ removal during Experiments 3-4, at 22%. Despite higher NO₃⁻ removal rates

during Experiments 3-4, N₂O export was 7.7-fold higher from the rings during Experiments 1-2. N₂O export was also 10-fold higher on average from ring US than from ring DS. This corresponded with 53% higher NO₃⁻ removal rates on average in ring US for each flux rate, and with observations of woody debris and POC in the stream sediments beneath ring US.

It is unlikely that the POC in ring US contributed to much more DOC production, or contributed to increases in O₂ removal (Stelzer, 2015), because DOC concentrations showed accumulation on average along the flowpath, but no difference in accumulation between the rings. Buried POC in stream sediments have been shown to be important to enhancing microbial activity even when not contributing to higher DOC concentrations (Sobczak *et al.*, 1998).

Despite the POC in ring US, ring DS was observed to have O₂ removal rates 29% higher on average across the experimental flux rates. Instead, POC within the sediment matrix likely reduced the SWI porosity and thereby promoted the presence of reactive anoxic microzones (Sexstone *et al.*, 1985; Briggs *et al.*, 2015; Kaufman *et al.*, 2017; Kravchenko *et al.*, 2017), thus indirectly contributing to the higher NO₃⁻ removal and N₂O emissions.

During Experiment 1, the POC in the sediments of ring US may have leached the most labile forms of carbon first (Stelzer *et al.*, 2014) because this was the experiment with the largest hydrologic flux, however, from Experiment 1 to 2 O₂ removal rates increased by 73% for the two rings, suggesting O₂ removal was not limited by labile DOC supply via leaching of POC. N₂O production is known to be promoted by more recalcitrant DOC sources, where the reduction of N₂O to N₂ is limited by DOC supply, leading to N₂O export (Burford and Bremner, 1975; Quick *et al.*, 2016). This further suggests that the high production rates of N₂O during Experiment 1 were not due to DOC sources and were likely instead due to increased abundance of anoxic microsites. Based on the SWI pore-network model of Briggs *et al.* (2015), an increase in flux

rate (as in Experiment 2, increase from 2 to 3 m/d) will cause a decrease in the proportion of reactive less mobile porosity, specifically in the proportion of flow-dependent less mobile porosity (i.e., flux rate tends to directly correlate with the abundance of microzones). With fewer anoxic microsites, production of N₂O would decrease, as was observed in Experiment 2. With the onset of complete anoxia at depth in Experiments 3-4, the further reduction of N₂O to N₂ was not limited by reaction site abundance, and would be controlled at the flowpath scale by electron donor abundance (Betlach and Tiedje, 1981; Quick *et al.*, 2016). Production of N₂ was highest at the longest residence times (Figure 23), suggesting more complete denitrification (i.e., higher N₂/N₂O ratios) can be achieved with additional exposure time (Marzadri *et al.*, 2017).

Although we did not monitor porewater deeper than 20 cm along each flowpath, due to limitation of the experimental apparatus, these shallow vertical flowpaths produced by the rings provide an analogue for hyporheic flowpaths of comparable length or residence time. Contrary to the assumptions of many models incorporating hydrodynamics and biogeochemical processes (e.g., Marzadri *et al.*, 2014), denitrification was not inhibited in bulk-oxic sediments, and N₂O production can actually be highest from flowpaths of intermediate length (Quick *et al.*, 2016) that may be mostly bulk-oxic (Figure 23). This is a key finding that highlights N processing conditions that are poorly characterized or not even accounted for in current stream N and SWI studies and models.

3.4.3. Implications of Dynamic Stream Hydrology for N export

Variable flow events, such as those produced by storm induced runoff, have been shown to result in increased chemical mixing of stream SWIs (Zimmer and Lautz, 2014), however the net effect on SWI exchange flow is less clear, with some studies suggesting that exchange flow can either increase or decrease at higher stream discharges depending upon a large range of

hydrogeomorphic conditions in the stream sediment and reach (Wondzell and Swanson, 1996; Wondzell, 2011; Boano et al., 2014). Still other studies have documented no relationship between hyporheic exchange rates and discharge (Ward et al., 2012, 2016), and many studies have found large spatial variability in SWI flux around specific reach features (Lautz and Fanelli, 2008; Briggs et al., 2013; Smidt et al., 2015). As we saw from the hydrologic data from our experiments, there were different relationships between biogeochemical fluxes and residence times within our two SWI rings (Figure 24), and sometimes large disparities of O₂, NO₃⁻, and denitrification reaction rates at the same hydrologic flow-through rates (Figure 21, Figure 23, Figure 26). This heterogeneity has been the source of inquiry for several empirical models (Marzadri et al., 2014; Tonina et al., 2016) suggesting that heterogeneity of streambed and reach-scale morphology unto itself has a large influence on hydrologic residence time distributions as well as NO₃ removal and N₂O production. Recent modeling incorporating process-based particle-tracking simulations by Li et al. (2017) starts to address this role of different scales of heterogeneity by showing that spatial heterogeneity of SWI flows and exchanges with surface water can enhance both NO₃ removal and denitrification.

While it may be true that net SWI flow is relatively small compared to overall stream flow out of watersheds in all but the smallest and steepest stream reaches (Wondzell, 2011), our results show that even if a small fraction of SWI flowpaths achieves the appropriate balance of reaction and transport timescales, rates of NO₃⁻ removal and production of the potent greenhouse gas, N₂O, will be high. The existence of many SWI flow path with NO₃⁻ removal and N₂O production along stream reaches may explain the high levels of dissolved N₂O that have been previous observed at the reach scale (Mulholland *et al.*, 2008; Beaulieu *et al.*, 2011; Wollheim *et al.*, 2014). This conclusion has previously been suggested by Quick *et al.* (2016), appropriately

referencing a "Goldilocks' Zone" where the balance of the controlling timescales leads to flowpaths that are net exporters of N₂O, whereas flowpaths that are too short are generally not anoxic enough and thus not conducive to denitrification, and flowpaths that are too long become net consumers of N₂O. SWI exchange generally produces a power-law distribution of flowpath residence times (Haggerty et al., 2002; Cardenas, 2008; Sawyer and Cardenas, 2009), with a strong bias towards flowpaths of short residence times, but also a large tail of longer residence time flowpaths. These more abundant, shorter SWI flowpaths are generally dominated by oxic conditions (Baker et al., 2000a; Arnon et al., 2007), which has been assumed to lead to lower emissions of N₂O (Marzadri et al., 2011; Quick et al., 2016), but here we show that the highest N₂O emissions were observed in Experiment 1 in ring US under oxic conditions (>100 μmol O₂/L), equaling an export of 948 μmol N₂O-N/d. Thus, the range of porewater residence times and SWI conditions where net N₂O production is possible may be much wider than previously estimated. The role of residence time heterogeneity in increased N₂O production under oxic conditions would vary depending on streambed morphology, which we do not address with our small-scale studies (Boano et al., 2014; Tonina et al., 2016).

Sawmill Brook is a stream with heavily urbanized headwaters, and it has been recognized that these urbanized catchments have higher stream NO₃⁻ concentrations and N₂O emissions than catchments draining native or unmanaged successional vegetation (Mulholland *et al.*, 2008; Beaulieu *et al.*, 2011). Still, the role of urbanization in altering the physical flow regime in the stream and streambed has not yet been detangled from proposed influences of elevated N_R inputs. While we do not know the Nr effects of land use in Sawmill Brook, we do know that our study targeted streambed morphologies that were a direct result of road sand application in the catchment (Paul and Meyer, 2001; Finkenbine J. K. *et al.*, 2007), and it is not known how

denitrification in native sediments compares to altered, increasingly sandy, bed composition. Research on a comparable environment, where a once clay-bedded stream ended up with a new sandy bed originating from road sand application, found that benthic algal growth was inhibited by constant bed movement, and thus respiration was higher within the sediment than the benthic zone or water column (Atkinson *et al.*, 2008). Our study and that of Atkinson et al. (2008) highlight a potentially exciting research gap of how highly reactive SWI conditions are altered by human-introduced sand to stream channels.

3.5. Conclusions

The role of the SWI in NO₃ removal has been emphasized by other studies as being dependent on the interplay between reactant supply (e.g., buried POC) and transport timescales (Ocampo et al., 2006; Gu et al., 2007; Zarnetske et al., 2012). Similarly, riparian zones have also been emphasized as an important stream-sediment interface in facilitating NO₃ removal (Hedin et al., 1998; Vidon and Hill, 2004). This study found that under varying hydrologic conditions O₂ and NO₃⁻ removal were enhanced at lower hydrologic flow-through rates and thus longer hydrologic residence times. The shift towards longer residence times also resulted in increased N₂ production via denitrification (by 3.3-fold) and an increase in the proportion of NO₃⁻ removal accounted for by denitrification end-products (by 4.5-fold). N₂O production peaked at intermediate porewater residence times, and longer residence time flowpaths exhibited further reduction of N₂O to N₂, such that N₂O export also peaked at intermediate flux rates. N₂O export was 12-fold greater from two high flux rate experiments (3 and 2 m/d) than from two low flux rate experiments (1.2 and 0.8 m/d). N₂O export was also 2.5-fold greater for all experiments from the experimental ring underlain by sediments with POC and woody debris, as opposed to well sorted sands. These experiments also reveal measurable denitrification and N₂O production

in bulk-oxic sediments (as in Experiments 1-2), emphasizing the importance of less-mobile porosity and anoxic microzones in heterogeneous stream sediments. Models relying on bulk properties and threshold-type behavior of O_2 inhibition of denitrification should consider the role of anoxic microzones in contributing to increased N_2O emissions from streams. Since these experiments maintained constant inflow chemistry, we are able to definitively show that hydrologic residence time is an important control on SWI biogeochemical reaction rates with respect to N transformations, an important function of the SWI that affects NO_3 - transport to downstream groundwaters and surface waters.

CHAPTER 4: SYNTHESIS & IMPLICATIONS

This thesis focused on the role of the sediment-water interface (SWI) in processing of nitrogen (N) across freshwater landscapes. The central research questions addressed in Chapters 2 and 3 were: 1) how do changing concentrations of dissolved organic carbon (DOC) and nitrate (NO₃⁻) influence NO₃⁻ removal in the SWI; and 2) how do hydrologic conditions (downwelling rates) change residence times along a SWI flowpath and affect rates of removal of oxygen (O₂), DOC, and NO₃-? To address these questions, two field studies were conducted during the summers of 2016 and 2017. Chapter 2 outlines experiments conducted in Snake Pond, Massachusetts, where I manipulated both reactant chemistry and hydrologic residence times entering vertical flowpaths through the lakebed SWI sediments within open-bottom mesocosms. I found that when NO₃⁻ and DOC abundance were varied in the SWI sediments, changes in hydrologic residence time actually had the largest effect on SWI N processing (NO₃⁻ removal and denitrification), not the abundance of NO₃⁻ and DOC. Longer residence times resulted in increased O₂, DOC, and NO₃⁻ removal, as well as denitrification and nitrous oxide (N₂O) production. While the Snake Pond experiments described in Chapter 2 explored the relationships between NO₃⁻ and DOC concentrations and NO₃⁻ removal rates in a lentic sediment, subsequent experiments conducted in Sawmill Brook, MA, and described in Chapter 3, solely explored how hydrologic flow-through affected biogeochemical function, and specifically NO₃ removal, in a lotic setting. The results of the Sawmill Brook experiments show that NO₃ removal does clearly increase with hydrologic residence times, with longer residence times promoting increased NO₃⁻ removal. While O₂ removal increased with residence time, NO₃⁻ removal and denitrification occurred frequently in oxic conditions before O₂ removal was complete along flowpaths. This implicates anoxic microzones providing embedded anaerobic processing in otherwise bulk oxic

SWI porewater. Furthermore, while NO_3^- removal rates were highest at long residence times, shorter residence times where bulk porewater was oxic resulted in the largest production and export of N_2O from the SWI sediments at Sawmill Brook.

Results from the Snake Pond Experiments (Chapter 2) also highlighted the role of particulate organic carbon (POC) in facilitating O₂ and NO₃⁻ removal, including via denitrification (Stelzer *et al.*, 2015). In other studies POC has been highlighted as supplying an additional DOC source, based on budgets constructed for O₂ and NO₃⁻ removal and molar ratios of those reactions (Findlay and Sobczak, 1996). These experiments corroborated findings that POC abundance decreased with depth (Inwood *et al.*, 2007; Harvey *et al.*, 2015), and this had the effect of highly reactive shallow sediments, with less modification with depth, especially under anoxic conditions. The Sawmill Brook Experiments (Chapter 3) targeted two sediment types (one with and one without abundant POC) with two identical experimental rings and the same hydrologic flow-through rates, and found different relationships between flow-through and residence time in each ring, as well as much higher NO₃⁻ removal and N₂O production in sediments with the most POC. Thus, these experiments indicate that POC can play a role as a source of DOC for reactions, but also a modifier of hydrologic flux rates, which can either promote or inhibit other controls on N processing in the SWI.

By exploring the change in NO₃⁻ removal and denitrification rates as a function of reactant (NO₃⁻ and DOC) concentrations in the Snake Pond experiments, and by solely manipulating flow-through rates in the Sawmill Brook experiments, the relative importance of biogeochemical and hydrologic factors was directly interrogated. Overall, I found that modifications of hydrologic flux in these two distinct SWIs had the largest effect O₂ and NO₃⁻ removal, denitrification, and N₂O production rates – more than increasing the concentrations of

NO₃⁻ and labile DOC. The results presented in Chapters 2 and 3 show that relatively small reductions in hydrologic flux (40-70%) resulted in large increases in rates of processes such as denitrification (700-4000%). With DOC and NO₃⁻ abundance limitations removed, hydrologic residence time is the dominant control on SWI biogeochemical functions that are driven by solutes in water moving through the SWI.

The results of this thesis raise important points to be addressed in future SWI studies. Many similar research questions to those addressed here concerning the role of chemical versus hydrologic controls have been addressed through controlled column studies (Gu *et al.*, 2007; Bourke *et al.*, 2014; Quick *et al.*, 2016; Liu *et al.*, 2017) and mesocosm experiments (Sobczak *et al.*, 2003; Stelzer *et al.*, 2014, 2015; Kurz *et al.*, 2017). The methods used in this thesis present some advances over these previous experiments, in that I have independently manipulated both chemical and hydrologic conditions in SWI sediments *in situ*. While my experiments have highlighted that controlled changes in both chemical inputs and hydrologic conditions resulted in changes in SWI function, other research questions have yet to be addressed. Specifically:

- 1) How does the naturally-occurring gradient of DOC quality (lability) affect NO₃⁻ removal and N₂O production? Decreased DOC lability was hypothesized to result in increased N₂O production by incomplete denitrification (Quick *et al.*, 2016), but this was not substantiated by qualitative measurements of DOC lability, such as spectrophotometric analysis (McKnight *et al.*, 2001; Cory *et al.*, 2011).
- 2) How do seasonal changes in DOC quality, paired with hydrologic variability in stage or flow, result in changing SWI function (Stoliker *et al.*, 2016)? While my experiments addressed the role of hydrologic residence time in NO₃⁻ processing in the absence of DOC abundance limitations, determining how these two controls interact on a seasonal

- basis requires longer-term sampling. It is also not known if microbial community composition in a natural setting responds to these controls over these time scales (Storey *et al.*, 1999; Li *et al.*, 2017; Kim *et al.*, 2018).
- 3) What is the scaling nature of the importance of less-mobile porosity in contributing to the abundance of anoxic microsites in SWI sediments under varying flow regimes (Briggs *et al.*, 2015)? These experiments identify that our studied SWI sediments were large sources of N₂O under fully oxic conditions, implicating anoxic microzones as important for N₂O production.
- 4) What was the importance of POC in contributing to N₂O production? POC can play a role as a DOC source to fuel aerobic and anaerobic respiration. However, it may also be possible that it impedes convective flow and thereby facilities diffusion-dominated transport and the development of anoxic microzones (Sawyer, 2015). There was also a large disparity in the hydrologic flow-through rates achieved within the rings with the same hydraulic head conditions, which implicates that the large fraction of POC in the sandy sediment of one ring played a role in regulating overall flow conditions through the SWI.
- 5) How does human alteration of the shallow SWI in urban environments, specifically through increased erosion and contribution of non-native sandy sediment such as from road sand application (Atkinson *et al.*, 2008), alter SWI biogeochemical function? Further, can we disentangle the role of the physical alteration of SWI sediments and residence time distributions from anthropogenic N loading in urban catchments (Wollheim *et al.*, 2005; Mulholland *et al.*, 2008), and which control is important for N₂O emissions from streams (Beaulieu *et al.*, 2011)?

APPENDICES

APPENDIX A

2016 Snake Pond Sampling Data

Table 4: Tabulated data from Figure 12. Concentrations are as either μ mol/L or nmol/L. Experiment is listed, with A for Ambient or the experiment number. Type is the mean with standard deviation of points in parentheses, when more than one measurement was available.

Exp	Depth	Time	N ₂	X ¹⁵ N ₂	N ₂ O	X ¹⁵ _{N2} O	X ¹⁵ NO ₃
r	(cm)	(h)	μM	%	nM	%	%
amb	0	0	414	0.366	8.97	0.429	0.379
			(0.933)	(5.26e-05)	(1.35)	(0.00161)	(0.00856)
amb	1.5	0.9	422	0.366	8.55	0.42	0.37
			(32.2)	(1.16e-05)	(0.706)	(0.00731)	(0.000248)
amb	7	4.2	417 (0)	0.366 (0)	7.35 (0)	0.408 (0)	0.367 (0)
amb	12	7.2	400 (0)	0.366 (0)	2.01 (0)	0.45 (0)	0.37 (0)
amb	18	10.8	404 (0)	0.366 (0)	1.64 (0)	0.497 (0)	0.386 (0)
1	0	0	NA	NA	NA	NA	NA
1	9.5	0.52	402	0.366	6.23	0.536	5.5 (0.905)
			(22.7)	(9.66e-05)	(1.51)	(0.0225)	
1	14.5	0.793	400	0.366 (6.4e-	7.06	0.432	0.978
			(13.5)	05)	(0.694)	(0.0409)	(0.182)
1	19.5	1.07	391	0.366	9.18	1.49	5.11 (1.97)
			(8.86)	(3.29e-05)	(0.921)	(0.182)	
2	0	0	NA	NA	NA	NA	NA
2	9.5	0.506	431	0.367	10.1	1.09	4.07
			(39.1)	(1.87e-05)	(0.999)	(0.152)	(0.054)
2	14.5	0.773	429	0.367	14.7	1.94	4.08
			(5.91)	(5.62e-05)	(1.69)	(0.272)	(0.0403)
2	19.5	1.04	411	0.367	10.5	1.52	4.11
			(4.94)	(1.07e-05)	(0.651)	(0.0954)	(0.0488)
3	0	0	386 (0)	0.367 (0)	0 (0)	2.47 (0)	3.92 (0)
3	9.5	0.49	474	0.367	4.82	1.18	3.84
		0.740	(8.18)	(6.65e-05)	(4.06)	(0.286)	(0.00257)
3	14.5	0.748	459	0.368	7.73 (3.4)	1.38	3.84
2	10.5	1.01	(30.4)	(4.55e-05)	0.00	(0.0241)	(0.00788)
3	19.5	1.01	427 (16)	0.367	9.88	1.14	3.84
4	0	0	0 (0)	(5.32e-05)	(0.584)	(0.0823)	(0.000759)
4	0	0	0 (0)	0 (0)	0 (0)	0 (0)	3.92 (0)
4	9.5	0.474	396	0.367	10.1 (1.6)	1.23	3.85
	145	0.724	(4.02)	(0.00012)	26.2	(0.259)	(0.00358)
4	14.5	0.724	416	0.37 (0.000993)	36.3 (31.8)	2.62 (0.763)	3.85
4	19.5	0.973	(25.5) 404 (6.2)	0.367	66.5	3.35	(0.00246)
4	17.3	0.973	+04 (0.2)	(0.000165)	(27.1)	(0.193)	(0.0044)
5	0	0	0 (0)	0.000103)	0 (0)	0 (0)	3.93 (0)
5	9.5	0.747	474	0.532	12.6	2.42	
)	7.3	0.747	(22.4)	(0.0596)	(15.9)	(0.662)	2.28 (1.32)
	1	l .	(44.4)	(0.0270)	(13.7)	(0.004)	j

Table 4 (cont'd)

5	14.5	1.14	431	0.631	38.5	2.42 (1.27)	1.31 (1.22)
			(21.1)	(0.105)	(53.9)		,
5	19.5	1.53	433	0.778	2140	3.92	3.86
			(24.9)	(0.0435)	(291)	(0.0015)	(0.0444)
Eve	Depth	Time	NO ₃ -	O_2	С	SO ₄ ²⁻	NO ₂ -
Exp	(cm)	(h)	μM	μM	μM	μM	μM
amb	0	0	1.04	231 (0)	222 (45.1)	54.1	0 (0)
			(0.0673)			(0.393)	
amb	1.5	0.9	1.2	230 (0.442)	166 (4.92)	54 (0.994)	0 (0)
			(0.0824)				
amb	7	4.2	1.31 (0)	10.9 (0)	123 (0)	53.5 (0)	0 (0)
amb	12	7.2	1.05 (0)	14.4 (0)	116 (0)	53 (0)	0 (0)
amb	18	10.8	1.05 (0)	35.6 (0)	107 (0)	56.2 (0)	0 (0)
1	0	0	NA	NA	NA	NA	NA
1	9.5	0.52	3.65	225 (1.7)	253 (7.92)	54.5	0 (0)
			(3.55)			(0.484)	
1	14.5	0.793	4.36	170 (1.38)	238 (9.87)	54.5	0 (0)
			(3.35)			(0.449)	
1	19.5	1.07	3.97	154 (3.76)	237 (16)	54.9	0 (0)
			(0.947)			(0.306)	
2	0	0	NA	NA	NA	NA	NA
2	9.5	0.506	180	225 (1.84)	226 (6.25)	53.5	0 (0)
			(4.04)			(0.888)	0 (0)
2	14.5	0.773	176	148 (3.68)	219 (7.45)	53.6 (0.19)	0 (0)
2	10.7	1.04	(2.98)	150 (7.02)	100 (5.16)	7.4.1	0 (0)
2	19.5	1.04	183	159 (7.83)	188 (5.16)	54.1	0 (0)
2	0	0	(4.72)	0 (0)	269 (0)	(0.143)	0 (0)
3	0	0	164 (0)	0 (0)	368 (0)	52.7 (0)	0 (0)
3	9.5	0.49	154	236 (5.45)	253 (27)	52.5 (1.35)	0 (0)
3	14.5	0.748	(3.42)	108 (2.64)	250 (38.1)	52.4	0 (0)
3	14.5	0.748	(4.06)	100 (2.04)	230 (36.1)	(0.797)	0 (0)
3	19.5	1.01	158 (2.8)	123 (0.895)	362 (33.6)	54 (0.313)	0 (0)
4	0	0	252 (0)	0 (0)	684 (0)	50.8 (0)	1.47 (0)
4	9.5	0.474	177	195 (4.26)	310 (4.4)	46.6 (11.3)	2.42
4	9.3	0.474	(1.93)	193 (4.20)	310 (4.4)	40.0 (11.3)	(0.215)
4	14.5	0.724	164	8.15 (3.66)	279 (58.1)	52.3	4.29 (1.86)
'	11.5	0.,2,	(5.91)	3.13 (3.00)	277 (30.1)	(0.871)	25 (1.00)
4	19.5	0.973	159	4.35 (0.281)	544 (65.3)	52.9 (1.21)	12.7 (3.91)
			(3.43)		(/		()
5	0	0	798 (0)	0 (0)	1610 (0)	45.7 (0)	19.3 (0)

Table 4 (cont'd)

5	9.5	0.747	27.9	197 (10)	326 (9.63)	50.2	0 (0)
			(23.7)			(0.929)	
5	14.5	1.14	27 (23)	4.32	302	50.6	0 (0)
				(0.0177)	(0.307)	(0.445)	
5	19.5	1.53	30 (22.4)	4.5	576 (53.8)	62.7 (1.58)	25 (5.45)
				(0.00766)			

Table 5: Tabulated data from Figure 13, as well as data for SO_4^{2-} and NO_2^{-} . Rates are calculated as in Section 2.2.5. For the ambient profile, rates are calculated between 0 and 18 cm depth. For gases $(O_2, N_2, \text{ and } N_2O)$, rates are between 9.5 and 19.5 cm depths. For NO_3^{-} and DOC, rates are calculated between 9.5 and 19.5 cm for Experiments 1-2, and between 0 and 19.5

cm for Experiments 3-5. Standard deviation is in parentheses.

	em for Emperations & &. Standard deviation is in parentileses.								
	N ₂ -N	N ₂ O-N	NO ₃ -	O_2	DOC	SO_4^{2-}	NO_2		
	$(\mu M/h)$	(nM/h)	(µM/h)	$(\mu M/h)$	$(\mu M/h)$	$(\mu M/h)$	$(\mu M/h)$		
Ambient	-0.889	-0.741	0.000719	-18.1	-10.6	0.193	0		
Conditions	(0.020)	(0.018)	(0.0673)	(0.0)	(45.1)	(0.393)	(0)		
Exp 1:	-1.36	3.46	0.596	-130	-29.8	0.849	0		
15 N	(0.09)	(0.03)	(3.67)	(4)	(17.8)	(0.572)	(0)		
Exp 2:	-3.18	2.24	5.95	-123	-72.0	1.22	0		
NO_3	(0.15)	(0.03)	(6.21)	(8)	(8.1)	(0.90)	(0)		
Exp 3:	-8.59	2.44	-6.36	-219	-5.2	1.3	0		
N+C	(0.07)	(0.06)	(2.8)	(6)	(33.6)	(0.3)	(0)		
Exp 4:	1.83	111	-96.1	-381	-144	2.21	11.5		
N++C	(0.03)	(1)	(3.4)	(4)	(65)	(1.21)	(3.9)		
Exp 5:	46.8	4660	-501	-245	-675	11.1	3.71		
Incr. R _T	(0.5)	(10)	(22)	(10)	(54)	(1.6)	(5.45)		

Table 6: Sediment core data from Snake Pond. Also including Loss on Ignition results from Figure 11.

<u> </u>				
Depth Interval	Dry Sediment	Porosity	Loss on	Sediment POC (g
(cm)	Mass (g)	(%)	Ignition (%)	loss/cm3)
0-1	39.0	26.7	0.477	0.0126
1-2	36.1	26.7	0.428	0.0113
2-3	34.2	28.7	0.448	0.0119
3-5	69.7	27.4	0.408	0.0108
5-7	69.7	35.2	0.384	0.0102
7-9	65.0	32.2	0.428	0.0113
9-11	67.2	29.9	0.404	0.0107

APPENDIX B

2017 Sawmill Brook Experimental Data

Table 7: Tabulated data from Figure 20 and Figure 22. Concentrations are as either μ mol/L or nmol/L. Experiment is listed, with the flux rate and ring (US or DS). Type is the mean with standard deviation of points in parentheses, when more than one measurement was available.

Evn	Depth	Time	N_2	$X^{15}_{N_2}$	N ₂ O	X ¹⁵ _{N2} O
Exp	(cm)	(h)	μM	%	nM	% ~
3 m/d US	0	0	384 (44)	0.367 (3.25e-05)	19.7 (0.557)	1.38 (0.012)
3 m/d US	5	0.33	421 (34.8)	0.367 (8.68e-06)	17.3 (1.08)	1.63 (0.0413)
3 m/d US	10	0.66	414 (65.6)	0.371 (0.000209)	39.4 (2.18)	4.91 (0.0214)
3 m/d US	15	0.991	408 (13.8)	0.37 (9.09e-05)	33.5 (0.268)	4.15 (0.0217)
3 m/d US	20	1.32	440 (56.8)	0.408 (0.00383)	155 (7.52)	7.08 (0.0115)
3 m/d DS	0	0	398 (47.5)	0.368 (0.00237)	23.4 (8.08)	1.98 (1.57)
3 m/d DS	5	0.249	423 (32)	0.367 (1.86e-05)	12.8 (6.88)	1.51 (0.0108)
3 m/d DS	10	0.499	426 (60.2)	0.367 (3.31e-05)	17.2 (0.409)	1.53 (0.027)
3 m/d DS	15	0.748	445 (60.2)	0.368 (2.41e-05)	27.8 (0.268)	3.65 (0.0252)
3 m/d DS	20	0.998	430 (48.7)	0.37 (9.11e-05)	31.5 (2.18)	4.53 (0.0923)
2 m/d US	0	0	452 (46.4)	0.367 (1.94e-05)	23.2 (2.46)	0.621 (0.0357)
2 m/d US	5	0.458	423 (10.9)	0.367 (2.48e-05)	21.5 (0.568)	0.884 (0.0197)
2 m/d US	10	0.917	354 (20)	0.371 (5.72e-05)	59.4 (0)	5.09 (0.0269)
2 m/d US	15	1.38	342 (25.5)	0.382 (0.00115)	220 (28.2)	6.95 (0.15)
2 m/d US	20	1.83	424 (62.8)	0.421 (0.00215)	499 (41.8)	7.49 (0.0136)
2 m/d DS	0	0	439 (81.9)	0.367 (3.08e-05)	20.1 (0.757)	0.624 (0.19)
2 m/d DS	5	0.318	468 (0.91)	0.367 (5.22e-05)	21.3 (0.568)	1.27 (0.0849)
2 m/d DS	10	0.637	364 (46.4)	0.367 (3.64e-05)	18.7 (0.379)	0.658 (0.00103)
2 m/d DS	15	0.955	369 (30.9)	0.369 (0.000109)	47.2 (1.33)	4.57 (0.0672)
2 m/d DS	20	1.27	390 (20)	0.385 (0.000398)	159 (9.28)	6.97 (0.0117)
1.2 m/d US	0	0	557 (0)	0.368 (0)	18.7 (0)	1.85 (0)
1.2 m/d US	5	0.708	581 (0)	0.41 (0)	319 (0)	8.61 (0)
1.2 m/d US	10	1.42	489 (0)	0.59 (0)	160 (0)	8.56 (0)
1.2 m/d US	15	2.12	470 (0)	0.643 (0)	137 (0)	8.64 (0)
1.2 m/d US	20	2.83	555 (0)	0.59 (0)	8.83 (0)	6.88 (0)
1.2 m/d DS	0	0	483 (0)	0.395 (0)	71.7 (0)	6.88 (0)
1.2 m/d DS	5	0.628	524 (0)	0.513 (0)	211 (0)	6.55 (0)
1.2 m/d DS	10	1.26	614 (0)	0.644 (0)	33.7 (0)	6.92 (0)
1.2 m/d DS	15	1.88	505 (0)	0.643 (0)	0.803 (0)	2.34 (0)
1.2 m/d DS	20	2.51	467 (0)	0.633 (0)	0.268 (0)	0.657 (0)
0.8 m/d US	0	0	495 (50.5)	0.367 (6.24e-05)	21 (0.674)	0.919 (0.00892)
0.8 m/d US	5	0.8	563 (32.4)	0.431 (0.0982)	400 (208)	7.4 (0.117)
0.8 m/d US	10	1.6	525 (96.9)	0.486 (0.0941)	467 (445)	7.5 (0.0467)

Table 7 (cont'd)

0.8 m/d US	15	2.4	479 (80.3)	0.583 (0.00197)	142 (7.35)	7.61 (0.00828)
0.8 m/d US	20	3.2	516 (86.5)	0.543 (0.00867)	32.5 (6.47)	7.28 (0.113)
0.8 m/d DS	0	0	451 (3.64)	0.367 (0.000252)	17.3 (3.45)	0.916 (0.197)
0.8 m/d DS	5	1.1	455 (29.6)	0.368 (0.000121)	17.9 (8.95)	3.59 (0.368)
0.8 m/d DS	10	2.19	486 (68.4)	0.37 (0.00104)	170 (86.6)	6.59 (0.552)
0.8 m/d DS	15	3.29	509 (76.6)	0.388 (0.0104)	533 (189)	7.18 (0.0766)
0.8 m/d DS	20	4.38	502 (75.8)	0.555 (0.0105)	259 (18.4)	7.23 (0.021)
Exp	Depth	Time	NO ₃ -	X ¹⁵ _{NO₃}	O_2	С
	(cm)	(h)	μM	%	μM	μM
	_	_				
3 m/d US	0	0	73.4 (0.161)	7.69 (0.453)	228 (0)	571 (27.2)
3 m/d US	5	0.33	67.8 (8.21)	7.64 (0.172)	151 (0)	591 (40)
3 m/d US	10	0.66	51.7 (1.39)	7.61 (0.097)	84.1 (0)	595 (29.8)
3 m/d US	15	0.991	57.4 (1.01)	7.69 (0.0659)	69.5 (0)	533 (42.4)
3 m/d US	20	1.32	41 (0.703)	7.6 (0.156)	55 (0)	549 (31.2)
3 m/d DS	0	0	71.4 (2.78)	7.92 (0.0581)	219 (0)	737 (302)
3 m/d DS	5	0.249	67.2 (0.518)	7.38 (0.0292)	173 (0)	591 (44.6)
3 m/d DS	10	0.499	63.4 (0.838)	7.37 (0.0309)	127 (0)	602 (40.8)
3 m/d DS	15	0.748	62.4 (0.246)	7.36 (0.0195)	95.8 (0)	549 (19)
3 m/d DS	20	0.998	56.1 (2.13)	6.93 (0.752)	64.7 (0)	492 (38.3)
2 m/d US	0	0	78.5 (5.25)	7.45 (0.784)	219 (0)	522 (142)
2 m/d US	5	0.458	71.9 (3.88)	7.77 (0.0386)	180 (0)	659 (38.3)
2 m/d US	10	0.917	58.8 (10.4)	7.62 (0.147)	141 (0)	636 (11.8)
2 m/d US	15	1.38	63.7 (0.456)	7.78 (0.0347)	125 (0)	669 (41.2)
2 m/d US	20	1.83	39.7 (0.456)	7.69 (0.0259)	109 (0)	743 (130)
2 m/d DS	0	0	80.4 (6.96)	7.47 (0.827)	227 (0)	548 (128)
2 m/d DS	5	0.318	76.3 (2.74)	7.5 (0.0266)	192 (0)	644 (83.6)
2 m/d DS	10	0.637	73.1 (2.05)	7.49 (0.0495)	166 (0)	762 (126)
2 m/d DS	15	0.955	75.5 (2.74)	7.44 (0.0403)	130 (0)	617 (85.4)
2 m/d DS	20	1.27	66.3 (0.456)	7.42 (0.0015)	93.8 (0)	765 (83)
1.2 m/d US	0	0	80 (0)	8.89 (0)	142 (0)	489 (0)
1.2 m/d US	5	0.708	24.7 (0)	8.89 (0)	0.01 (0)	890 (0)
1.2 m/d US	10	1.42	16.9 (0)	8.89 (0)	0.01 (0)	941 (0)
1.2 m/d US	15	2.12	19.7 (0)	8.89 (0)	0.01 (0)	662 (0)
1.2 m/d US	20	2.83	12.1 (0)	8.89 (0)	0.01 (0)	664 (0)
L	L	l		I		

Table 7 (cont'd)

1.2 m/d DS	0	0	71.3 (0)	8.46 (0)	229 (0)	466 (0)
1.2 m/d DS	5	0.628	15 (0)	8.46 (0)	0.01 (0)	1030 (0)
1.2 m/d DS	10	1.26	15.8 (0)	8.46 (0)	0.01 (0)	1070 (0)
1.2 m/d DS	15	1.88	16.9 (0)	8.46 (0)	0.01 (0)	1090 (0)
1.2 m/d DS	20	2.51	18.5 (0)	8.46 (0)	0.01 (0)	739 (0)
0.8 m/d US	0	0	76.3 (0.652)	7.86 (0.156)	253 (0)	427 (15.1)
0.8 m/d US	5	0.8	37 (8.81)	7.48 (0.135)	11.3 (0)	789 (36.1)
0.8 m/d US	10	1.6	11.9 (7.92)	6.81 (0.23)	0.01 (0)	863 (80.5)
0.8 m/d US	15	2.4	16.8 (0.945)	6.61 (0.504)	0.01 (0)	612 (37.4)
0.8 m/d US	20	3.2	14.6 (0.566)	1.4 (0.482)	0.01 (0)	805 (17.4)
0.8 m/d DS	0	0	76.2 (1.99)	7.88 (0.118)	273 (0)	427 (41.2)
0.8 m/d DS	5	1.1	54.8 (3.81)	7.18 (0.167)	28.8 (0)	816 (50.8)
0.8 m/d DS	10	2.19	37.7 (5.5)	7.35 (0.0379)	0.01 (0)	845 (45.4)
0.8 m/d DS	15	3.29	16.7 (11.1)	7.25 (0.0211)	0.01 (0)	962 (80.4)
0.8 m/d DS	20	4.38	17.5 (1.3)	5.91 (1.13)	0.01 (0)	624 (56.2)

Table 8: Tabulated data from Figure 21 and Figure 23. Rates are calculated as in Section 2.2.5, as μ mol/L/h or nmol/L/h, with standard deviation in parentheses, when multiple points were available for the calculation.

	N ₂ -N	N ₂ O-N	NO ₃ -	O_2	DOC
Experiment	(µM/h)	(nM/h)	(µM/h)	(µM/h)	(µM/h)
3 m/d US	3.77 (0.27)	105 (1)	-24.5 (0.7)	-131 (0)	-16.6 (41.4)
3 m/d DS	1.59 (0.25)	11.1 (0.6)	-15.3 (3.5)	-154 (0)	-245 (305)
2 m/d US	0.929 (0.307)	272 (3)	-21.2 (5.3)	-60 (0)	120 (193)
2 m/d DS	-1.16 (0.31)	115 (1)	-11.1 (7)	-105 (0)	170 (153)
1.2 m/d US	4.86 (0)	1.03 (0)	-24 (0)	-50 (0)	62.1 (0)
1.2 m/d DS	4.96 (0)	-23.2 (0)	-21 (0)	-91 (0)	109 (0)
0.8 m/d US	3.92 (0.51)	8.66 (0.51)	-19.3 (0.9)	-79 (0)	118 (23)
0.8 m/d DS	3.28 (0.38)	53.9 (1.4)	-13.4 (2.4)	-62.3 (0)	44.9 (69.7)

Table 9: Injection and Flush porewater velocities from the Sawmill Brook Experiments. Velocities were determined by the depth (10 or 20 cm) divided by the median arrival time of the conductivity plume at that depth, as shown in Figure .

		Flush
Experiment,	Injection Velocity	Velocity
Ring, Depth	(m/d)	(m/d)
Exp1 DS-10cm	3.60	4.23
Exp1 DS-20cm	3.30	3.95
Exp1 US-10cm	2.38	3.21
Exp1 US-20cm	1.74	3.14
Exp2 DS-10cm	4.72	5.56
Exp2 DS-20cm	4.24	4.72
Exp2 US-10cm	3.50	3.01
Exp2 US-20cm	3.51	4.51
Exp3 DS-10cm	1.08	NA
Exp3 DS-20cm	1.11	NA
Exp3 US-10cm	1.51	NA
Exp3 US-20cm	1.49	NA

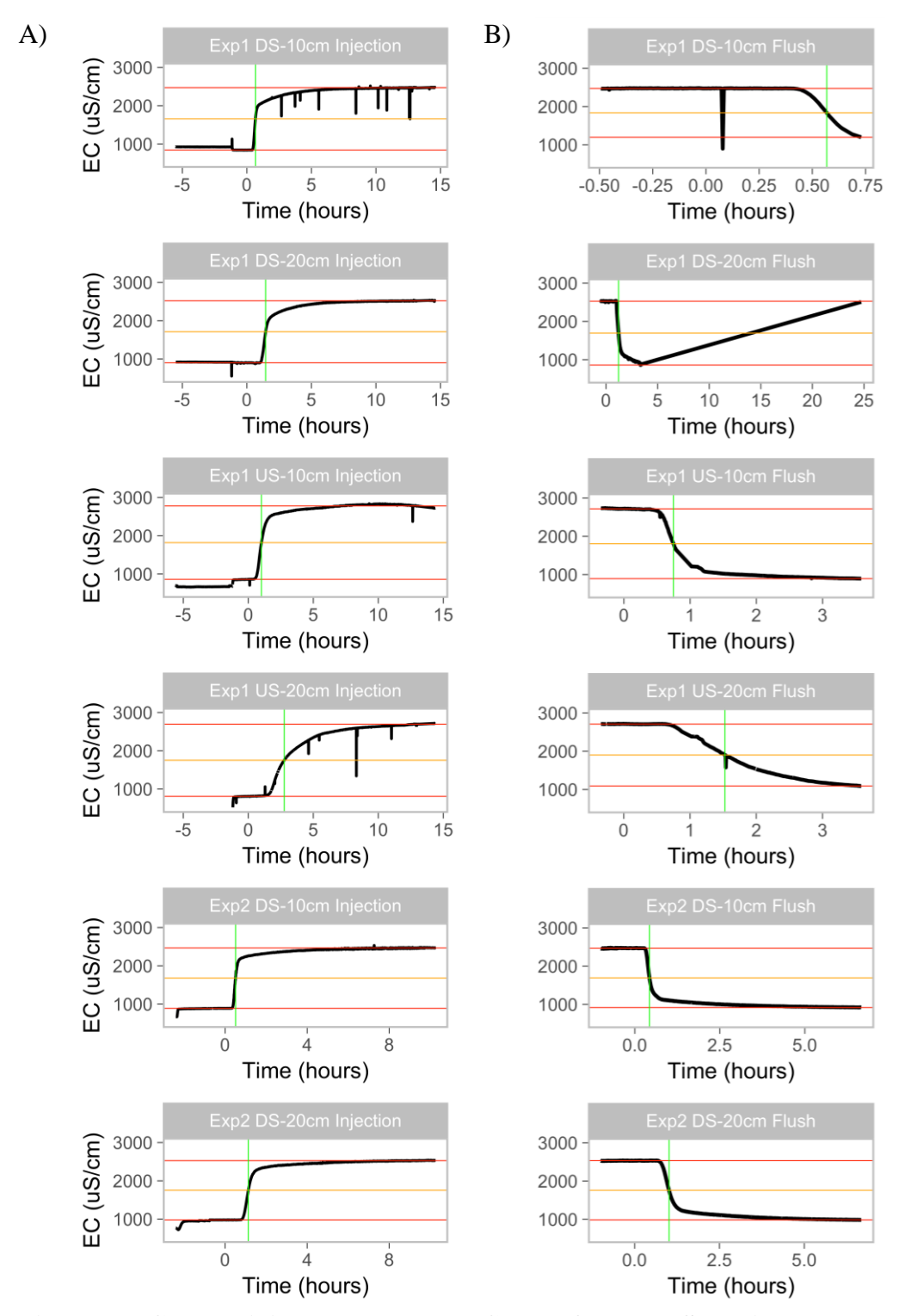
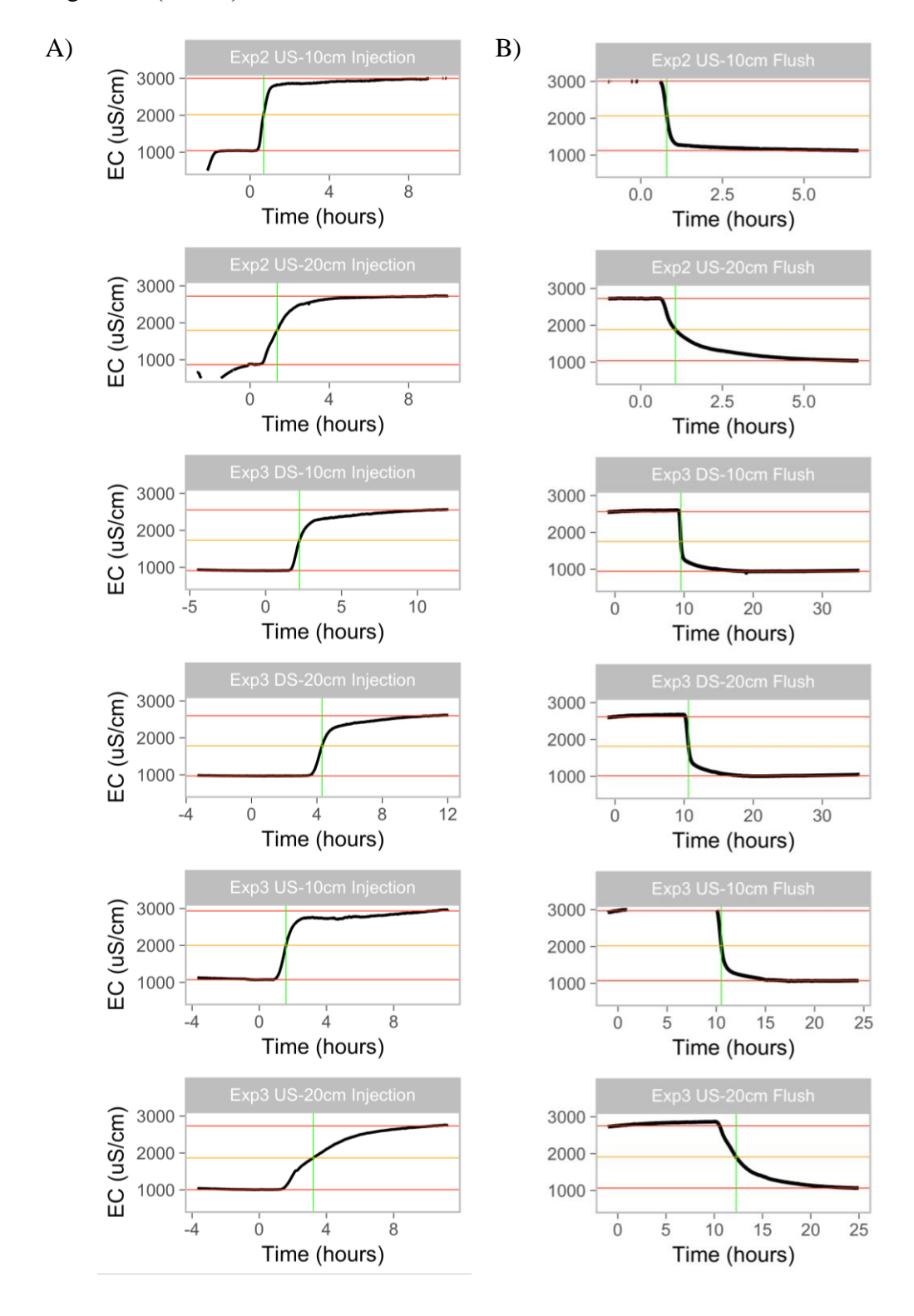


Figure 27: Conductivity Breakthrough Curves from the Sawmill Brook Experiments. Data are plotted as electrical conductivity over time for the first three experiments, for both 10 and 20 cm depth on the injection (A) and flush (B) phases of the high-conductivity injections. Time is normalized to the beginning of injection or flush. Red lines mark the initial concentration and plateau; the orange line marks the median concentration between those two, and the green line marks the time of median arrival time, which was used to calculate velocities as in Table 9.

Figure 27 (cont'd)



REFERENCES

REFERENCES

- Abbott BW, Baranov V, Mendoza-Lera C, Nikolakopoulou M, Harjung A, Kolbe T, Balasubramanian MN, Vaessen TN, Ciocca F, Campeau A, et al. 2016. Using multi-tracer inference to move beyond single-catchment ecohydrology. *Earth-Science Reviews* **160**: 19–42 DOI: 10.1016/j.earscirev.2016.06.014
- Abbott BW, Gruau G, Zarnetske JP, Moatar F, Barbe L, Thomas Z, Fovet O, Kolbe T, Gu S, Pierson-Wickmann A-C, et al. 2018. Unexpected spatial stability of water chemistry in headwater stream networks. *Ecology Letters* **21** (2): 296–308 DOI: 10.1016/j.earscirev.2016.06.014
- Ahrens TD, Siver PA. 2000. Trophic Conditions and Water Chemistry of Lakes on Cape Cod, Massachusetts, USA. *Lake and Reservoir Management* **16** (4): 268–280 DOI: 10.1080/07438140009354235
- Anderson JK, Wondzell SM, Gooseff MN, Haggerty R. 2005. Patterns in stream longitudinal profiles and implications for hyporheic exchange flow at the H.J. Andrews Experimental Forest, Oregon, USA. *Hydrological Processes* **19** (15): 2931–2949 DOI: 10.1002/hyp.5791
- Anderson MP, Munter JA. 1981. Seasonal reversals of groundwater flow around lakes and the relevance to stagnation points and lake budgets. *Water Resources Research* **17** (4): 1139–1150 DOI: 10.1029/WR017i004p01139
- Arnon S, Gray KA, Packman AI. 2007. Biophysicochemical process coupling controls nitrogen use by benthic biofilms. *Limnology and Oceanography* **52** (4): 1665–1671 DOI: 10.4319/lo.2007.52.4.1665
- Atkinson BL, Grace MR, Hart BT, Vanderkruk KEN. 2008. Sediment instability affects the rate and location of primary production and respiration in a sand-bed stream. *Journal of the North American Benthological Society* **27** (3): 581–592 DOI: 10.1899/07-143.1
- Baker MA, Dahm CN, Valett HM. 1999. Acetate retention and metabolism in the hyporheic zone of a mountain stream. *Limnology and Oceanography* **44** (6): 1530–1539 DOI: 10.4319/lo.1999.44.6.1530
- Baker MA, Dahm CN, Valett HM. 2000a. Anoxia, anaerobic metabolism biogeochemistry of the stream water-ground water interface. In *Streams and Ground Waters*, Jones JA, , Mullholland PJ (eds). Academic Press: San Diego, California, USA; 259–283.
- Baker MA, Valett HM, Dahm CN. 2000b. Organic carbon supply and metabolism in a shallow groundwater ecosystem. *Ecology* **81** (11): 3133–3148 DOI: 10.1890/0012-9658(2000)081[3133:OCSAMI]2.0.CO;2

- Barbaro JR, Walter DA, LeBlanc DR. 2013. Transport of nitrogen in a treated-wastewater plume to coastal discharge areas, Ashumet Valley, Cape Cod, Massachusetts. U.S. Geological Survey Scientific Investigations Report 2013-5061. US Geological Survey, Reston, VA. Available at: http://pubs.er.usgs.gov/publication/sir20135061 [Accessed 17 March 2017]
- Baulch HM, Schiff SL, Maranger R, Dillon PJ. 2011. Nitrogen enrichment and the emission of nitrous oxide from streams. *Global Biogeochemical Cycles* **25** (4) DOI: 10.1029/2011GB004047
- Beaulieu JJ, Tank JL, Hamilton SK, Wollheim WM, Hall Jr RO, Mulholland PJ, Peterson BJ, Ashkenas LR, Cooper LW, Dahm CN, et al. 2011. Nitrous oxide emission from denitrification in stream and river networks. *Proceedings of the National Academy of Sciences* **108** (1): 214–219 DOI: 10.1073/pnas.1011464108
- Bernhardt ES, Likens GE. 2002. Dissolved organic carbon enrichment alters nitrogen dynamics in a forest stream. *Ecology* **83** (6): 1689–1700 DOI: 10.1890/0012-9658(2002)083[1689:DOCEAN]2.0.CO;2
- Betlach MR, Tiedje JM. 1981. Kinetic Explanation for Accumulation of Nitrite, Nitric Oxide, and Nitrous Oxide During Bacterial Denitrification. *Applied and Environmental Microbiology* **42** (6): 1074–1084
- Boano F, Harvey JW, Marion A, Packman AI, Revelli R, Ridolfi L, Wörman A. 2014. Hyporheic flow and transport processes: Mechanisms, models, and biogeochemical implications. *Reviews of Geophysics* **52** (4): 603–679 DOI: 10.1002/2012RG000417
- Born SM, Smith SA, Stephenson DA. 1974. The hydrogeological regime of glacialterrain lakes, with management and planning applications: Madison. *University of Wisconsin Extension*
- Born SM, Smith SA, Stephenson DA. 1979. Hydrogeology of glacial-terrain lakes, with management and planning applications. *Journal of Hydrology* **43** (1–4): 7–43 DOI: 10.1016/0022-1694(79)90163-X
- Boulton AJ, Findlay S, Marmonier P, Stanley EH, Valett HM. 1998. The functional significance of the hyporheic zone in streams and rivers. *Annual Review of Ecology and Systematics*: 59–81 DOI: 10.1146/annurev.ecolsys.29.1.59
- Bourke MF, Kessler AJ, Cook PLM. 2014. Influence of buried Ulva lactuca on denitrification in permeable sediments. *Marine Ecology Progress Series* **498**: 85–94 DOI: 10.3354/meps10611
- Boyer EW, Howarth RW, Galloway JN, Dentener FJ, Green PA, Vörösmarty CJ. 2006. Riverine nitrogen export from the continents to the coasts. *Global Biogeochemical Cycles* **20** (1) DOI: 10.1029/2005GB002537
- Briggs MA, Day-Lewis FD, Zarnetske JP, Harvey JW. 2015. A physical explanation for the development of redox microzones in hyporheic flow. *Geophysical Research Letters* **42** (11): 4402–4410 DOI: 10.1002/2015GL064200

- Briggs MA, Gooseff MN, Peterson BJ, Morkeski K, Wollheim WM, Hopkinson CS. 2010. Surface and hyporheic transient storage dynamics throughout a coastal stream network. *Water Resources Research* **46** (6) DOI: 10.1029/2009WR008222
- Briggs MA, Lautz LK, Buckley SF, Lane JW. 2014a. Practical limitations on the use of diurnal temperature signals to quantify groundwater upwelling. *Journal of hydrology* **519**: 1739–1751 DOI: 10.1016/j.jhydrol.2014.09.030
- Briggs MA, Lautz LK, Hare DK. 2014b. Residence time control on hot moments of net nitrate production and uptake in the hyporheic zone. *Hydrological Processes* **28** (11): 3741–3751 DOI: 10.1002/hyp.9921
- Briggs MA, Lautz LK, Hare DK, González-Pinzón R. 2013. Relating hyporheic fluxes, residence times, and redox-sensitive biogeochemical processes upstream of beaver dams. *Freshwater Science* **32** (2): 622–641 DOI: 10.1899/12-110.1
- Brunke M, Gonser T. 1997. The ecological significance of exchange processes between rivers and groundwater. *Freshwater Biology* **37** (1): 1–33 DOI: 10.1046/j.1365-2427.1997.00143.x
- Burford JR, Bremner JM. 1975. Relationships between the denitrification capacities of soils and total, water-soluble and readily decomposable soil organic matter. *Soil Biology and Biochemistry* **7** (6): 389–394 DOI: 10.1016/0038-0717(75)90055-3
- Burgin AJ, Hamilton SK. 2007. Have we overemphasized the role of denitrification in aquatic ecosystems? A review of nitrate removal pathways. *Frontiers in Ecology and the Environment* **5** (2): 89–96 DOI: 10.1890/1540-9295(2007)5[89:HWOTRO]2.0.CO;2
- Burgin AJ, Hamilton SK. 2008. NO3–driven SO42- production in freshwater ecosystems: implications for N and S cycling. *Ecosystems* **11** (6): 908–922 DOI: <u>10.1007/s10021-008-9169-5</u>
- Burgin AJ, Yang WH, Hamilton SK, Silver WL. 2011. Beyond carbon and nitrogen: how the microbial energy economy couples elemental cycles in diverse ecosystems. *Frontiers in Ecology and the Environment* **9** (1): 44–52 DOI: 10.1890/090227
- Bussey KW, Walter DA. 1996. Spatial and temporal distribution of specific conductance, boron, and phosphorus in a sewage-contaminated aquifer near Ashumet Pond, Cape Cod, Massachusetts. US Geological Survey; Branch of Information Services [distributor]. Available at: http://pubs.er.usgs.gov/publication/ofr96472
- Cardenas MB. 2008. Surface water-groundwater interface geomorphology leads to scaling of residence times. *Geophysical Research Letters* **35** (8) DOI: <u>10.1029/2008GL033753</u>
- Cardenas MB. 2015. Hyporheic zone hydrologic science: A historical account of its emergence and a prospectus. *Water Resources Research* **51** (5): 3601–3616 DOI: 10.1002/2015WR017028

- Carlozzi CA, King K, Newbold WF. 1975. *Ecosystems and resources of the Massachusetts Coast*. Massachusetts Coastal Zone Management Program, Boston. Available at: http://masslib-dspace.longsight.com/handle/2452/69134
- Chen RL, Keeney DR, Graetz DA, Holding AJ. 1972. Denitrification and Nitrate Reduction in Wisconsin Lake Sediments. *Journal of Environmental Quality* **1** (2): 158–162 DOI: 10.2134/jeq1972.00472425000100020011x
- Cherkauer DS, McKereghan PF, Schalch LH. 1992. Delivery of Chloride and Nitrate by Ground Water to the Great Lakes: Study for the Door Peninsula, Wisconsin. *Groundwater* (30): 885–894 DOI: 10.1111/j.1745-6584.1992.tb01571.x
- Cory RM, Boyer EW, McKnight DM. 2011. Spectral methods to advance understanding of dissolved organic carbon dynamics in forested catchments. *Forest Hydrology and Biogeochemistry*: 117–135 DOI: 10.1007/978-94-007-1363-5_6
- Danczak RE, Sawyer AH, Williams KH, Stegen JC, Hobson C, Wilkins MJ. 2016. Seasonal hyporheic dynamics control coupled microbiology and geochemistry in Colorado River sediments. *Journal of Geophysical Research-Biogeosciences* **121** (12): 2976–2987 DOI: 10.1002/2016JG003527
- Downing JA, Cole JJ, Duarte CA, Middelburg JJ, Melack JM, Prairie YT, Kortelainen P, Striegl RG, McDowell WH, Tranvik LJ. 2012. Global abundance and size distribution of streams and rivers. *Inland waters* **2** (4): 229–236 DOI: 10.5268/IW-2.4.502
- Duff JH, Triska FJ. 1990. Denitrifications in sediments from the hyporheic zone adjacent to a small forested stream. *Canadian Journal of Fisheries and Aquatic Sciences* **47** (6): 1140–1147 DOI: 10.1139/f90-133
- Farrell TB, Quick AM, Reeder WJ, Tonina D, Benner SG, Feris KP. 2013. Carbon availability and the distribution of denitrifying organisms influence N2O production in the hyporheic zone. In *AGU Fall Meeting Abstracts*L05. Available at: http://adsabs.harvard.edu/abs/2013AGUFM.H31L..05F [Accessed 9 November 2016]
- Findlay S. 1995. Importance of surface-subsurface exchange in stream ecosystems: The hyporheic zone. *Limnology and Oceanography* **40** (1): 159–164 DOI: 10.4319/lo.1995.40.1.0159
- Findlay S, Sinsabaugh RL. 2003. Response of hyporheic biofilm metabolism and community structure to nitrogen amendments. *Aquatic microbial ecology* **33** (2): 127–136 DOI: 10.3354/ame033127
- Findlay S, Sobczak WV. 1996. Variability in removal of dissolved organic carbon in hyporheic sediments. *Journal of the North American Benthological Society* **15** (1): 35–41 DOI: 10.2307/1467431

- Finkenbine J. K., Atwater J. W., Mavinic D. S. 2007. Stream health after urbanization. *JAWRA Journal of the American Water Resources Association* **36** (5): 1149–1160 DOI: 10.1111/j.1752-1688.2000.tb05717.x
- Firestone MK, Davidson EA. 1989. Microbiological basis of NO and N2O production and consumption in soil. *Exchange of trace gases between terrestrial ecosystems and the atmosphere* **47**: 7–21
- Firestone MK, Tiedje JM. 1979. Temporal Change in Nitrous Oxide and Dinitrogen from Denitrification Following Onset of Anaerobiosis. *Applied and Environmental Microbiology* **38** (4): 673–679
- Firestone MK, Firestone RB, Tiedje JM. 1980. Nitrous oxide from soil denitrification: factors controlling its biological production. *Science* **208** (4445): 749–751 DOI: 10.1126/science.208.4445.749
- Forster P, Ramaswamy V, Artaxo P, Berntsen T, Betts R, Fahey DW, Haywood J, Lean J, Lowe DC, Myhre G, et al. 2007. Changes in atmospheric constituents and in radiative forcing. In *Climate Change 2007. The Physical Science Basis* Cambridge University Press: New York.
- Galloway JN, Dentener FJ, Capone DG, Boyer EW, Howarth RW, Seitzinger SP, Asner GP, Cleveland CC, Green PA, Holland EA, et al. 2004. Nitrogen cycles: past, present, and future. *Biogeochemistry* **70** (2): 153–226 DOI: 10.1007/s10533-004-0370-0
- Gardner JR, Doyle MW. 2018. Sediment–Water Surface Area Along Rivers: Water Column Versus Benthic. *Ecosystems* DOI: 10.1007/s10021-018-0236-2
- Gu C, Hornberger GM, Herman JS, Mills AL. 2008. Effect of freshets on the flux of groundwater nitrate through streambed sediments. *Water resources research* **44** (5) DOI: 10.1029/2007WR006488
- Gu C, Hornberger GM, Mills AL, Herman JS, Flewelling SA. 2007. Nitrate reduction in streambed sediments: Effects of flow and biogeochemical kinetics. *Water Resources Research* **43** (12) DOI: 10.1029/2007WR006027
- Haggerty R, Wondzell SM, Johnson MA. 2002. Power-law residence time distribution in the hyporheic zone of a 2nd-order mountain stream. *Geophysical Research Letters* **29** (13) DOI: http://dx.doi.org/10.1029/2002GL014743
- Hall Jr RO, Tank JL, Sobota DJ, Mulholland PJ, O'Brien JM, Dodds WK, Webster JR, Valett HM, Poole GC, Peterson BJ, et al. 2009. Nitrate removal in stream ecosystems measured by 15N addition experiments: Total uptake. *Limnology and Oceanography* **54** (3): 653–665 DOI: 10.4319/lo.2009.54.3.0653
- Harvey JW, Böhlke JK, Voytek MA, Scott D, Tobias CR. 2013. Hyporheic zone denitrification: Controls on effective reaction depth and contribution to whole-stream mass balance. *Water Resources Research* **49** (10): 6298–6316 DOI: 10.1002/wrcr.20492

- Harvey RW, Metge DW, LeBlanc DR, Underwood J, Aiken GR, Butler K, McCobb TD, Jasperse J. 2015. Importance of the Colmation Layer in the Transport and Removal of Cyanobacteria, Viruses, and Dissolved Organic Carbon during Natural Lake-Bank Filtration. *Journal of Environmental Quality* **44** (5): 1413–1423 DOI: 10.2134/jeq2015.03.0151
- Hedin LO, von Fischer JC, Ostrom NE, Kennedy BP, Brown MG, Robertson GP. 1998. Thermodynamic constraints on nitrogen transformations and other biogeochemical processes at soil–stream interfaces. *Ecology* **79** (2): 684–703 DOI: <u>10.1890/0012-9658(1998)079[0684:TCONAO]2.0.CO;2</u>
- Helton AM, Wright MS, Bernhardt ES, Poole GC, Cory RM, Stanford JA. 2015. Dissolved organic carbon lability increases with water residence time in the alluvial aquifer of a river floodplain ecosystem. *Journal of Geophysical Research: Biogeosciences* **120** (4): 693–706 DOI: 10.1002/2014JG002832
- Howarth RW, Billen G, Swaney D, Townsend A, Jaworski N, Lajtha K, Downing JA, Elmgren R, Caraco N, Jordan T, et al. 1996. Regional nitrogen budgets and riverine N & P fluxes for the drainages to the North Atlantic Ocean: Natural and human influences. *Biogeochemistry* **35**: 75–139 DOI: 10.1007/978-94-009-1776-7_3
- Inwood SE, Tank JL, Bernot MJ. 2007. Factors Controlling Sediment Denitrification in Midwestern Streams of Varying Land Use. *Microbial Ecology* **53** (2): 247–258 DOI: 10.1007/s00248-006-9104-2
- Irvine DJ, Lautz LK, Briggs MA, Gordon RP, McKenzie JM. 2015. Experimental evaluation of the applicability of phase, amplitude, and combined methods to determine water flux and thermal diffusivity from temperature time series using VFLUX 2. *Journal of Hydrology* **531**: 728–737 DOI: 10.1016/j.jhydrol.2015.10.054
- Kaufman MH, Cardenas MB, Buttles J, Kessler AJ, Cook PLM. 2017. Hyporheic hot moments: Dissolved oxygen dynamics in the hyporheic zone in response to surface flow perturbations. *Water Resources Research* **53** (8): 6642–6662 DOI: 10.1002/2016WR020296
- Kaushal SS, Likens GE, Pace ML, Utz RM, Haq S, Gorman J, Grese M. 2018. Freshwater salinization syndrome on a continental scale. *Proceedings of the National Academy of Sciences*: 201711234 DOI: 10.1073/pnas.1711234115
- Kidmose J, Engesgaard P, Ommen DAO, Nilsson B, Flindt MR, Andersen FØ. 2015. The Role of Groundwater for Lake-Water Quality and Quantification of N Seepage. *Groundwater* **53** (5): 709–721 DOI: 10.1111/gwat.12281
- Kim H, Kaown D, Mayer B, Lee J-Y, Lee K-K. 2018. Combining pyrosequencing and isotopic approaches to assess denitrification in a hyporheic zone. *Science of The Total Environment* **631–632**: 755–764 DOI: <u>10.1016/j.scitotenv.2018.03.073</u>

- Kravchenko AN, Fry JE, Guber AK. 2018. Water absorption capacity of soil-incorporated plant leaves can affect N 2 O emissions and soil inorganic N concentrations. *Soil Biology and Biochemistry* **121**: 113–119 DOI: 10.1016/j.soilbio.2018.03.013
- Kravchenko AN, Toosi ER, Guber AK, Ostrom NE, Yu J, Azeem K, Rivers ML, Robertson GP. 2017. Hotspots of soil N 2 O emission enhanced through water absorption by plant residue. *Nature Geoscience* **10** (7): 496 DOI: 10.1038/ngeo2963
- Kroeze C, Mosier A, Bouwman L. 1999. Closing the global N2O budget: a retrospective analysis 1500–1994. *Global Biogeochemical Cycles* **13** (1): 1–8 DOI: 10.1029/1998GB900020
- Kurz MJ, Drummond JD, Martí E, Zarnetske JP, Lee-Cullin J, Klaar MJ, Folegot S, Keller T, Ward AS, Fleckenstein JH. 2017. Impacts of water level on metabolism and transient storage in vegetated lowland rivers: Insights from a mesocosm study. *Journal of Geophysical Research: Biogeosciences* **122** (3): 628–644 DOI: 10.1002/2016JG003695
- Lansdown K, Heppell CM, Dossena M, Ullah S, Heathwaite AL, Binley A, Zhang H, Trimmer M. 2014. Fine-scale in situ measurement of riverbed nitrate production and consumption in an armored permeable riverbed. *Environmental Science & Technology* **48** (8): 4425–4434 DOI: 10.1021/es4056005
- Lansdown K, Heppell CM, Trimmer M, Binley A, Heathwaite AL, Byrne P, Zhang H. 2015. The interplay between transport and reaction rates as controls on nitrate attenuation in permeable, streambed sediments. *Journal of Geophysical Research-Biogeosciences* **120** (6): 1093–1109 DOI: 10.1002/2014JG002874
- Lansdown K, Trimmer M, Heppell CM, Sgouridis F, Ullah S, Heathwaite AL, Binley A, Zhang H. 2012. Characterization of the key pathways of dissimilatory nitrate reduction and their response to complex organic substrates in hyporheic sediments. *Limnology and Oceanography* **57** (2): 387–400 DOI: 10.4319/lo.2012.57.2.0387
- Lautz LK, Fanelli RM. 2008. Seasonal biogeochemical hotspots in the streambed around restoration structures. *Biogeochemistry* **91** (1): 85–104 DOI: 10.1007/s10533-008-9235-2
- LeBlanc DR, Garabedian SP, Hess KM, Gelhar LW, Quadri RD, Stollenwerk KG, Wood WW. 1991. Large-scale natural gradient tracer test in sand and gravel, Cape Cod, Massachusetts: 1. Experimental design and observed tracer movement. *Water Resources Research* **27** (5): 895–910 DOI: 10.1029/91WR00241
- Lewandowski J, Meinikmann K, Nützmann G, Rosenberry DO. 2015. Groundwater—the disregarded component in lake water and nutrient budgets. Part 2: effects of groundwater on nutrients. *Hydrological Processes* **29** (13): 2922–2955 DOI: 10.1002/hyp.10384
- Li S, Peng C, Wang C, Zheng J, Hu Y, Li D. 2017. Microbial Succession and Nitrogen Cycling in Cultured Biofilms as Affected by the Inorganic Nitrogen Availability. *Microbial Ecology* **73** (1): 1–15 DOI: 10.1007/s00248-016-0827-4

- Liu Y, Liu C, Nelson WC, Shi L, Xu F, Liu Y, Yan A, Zhong L, Thompson C, Fredrickson JK, et al. 2017. Effect of Water Chemistry and Hydrodynamics on Nitrogen Transformation Activity and Microbial Community Functional Potential in Hyporheic Zone Sediment Columns. *Environmental Science & Technology* **51** (9): 4877–4886 DOI: 10.1021/acs.est.6b05018
- Lloyd D. 1993. Aerobic denitrification in soils and sediments: From fallacies to factx. *Trends in Ecology & Evolution* **8** (10): 352–356 DOI: 10.1016/0169-5347(93)90218-E
- Lloyd D, Boddy L, Davies KJP. 1987. Persistence of bacterial denitrification capacity under aerobic conditions: The rule rather than the exception. *FEMS Microbiology Ecology* **3** (3): 185–190 DOI: 10.1111/j.1574-6968.1987.tb02354.x
- Luce CH, Tonina D, Gariglio F, Applebee R. 2013. Solutions for the diurnally forced advection-diffusion equation to estimate bulk fluid velocity and diffusivity in streambeds from temperature time series. *Water Resources Research* **49** (1): 488–506 DOI: 10.1029/2012WR012380
- van Luijn F, Boers PCM, Lijklema L. 1996. Comparison of denitrification rates in lake sediments obtained by the N2 flux method, the 15N isotope pairing technique and the mass balance approach. *Water Research* **30** (4): 893–900 DOI: 10.1016/0043-1354(95)00250-2
- Marzadri A, Dee MM, Tonina D, Bellin A, Tank JL. 2017. Role of surface and subsurface processes in scaling N2O emissions along riverine networks. *Proceedings of the National Academy of Sciences*: 201617454 DOI: 10.1073/pnas.1617454114
- Marzadri A, Tonina D, Bellin A. 2011. A semianalytical three-dimensional process-based model for hyporheic nitrogen dynamics in gravel bed rivers. *Water Resources Research* **47** (11) DOI: 10.1029/2011WR010583
- Marzadri A, Tonina D, Bellin A, Tank JL. 2014. A hydrologic model demonstrates nitrous oxide emissions depend on streambed morphology. *Geophysical Research Letters* **41** (15): 5484–5491 DOI: 10.1002/2014GL060732
- Massachusetts Division of Fisheries and Wildlife. 1993. Pond maps of Massachusetts: Cape Cod. publication no. 17455-60-1M-12/93.
- Masterson JP, Walter DA, Savoie, J. 1996. Use of particle tracking to improve numerical model calibration and to analyze ground-water flow and contaminant migration, Massachusetts Military Reservation, Cape Cod, Massachusetts. U.S. Geological Survey Water-Supply Paper 2482. Available at: http://pubs.er.usgs.gov/publication/ofr96214
- Mather KF, Goldthwait RP, Thiesmeyer LR. 1942. Pleistocene geology of western Cape Cod, Massachusetts. *Geological Society of America Bulletin* **53** (8): 1127–1174 DOI: 10.1130/GSAB-53-1127

- McCallum AM, Andersen MS, Rau GC, Acworth RI. 2012. A 1-D analytical method for estimating surface water—groundwater interactions and effective thermal diffusivity using temperature time series. *Water Resources Research* **48** (11): W11532 DOI: 10.1029/2012WR012007
- McClain ME, Boyer EW, Dent CL, Gergel SE, Grimm NB, Groffman PM, Hart SC, Harvey JW, Johnston CA, Mayorga E, et al. 2003. Biogeochemical hot spots and hot moments at the interface of terrestrial and aquatic ecosystems. *Ecosystems* **6** (4): 301–312 DOI: 10.1007/s10021-003-0161-9
- McCobb TD, LeBlanc DR, Walter DA, Hess KM, Kent DB, Smith RL. 2003. Phosphorus in a ground-water contaminant plume discharging to Ashumet Pond, Cape Cod, Massachusetts, 1999 Available at: http://pubs.usgs.gov/wri/wri024306/pdfs/wrir024306.pdf [Accessed 2 April 2017]
- McGuire KJ, Torgersen CE, Likens GE, Buso DC, Lowe WH, Bailey SW. 2014. Network analysis reveals multiscale controls on streamwater chemistry. *Proceedings of the National Academy of Sciences* **111** (19): 7030–7035 DOI: 10.1073/pnas.1404820111
- McKnight DM, Boyer EW, Westerhoff PK, Doran PT, Kulbe T, Andersen DT. 2001. Spectrofluorometric characterization of dissolved organic matter for indication of precursor organic material and aromaticity. *Limnology and Oceanography* **46** (1): 38–48 DOI: 10.4319/lo.2001.46.1.0038
- Minnesota Department of Natural Resources, Division of Ecological Services D. 2003. Healthy Rivers: A Water Course How Rivers Run Connections. *Minnesota Department of Natural Resources* Available at:

 http://files.dnr.state.mn.us/assistance/backyard/healthyrivers/course/200/203_130.htm
 [Accessed 15 January 2017]
- Mosier AR, Doran JW, Freney JR. 2002. Managing soil denitrification. *Journal of soil and water conservation* **57** (6): 505–512
- Mulholland PJ, Hall Jr RO, Sobota DJ, Dodds WK, Findlay SE, Grimm NB, Hamilton SK, McDowell WH, O'Brien JM, Tank JL, et al. 2009. Nitrate removal in stream ecosystems measured by 15N addition experiments: denitrification. *Limnology and Oceanography* **54** (3): 666–680 DOI: 10.4319/lo.2009.54.3.0666
- Mulholland PJ, Helton AM, Poole GC, Hall Jr RO, Hamilton SK, Peterson BJ, Tank JL, Ashkenas LR, Cooper LW, Dahm CN, et al. 2008. Stream denitrification across biomes and its response to anthropogenic nitrate loading. *Nature* **452** (7184): 202–205 DOI: 10.1038/nature06686
- Ocampo CJ, Oldham CE, Sivapalan M. 2006. Nitrate attenuation in agricultural catchments: Shifting balances between transport and reaction. *Water Resources Research* **42** (1) DOI: 10.1029/2004WR003773

- Ostrom NE, Gandhi H, Trubl G, Murray AE. 2016. Chemodenitrification in the cryoecosystem of Lake Vida, Victoria Valley, Antarctica. *Geobiology* **14** (6): 575–587 DOI: 10.1111/gbi.12190
- Ostrom NE, Hedin LO, Von Fischer JC, Robertson GP. 2002. Nitrogen transformations and NO3- removal at a soil–stream interface: a stable isotope approach. *Ecological Applications* **12** (4): 1027–1043 DOI: 10.1890/1051-0761(2002)012[1027:NTANRA]2.0.CO;2
- Paul MJ, Meyer JL. 2001. Streams in the Urban Landscape. *Annual Review of Ecology and Systematics* **32** (1): 333–365 DOI: 10.1146/annurev.ecolsys.32.081501.114040
- Payne WJ. 1973. Reduction of nitrogenous oxides by microorganisms. *Bacteriological Reviews* **37** (4): 409–452
- Peterson BJ, Wollheim WM, Mulholland PJ, Webster JR, Meyer JL, Tank JL, Martí E, Bowden WB, Valett HM, Hershey AE, et al. 2001. Control of nitrogen export from watersheds by headwater streams. *Science* **292** (5514): 86–90 DOI: 10.1126/science.1056874
- Quick AM, Reeder WJ, Farrell TB, Tonina D, Feris KP, Benner SG. 2016. Controls on nitrous oxide emissions from the hyporheic zones of streams. *Environmental Science & Technology* **50** (21): 11491–11500 DOI: 10.1021/acs.est.6b02680
- Ravishankara AR, Daniel JS, Portmann RW. 2009. Nitrous oxide (N2O): the dominant ozone-depleting substance emitted in the 21st century. *Science* **326** (5949): 123–125 DOI: 10.1126/science.1176985
- Reddy KR, Patrick WH. 1975. Effect of alternate aerobic and anaerobic conditions on redox potential, organic matter decomposition and nitrogen loss in a flooded soil. *Soil Biology and Biochemistry* **7** (2): 87–94 DOI: 10.1016/0038-0717(75)90004-8
- Repert DA, Barber LB, Hess KM, Keefe SH, Kent DB, LeBlanc DR, Smith RL. 2006. Long-term natural attenuation of carbon and nitrogen within a groundwater plume after removal of the treated wastewater source. *Environmental science & technology* **40** (4): 1154–1162 DOI: 10.1021/es051442j
- Robertson GP, Tiedje JM. 1987. Nitrous oxide sources in aerobic soils: Nitrification, denitrification and other biological processes. *Soil Biology and Biochemistry* **19** (2): 187–193 DOI: 10.1016/0038-0717(87)90080-0
- Robertson LA, Kuenen JG. 1984. Aerobic denitrification: a controversy revived. *Archives of Microbiology* **139** (4): 351–354 DOI: <u>10.1007/BF00408378</u>
- Rockström J, Steffen W, Noone K, Persson Å, Chapin FSI, Lambin E, Lenton T, Scheffer M, Folke C, Schellnhuber HJ, et al. 2009. Planetary Boundaries: Exploring the Safe Operating Space for Humanity. *Ecology and Society* **14** (2) DOI: <u>10.5751/ES-03180-140232</u>

- Rosamond MS, Thuss SJ, Schiff SL. 2012. Dependence of riverine nitrous oxide emissions on dissolved oxygen levels. *Nature geoscience* **5** (10): 715 DOI: 10.1038/ngeo1556
- Rosenberry DO, LaBaugh JW. 2008. Field techniques for estimating water fluxes between surface water and ground water. Techniques and Methods 4-D2. Geological Survey (US). Available at: http://pubs.usgs.gov/tm/04d02/ [Accessed 16 June 2015]
- Rosenberry DO, Lewandowski J, Meinikmann K, Nützmann G. 2015. Groundwater–the disregarded component in lake water and nutrient budgets. Part 1: effects of groundwater on hydrology. *Hydrological Processes* **29** (13): 2895–2921 DOI: 10.1002/hyp.10403
- Rosenberry DO, Sheibley RW, Cox SE, Simonds FW, Naftz DL. 2013. Temporal variability of exchange between groundwater and surface water based on high-frequency direct measurements of seepage at the sediment-water interface. *Water Resources Research* **49** (5): 2975–2986 DOI: 10.1002/wrcr.20198
- Ruhala SS, Zarnetske JP, Long DT, Lee-Cullin JA, Plont S, Wiewiora ER. 2018. Exploring dissolved organic carbon cycling at the stream—groundwater interface across a third-order, lowland stream network. *Biogeochemistry* **137** (1–2): 105–126 DOI: 10.1007/s10533-017-0404-z
- Rysgaard S, Risgaard-Petersen N, Nielsen LP, Revsbech NP. 1993. Nitrification and Denitrification in Lake and Estuarine Sediments Measured by the 15N Dilution Technique and Isotope Pairing. *Applied and Environmental Microbiology* **59** (7): 2093–2098
- Santelli CM, Chaput DL, Hansel CM. 2014. Microbial communities promoting Mn (II) oxidation in Ashumet Pond, a historically polluted freshwater pond undergoing remediation. *Geomicrobiology Journal* **31** (7): 605–616 DOI: 10.1080/01490451.2013.875605
- Sawyer AH. 2015. Enhanced removal of groundwater-borne nitrate in heterogeneous aquatic sediments. *Geophysical Research Letters* **42** (2): DOI: <u>10.1002/2014GL062234</u>
- Sawyer AH, Cardenas MB. 2009. Hyporheic flow and residence time distributions in heterogeneous cross-bedded sediment. *Water Resources Research* **45** (8) DOI: 10.1029/2008WR007632
- Schlesinger WH, Reckhow KH, Bernhardt ES. 2006. Global change: The nitrogen cycle and rivers. *Water Resources Research* **42** (3) DOI: <u>10.1029/2005WR004300</u>
- Scruggs CR, Mitzman R, MahmoodPoor Dehkordyt F, Briggs MA, Day-Lewis FD, Lane JW. 2016. 'Using a dual-domain porosity apparatus to study water exchange with less-mobile pore spaces in the shallow subsurface of Snake Pond, Cape Cod, MA,' 2016 AGU Fall Meeting, Graduate Virtual Poster Showcase, San Francisco, California, 2016.

- Seitzinger S, Harrison JA, Böhlke JK, Bouwman AF, Lowrance R, Peterson B, Tobias C, Drecht GV. 2006. Denitrification across landscapes and waterscapes: a synthesis. *Ecological Applications* **16** (6): 2064–2090 DOI: 10.1890/1051-0761(2006)016%5B2064:DALAWA%5D2.0.CO;2
- Seitzinger SP, Kroeze C. 1998. Global distribution of nitrous oxide production and N inputs in freshwater and coastal marine ecosystems. *Global biogeochemical cycles* **12** (1): 93–113 DOI: 10.1029/97GB03657
- Seitzinger SP, Styles RV, Boyer EW, Alexander RB, Billen G, Howarth RW, Mayer B, Van Breemen N. 2002. Nitrogen retention in rivers: model development and application to watersheds in the northeastern USA. *Biogeochemistry* **57/58**: 199–237 DOI: 10.1007/978-94-017-3405-9 6
- Sexstone AJ, Revsbech NP, Parkin TB, Tiedje JM. 1985. Direct Measurement of Oxygen Profiles and Denitrification Rates in Soil Aggregates 1. *Soil science society of America journal* **49** (3): 645–651 DOI: 10.2136/sssaj1985.03615995004900030024x
- Smidt SJ, Cullin JA, Ward AS, Robinson J, Zimmer MA, Lautz LK, Endreny TA. 2015. A Comparison of Hyporheic Transport at a Cross-Vane Structure and Natural Riffle. *Groundwater* **53** (6): 859–871 DOI: 10.1111/gwat.12288
- Smith RL, Bohlke JK, Song B, Tobias CR. 2015. Role of anaerobic ammonium oxidation (anammox) in nitrogen removal from a freshwater aquifer. *Environmental Science & Technology* **49** (20): 12169–12177 DOI: 10.1021/acs.est.5b02488
- Smith RL, Howes BL, Duff JH. 1991. Denitrification in nitrate-contaminated groundwater: occurrence in steep vertical geochemical gradients. *Geochimica et Cosmochimica Acta* **55** (7): 1815–1825 DOI: 10.1016/0016-7037(91)90026-2
- Sobczak WV, Findlay S, Dye S. 2003. Relationships between DOC bioavailability and nitrate removal in an upland stream: An experimental approach. *Biogeochemistry* **62** (3): 309–327 DOI: 10.1023/A:1021192631423
- Sobczak WV, Hedin LO, Klug MJ. 1998. Relationships between bacterial productivity and organic carbon at a soil—stream interface. *Hydrobiologia* **386** (1–3): 45–53
- Sophocleous M. 2002. Interactions between groundwater and surface water: the state of the science. *Hydrogeology journal* **10** (1): 52–67 DOI: 10.1007/s10040-001-0170-8
- Steffen W, Richardson K, Rockström J, Cornell SE, Fetzer I, Bennett EM, Biggs R, Carpenter SR, Vries W de, Wit CA de, et al. 2015. Planetary boundaries: Guiding human development on a changing planet. *Science* **347** (6223): 1259855 DOI: 10.1126/science.1259855
- Stelzer RS. 2015. Yearlong Impact of Buried Organic Carbon on Nitrate Retention in Stream Sediments. *Journal of Environmental Quality* **44** (6): 1711–1719 DOI: 10.2134/jeq2015.02.0073

- Stelzer RS, Scott JT, Bartsch LA. 2015. Buried particulate organic carbon stimulates denitrification and nitrate retention in stream sediments at the groundwater–surface water interface. *Freshwater Science* **34** (1): 161–171 DOI: 10.1086/678249
- Stelzer RS, Scott JT, Bartsch LA, Parr TB. 2014. Particulate organic matter quality influences nitrate retention and denitrification in stream sediments: evidence from a carbon burial experiment. *Biogeochemistry* **119** (1–3): 387–402 DOI: 10.1007/s10533-014-9975-0
- Stoliker DL, Repert DA, Smith RL, Song B, LeBlanc DR, McCobb TD, Conaway CH, Hyun SP, Koh D-C, Moon HS, et al. 2016. Hydrologic Controls on Nitrogen Cycling Processes and Functional Gene Abundance in Sediments of a Groundwater Flow-Through Lake. *Environmental Science & Technology* **50** (7): 3649–3657 DOI: 10.1021/acs.est.5b06155
- Storey RG, Fulthorpe RR, Williams DD. 1999. Perspectives and predictions on the microbial ecology of the hyporheic zone. *Freshwater Biology* **41** (1): 119–130 DOI: 10.1046/j.1365-2427.1999.00377.x
- Syakila A, Kroeze C. 2011. The global nitrous oxide budget revisited. *Greenhouse Gas Measurement and Management* **1** (1): 17–26 DOI: 10.3763/ghgmm.2010.0007
- Thomas SA, Valett HM, Mulholland PJ, Fellows CS, Webster JR, Dahm CN, Peterson CG. 2001. Nitrogen Retention in Headwater Streams: The Influence of Groundwater-Surface Water Exchange. *The Scientific World Journal* DOI: 10.1100/tsw.2001.272
- Tiedje JM, Sexstone AJ, Myrold DD, Robinson JA. 1983. Denitrification: ecological niches, competition and survival. *Antonie van Leeuwenhoek* **48** (6): 569–583 DOI: 10.1007/BF00399542
- Tiedje JM, Sexstone AJ, Parkin TB, Revsbech NP. 1984. Anaerobic processes in soil. *Plant and Soil* **76** (1–3): 197–212 DOI: 10.1007/BF02205580
- Tonina D, de Barros FPJ, Marzadri A, Bellin A. 2016. Does streambed heterogeneity matter for hyporheic residence time distribution in sand-bedded streams? *Advances in Water Resources* **96**: 120–126 DOI: 10.1016/j.advwatres.2016.07.009
- Triska FJ, Duff JH, Avanzino RJ. 1990. Influence of exchange flow between the channel and hyporheic zone on nitrate production in a small mountain stream. *Canadian Journal of Fisheries and Aquatic Sciences* **47** (11): 2099–2111 DOI: 10.1139/f90-235
- Triska FJ, Duff JH, Avanzino RJ. 1993. The role of water exchange between a stream channel and its hyporheic zone in nitrogen cycling at the terrestrial—aquatic interface. *Hydrobiologia* **251** (1–3): 167–184 DOI: 10.1007/BF00007177
- US EPA O. 2016. EPA Approves Massachusetts Plan to Protect Cape Cod Waters. *US EPA*Available at: http://www.epa.gov/newsreleases/epa-approves-massachusetts-plan-protect-cape-cod-waters [Accessed 13 June 2017]

- Vidon PG, Hill AR. 2004. Landscape controls on the hydrology of stream riparian zones. *Journal of Hydrology* **292** (1): 210–228 DOI: 10.1016/j.jhydrol.2004.01.005
- Vitousek PM, Aber JD, Howarth RW, Likens GE, Matson PA, Schindler DW, Schlesinger WH, Tilman DG. 1997. Human Alteration of the Global Nitrogen Cycle: Sources and Consequences. *Ecological Applications* **7** (3): 737–750 DOI: 10.1890/1051-0761(1997)007%5B0737:HAOTGN%5D2.0.CO;2
- Walter DA, LeBlanc DR. 1997. Geochemical and hydrologic considerations in remediating phosphorus-contaminated ground water in a sewage plume near Ashumet Pond, Cape Cod, Massachusetts. US Geological Survey; Branch of Information Services [distributor]. Available at: http://pubs.er.usgs.gov/publication/ofr97202
- Walter DA, Masterson JP. 2011. Estimated Hydrologic Budgets of Kettle-Hole Ponds in Coastal Aquifers of Southeastern Massachusetts. U.S. Geological Survey Scientific Investigations Report 2011–5137. Available at: http://pubs.usgs.gov/sir/2011/5137/
- Walter DA, Whealan AT. 2004. Simulated Water Sources and Effects of Pumping on Surface and Ground Water, Sagamore and Monomoy Flow Lenses, Cape Cod, Massachusetts. U.S. Geological Survey Scientific Investigations Report 2004-5181. Available at: http://pubs.er.usgs.gov/publication/sir20045181
- Ward AS, Fitzgerald M, Gooseff MN, Voltz TJ, Binley AM, Singha K. 2012. Hydrologic and geomorphic controls on hyporheic exchange during base flow recession in a headwater mountain stream. *Water Resources Research* **48** (4) DOI: 10.1029/2011WR011461
- Ward AS, Schmadel NM, Wondzell SM, Harman C, Gooseff MN, Singha K. 2016. Hydrogeomorphic controls on hyporheic and riparian transport in two headwater mountain streams during base flow recession. *Water Resources Research* DOI: 10.1002/2015WR018225
- Weiss RF. 1970. The solubility of nitrogen, oxygen and argon in water and seawater. *Deep Sea Research and Oceanographic Abstracts* **17** (4): 721–735 DOI: 10.1016/0011-7471(70)90037-9
- Weiss RF, Price BA. 1980. Nitrous oxide solubility in water and seawater. *Marine chemistry* **8** (4): 347–359 DOI: 10.1016/0304-4203(80)90024-9
- Whitmire SL, Hamilton SK. 2005. Rapid removal of nitrate and sulfate in freshwater wetland sediments. *Journal of Environmental Quality* **34** (6): 2062–2071 DOI: 10.2134/jeq2004.0483
- Williams M, Hopkinson C, Rastetter E, Vallino J. 2004. N budgets and aquatic uptake in the Ipswich River basin, northeastern Massachusetts. *Water Resources Research* **40** (11) DOI: 10.1029/2004WR003172
- Winter TC. 1999. Relation of streams, lakes, and wetlands to groundwater flow systems. *Hydrogeology Journal* **7** (1): 28–45 DOI: 10.1007/s100400050178

- Winter TC, Harvey JW, Franke OL, Alley WM. 1998. *Ground water and surface water: a single resource*. DIANE Publishing Inc. Available at: http://pubs.usgs.gov/circ/circ1139/ [Accessed 25 March 2018]
- Wollheim WM, Harms TK, Peterson BJ, Morkeski K, Hopkinson CS, Stewart RJ, Gooseff MN, Briggs MA. 2014. Nitrate uptake dynamics of surface transient storage in stream channels and fluvial wetlands. *Biogeochemistry* **120** (1–3): 239–257 DOI: 10.1007/s10533-014-9993-y
- Wollheim WM, Pellerin BA, Vörösmarty CJ, Hopkinson CS. 2005. N Retention in Urbanizing Headwater Catchments. *Ecosystems* **8** (8): 871–884 DOI: 10.1007/s10021-005-0178-3
- Wondzell SM. 2011. The role of the hyporheic zone across stream networks. *Hydrological Processes* **25** (22): 3525–3532 DOI: <u>10.1002/hyp.8119</u>
- Wondzell SM, Swanson FJ. 1996. Seasonal and Storm Dynamics of the Hyporheic Zone of a 4th-Order Mountain Stream. I: Hydrologic Processes. *Journal of the North American Benthological Society* **15** (1): 3–19 DOI: 10.2307/1467429
- Wörman A, Packman AI, Johansson H, Jonsson K. 2002. Effect of flow-induced exchange in hyporheic zones on longitudinal transport of solutes in streams and rivers. *Water Resources Research* **38** (1) DOI: 10.1029/2001WR000769
- Zarnetske JP, Haggerty R, Wondzell SM, Baker MA. 2011a. Dynamics of nitrate production and removal as a function of residence time in the hyporheic zone. *Journal of Geophysical Research: Biogeosciences* **116** (1): 72 DOI: 10.1029/2010JG001356
- Zarnetske JP, Haggerty R, Wondzell SM, Baker MA. 2011b. Labile dissolved organic carbon supply limits hyporheic denitrification. *Journal of Geophysical Research: Biogeosciences* **116** (March 2010): G04036 DOI: 10.1029/2011JG001730
- Zarnetske JP, Haggerty R, Wondzell SM, Bokil VA, González-Pinzón R. 2012. Coupled transport and reaction kinetics control the nitrate source-sink function of hyporheic zones. *Water Resources Research* **48** (11): W11508 DOI: 10.1029/2012WR013291
- Zimmer MA, Lautz LK. 2014. Temporal and spatial response of hyporheic zone geochemistry to a storm event. *Hydrological Processes* **28** (4): 2324–2337 DOI: 10.1002/hyp.9778